

NANOPORE STOCHASTIC SENSING WITH IONIC LIQUID SUPPORTING
ELECTROLYTE AND IONIC LIQUID BASED WATER QUANTITATION
USING GAS CHROMATOGRAPHY

By

DILANI A. JAYAWARDHANA

Presented to the Faculty of the Graduate School of
The University of Texas at Arlington in Partial Fulfillment
of the Requirements
for the Degree of

DOCTOR OF PHILOSOPHY

THE UNIVERSITY OF TEXAS AT ARLINGTON

December 2010

Copyright © by Dilani Jayawardhana 2010

All Rights Reserved

This dissertation is dedicated to my parents; who raised me, educated me,
encouraged me and loved me.

ACKNOWLEDGEMENTS

There are always far more people who helped me to achieve the goals than I could ever be able to acknowledge.

First and foremost, I would like to thank both my co-advisors, Professor Daniel W. Armstrong and Professor Richard X. Guan for the guidance, supervision and encouragement that they have provided me throughout my graduate studies. I am extremely fortunate to learn under both of them.

I would like to acknowledge my dissertation committee members: Professor Richard B. Timmons and Professor Carl J. Lovely, for their suggestions and corrections provided during my study. Most importantly, they encouraged me toward more enthusiastic research.

I would like to thank current and former members of the Guan research group: Dr. Mrinal Sengupta, Dr. Milan Dissanayaka, Dr. Jyoti Gupta, Dr. Qitao Zhao, Dr. Deqiang Wang, and Miss Samantha de Zoysa, for their support during my PhD study. I cannot forget the former and current members in Armstrong research group. It is really difficult to list each individual as we have a huge group, but please know that I have appreciated all you have done.

Additional thanks goes to Professor Zoltan A. Schelly for allowing me to use his Karl Fischer titrator and to Professor Subhrangsu S. Mandal for giving me the opportunity of using his resources for protein preparation. Further, I greatly

appreciate the assistance of Mrs. Barbara Smith, Dr. Brian Edwards, Mr. Charles Savage, and the entire chemistry staff.

This journey would not be possible if it weren't for the love and support from my parents, who taught me the value of education. They not only raised me with teaching the good and bad of the world, but also helped me to take care of my son. My sister and brother have always been there with every step that I took. I would also like to thank my husband, for his endless love and countless sacrifices. I know, the life was not easy, but together, we made our goal a success. I should acknowledge the most precious gift, my son for the unconditional love and joy that he brought to our lives.

Finally, I would like to thank all my friends who have been there with me through my life, especially in the difficult situations.

November 10, 2010

ABSTRACT

NANOPORE STOCHASTIC SENSING WITH IONIC LIQUID SUPPORTING ELECTROLYTE AND IONIC LIQUID BASED WATER QUANTITATION USING GAS CHROMATOGRAPHY

Dilani A. Jayawardhana, PhD

The University of Texas at Arlington, 2010

Supervising Professors: Richard X. Guan, Daniel W. Armstrong

This dissertation focuses toward finding two new avenues to explore the properties of ionic liquids (ILs). First, ILs has been used as a novel, and advantageous supporting electrolytes in nanopore stochastic sensing technology. Here, the sensing element is the α -hemolysin protein, while a solution containing an ionic liquid will be used as the background electrolyte, instead of the typical used NaCl/KCl solution. This method employs single-channel recording with the planar lipid bilayer technique, where current modulation represents individual binding events. In this study, a useful means of implementing IL salt solutions will be demonstrated. Specifically, its great enhancements of sensitivity and selectivity of the nanopore for some analytes in stochastic sensing will be discussed. Further, the pH triggered ligand gating of α -hemolysin pore, by phosphonium IL will also be discussed

The goal of the second study is, use of IL as the stationary phase in capillary gas chromatography (GC), with thermal conductivity detector (TCD) for the detection of water content in liquid samples. The detection and quantitation of the amount of water in 50 different solvent samples, with increased sensitivity will be presented.

TABLE OF CONTENTS

ACKNOWLEDGEMENTS	iv
ABSTRACT	vi
LIST OF ILLUSTRATIONS	xii
LIST OF TABLES	xvi
Chapter	Page
1. INTRODUCTION	1
1.1 Nanopore stochastic sensing	1
1.2 Biological nanopore.....	2
1.3 Experimental details.....	4
1.3.1 Single-channel recordings	4
1.3.2 Data analysis	5
1.4 Synthetic nanopore	6
1.5 Nanopore stochastic sensing with ionic liquid supporting electrolytes.....	7
1.6 Ionic liquid based water quantitation using gas chromatography	9
1.7 Organization of dissertation.....	11
2. STOCHASTIC SENSING OF PEPTIDES IN AN ENGINEERED PROTEIN CHANNEL	12
2.1 Introduction	12
2.2 Experimental methods	14
2.2.1 Reagents	14

2.2.2	Preparation and formation of protein pores	14
2.2.3	Electrical recording	15
2.2.4	Data analysis	16
2.2.5	Activities of NaCl used in buffers	16
2.2.6	Ion selectivity of α HL pores.....	17
2.2.7	Estimate of debye length	18
2.2.8	Molecular graphics.....	19
2.3	Results and discussion	19
2.3.1	The Effect of structures of peptides on binding affinities	19
2.3.2	Effects of peptide concentration and applied voltage on the binding kinetics.....	31
2.3.3	Application of peptide-protein pore interaction for peptide detection.....	35
2.4	Conclusions	45
3.	NANOPORE STOCHASTIC DETECTION OF A LIQUID EXPLOSIVE COMPONENT AND SENSITIZERS USING BOROMYCIN AND AN IONIC LIQUID SUPPORTING ELECTROLYTE.....	47
3.1	Introduction	47
3.2	Experimental section.....	50
3.2.1	Materials.....	50
3.2.2	Methods.....	51
3.2.3	Results and discussion	52
4.	SLOWING DNA TRANSLOCATION THROUGH NANOPORES USING A SOLUTION CONTAINING ORGANIC SALTS	66
4.1	Introduction	66
4.2	Experimental methods	67

4.2.1	Materials and reagents	67
4.2.2	Planar bilayer experiments	68
4.2.3	Data analysis	69
4.3	Results and discussion	72
4.4	Conclusions	87
5.	LIGAND GATED α -HEMOLYSIN CHANNEL, TRIGGERED BY PH EFFECT	88
5.1	Introduction	88
5.2	Experimental section.....	90
5.2.1	Materials.....	90
5.2.2	Methods.....	90
5.2.3	Flow nanopore sensing device.....	91
5.3	Results and discussion	93
5.3.1	The effect of pH on the binding of β CD to the α HL pore in the P(CH ₂ OH) ₄ -Cl solution.....	93
5.3.2	The effect of pH on the α HL channel in other electrolytes	95
5.3.3	Understanding the gating phenomenon	96
5.3.4	Investigating the gating mechanism in the α HL pore.....	101
5.4	Conclusion	102
6.	A RAPID GAS CHROMATOGRAPHIC WATER QUANTITATION METHOD, USING IONIC LIQUID STATIONARY PHASES.....	104
6.1	Introduction	104
6.2	Experimental.....	106
6.2.1	Apparatus	106
6.2.2	Materials	107

6.2.3	Calibration standard and sample preparation.....	108
6.2.4	Methods.....	108
6.2.5	Preparation of IS calibration plots	109
6.2.6	Sample preparation and analysis.....	110
6.2.7	Detection limit and quantitation limit.....	110
6.3	Results and discussion	111
6.4	Conclusions.	119
7.	SUMMARY	120
	APPENDIX	122
A.	DESCRIPTION OF SOLVENTS THAT ARE USED TO DETECT THE WATER CONTENT.....	122
B.	STRUCTURES OF ILS THAT ARE TESTED AS GC STATIONARY PHASES FOR THE DETECTION OF WATER.....	126
C.	CALIBRATION PLOTS FOR WATER DETECTION STUDY.....	129
D.	THE STUDY OF ATMOSPHERIC WATER ABSORPTION ON DIFFERENT SOLVENTS: THE INCREMENT OF WATER PEAK AREA AS A FUNCTION OF TIME.....	139
E.	STUDY OF THE EFFECT OF DIFFERENT ILS ON STOCHASTIC SENSING.....	145
F.	RIGHTS AND PERMISSIONS.....	148
	REFERENCES	155
	BIOGRAPHICAL INFORMATION	166

LIST OF ILLUSTRATIONS

Figure		Page
1.1	Schematic representation of stochastic sensing	2
1.2	Structure and dimensions of α -hemolysin channel	3
1.3	Schematic representation of the chamber	5
1.4	Structures of common cations	8
1.5	Structures of common anions	8
2.1	Molecular graphics representation of the staphylococcal α HL protein pore and relative size of the amyloid- β peptide (10-20).	20
2.2	Representative single-channel traces showing the effect of peptide length and structure on the transport of peptides through a single (M113Y) ₇ pore.....	21
2.3	Effect of peptide length and structure on the transport of peptides through a single (M113Y) ₇ pore. (a) Current blockage amplitudes; and (b) Event mean dwell times.	22
2.4	Effect of structure of protein pores on peptide translocation. Typical single-channel recording traces: (a) (WT) ₇ , (b) (M113F) ₇ , and (c) (2FN) ₇ , showing the interaction between peptide Y6 and three different protein pores.....	26
2.5	The interaction between peptide Y6 and three different protein pores; (a) event residual currents; and (b) formation constants	27
2.6	Representative single-channel recordings, showing the effect of engineered protein pores on the peptide transport. (a) (WT) ₇ ; (b) (M113F) ₇ ; and (c) (2FN) ₇	29
2.7	The effect of peptide concentration on the residence time of binding events.	33

2.8	The effect of peptide concentration on the frequency of binding events.....	33
2.9	The effect of the applied voltage on the residence time of binding events.	34
2.10	The effect of the applied voltage on the frequency of binding events.....	34
2.11	Simultaneous detection of a mixture of peptides.....	36
2.12	(a) a mixture of Y6, YPFW, YWPF and YPWG, where the concentration of YPFW was three times larger than that of (2.9d); and (b) the corresponding representative single-channel current trace of (2.9d), in which the individual Y6, YPFW, YWPF and YPWG events were arrow-marked at different levels.	37
2.13	Simultaneous detection of a two-peptide mixture in the (M113F) ₇ pore. Event histograms of (a) YFF, (b) YPF, and (c) a mixture of YFF and YPF.	40
2.14	Simultaneous detection of a two-peptide mixture in the (2FN) ₇ pore. Event histograms of (a) YFF, (b) YPF, and (c) a mixture of YFF and YPF.	41
2.15	Differentiation of peptide sequences. (a) Event residual currents; and (b) Mean dwell times.	42
2.16	Typical single-channel recordings, showing the detection of a series of peptides with the same length and amino acid composition but different sequences in positive voltage bias.....	43
2.17	Typical single-channel recordings, showing the detection of a series of peptides with the same length and amino acid composition but different sequences in negative voltage bias.	44
3.1	a) Structure of boromycin, b) structure of BMIM-Cl, and c) complexation of guest molecule with boromycin.	49
3.2	Typical single channel current recording traces for the detection of tetramethylammonium chloride.....	53
3.3	Typical single channel current recording traces of boromycin in (a) 1 M NaCl (aq); and (b) 1 M BMIM-Cl (aq).....	55

3.4	The effect of applied potential on the detection of mono-valent cations.	58
3.5	Typical single channel current recording traces showing the stochastic sensing of analytes in 1M BMIM-Cl solution and using boromycin as a host. a) TEA, b) DEA, c) CM, d) HZ, e) NH ₄ ⁺ , and f) K ⁺	60
3.6	Stochastic sensing of analytes in 1M BMIM-Cl solution and using boromycin as a host. (<i>Left</i>) Dwell time histograms. (<i>Right</i>) Amplitude histograms. a) TEA, b) DEA, c) CM, d) HZ, e) NH ₄ ⁺ , and f) K ⁺	61
3.7	Typical single channel current recording traces for the simultaneous detection of TEA and HZ in 1 M BMIM-Cl (aq). a) Boromycin + TEA; b) boromycin + HZ; and c) boromycin + HZ + TEA.	63
3.8	Amplitude histograms for simultaneous detection of TEA and HZ.	64
4.1	Translocation of (dA) ₂₀ in the mutant (M113F) ₇ αHL pore in 1M NaCl solution.	71
4.2	Translocation of (dA) ₂₀ in the mutant (M113F) ₇ αHL pore in 1M BMIM-Cl solution.	73
4.3	Effect of DNA length on the mean residence time of (a) long-lived events; and (b) short-lived events, suggesting that the long duration events are caused by DNA's threading through the αHL pore.	75
4.4	Event dwell time histograms of (a) (dA) ₂₀ ; (b) (dT) ₂₀ ; (c) (dC) ₂₀ ; (d) (dC) ₁₀ (dT) ₁₀ ; and (e) (dCdT) ₁₀	76
4.5	Event dwell time histograms of (a) (dA) ₂₀ ; (b) (dT) ₂₀ ; (c) (dC) ₂₀ ; (d) (dC) ₁₀ (dT) ₁₀ ; and (e) (dCdT) ₁₀	81
4.6	The mean residence times and current blockage amplitudes of five ssDNA samples in the wild-type αHL protein channel.	82
4.7	Determination of the streaming potentials of αHL channels in NaCl solution.	83
4.8	Determination of the streaming potentials of αHL channels in BMIM-Cl solution.	84

4.9	Translocation of (dA) ₂₀ in the mutant (M113F) ₇ αHL pore in 1 M tetramethylammonium chloride solution.	86
5.1	Schematic representation of the flow set-up.	93
5.2	The effect of pH on the current of the α-hemolysin channel and the interaction between βCD and the α-hemolysin pore.	94
5.3	pH Dependence of the β-CD's binding to αHL channel.	96
5.4	Voltage effect on both gated and open channels.	97
5.5	Online study of pH dependence while adding NaOH, up to pH 7.0.	99
5.6	On-line monitoring of the pH effect on the αHL channel in the presence of 80 μM βCD.	101
6.1	The structures of ILs that gave the best separation of water, when coated on fused silica capillary columns.	112
6.2	Separation of water from CH ₂ Cl ₂ in examined columns at 80 °C.	112
6.3	Summary of the detection of water by two IL columns; green is HMHM-PEG and pink is TPT.	117

LIST OF TABLES

Table		Page
2.1	Mean activities of 0.2 M and 1.0 M NaCl solutions at 22 ± 1 °C.....	18
2.2	Kinetic and thermodynamic constants of the non-covalent interactions between various peptides and the (M113F) ₇ pore.	24
2.3	Charge selectivities of α HL pores. Single-channel currents were recorded under asymmetric conditions: 1 M NaCl, 10 mM Tris-HCl (pH 7.5) (<i>cis</i>), and 0.2 M NaCl, 10 mM Tris-HCl (pH 7.5) (<i>trans</i>)	31
3.1	The dwell time and amplitude values for analyte-boromycin complexes	62
4.1	The mean residence times and current blockage amplitudes of five ssDNA samples in the (M113F) ₇ protein pore	78
4.2	The mean residence times and current blockage amplitudes of five ssDNA samples in the wild-type α HL protein channel	79
6.1	GC/TCD parameters for the analysis of water	107
6.2	Limits of detection and limits of quantitation of water in evaluated columns	113
6.3	Detection of water in 50 solvents. X- couldn't separate the water peak from the solvent peak.....	114

CHAPTER 1

INTRODUCTION

1.1 Nanopore stochastic sensing

Stochastic sensing is currently an active research area, as a highly-sensitive, rapid, and multi-functional sensing system.¹ The stochastic sensor element is a biological ion channel embedded in a planar lipid bilayer or a single artificial nanopore fabricated in a solid-state membrane. When individual molecules pass through the nanometer-sized pore at a fixed applied potential, the modulations of the ionic current flowing through the pore can be observed as random events.² The concentration of the analyte can be obtained by the frequency of occurrence ($1/\tau_{\text{on}}$) of the recorded blockades, while the mean residence time (τ_{off}) of the analyte coupled with the extent of current blockage (amplitude) allows to determine its identity (Figure 1.1).

Since each analyte produces a characteristic signature, the sensor element itself need not be highly selective and multiple analytes can be quantitated simultaneously using a single sensor element, as long as the sensor itself can provide enough resolution. Moreover, nanopore stochastic sensing does not require the use of expensive reagents or chemical tags with no loss of signal-to-noise at lower concentrations of the analyte.

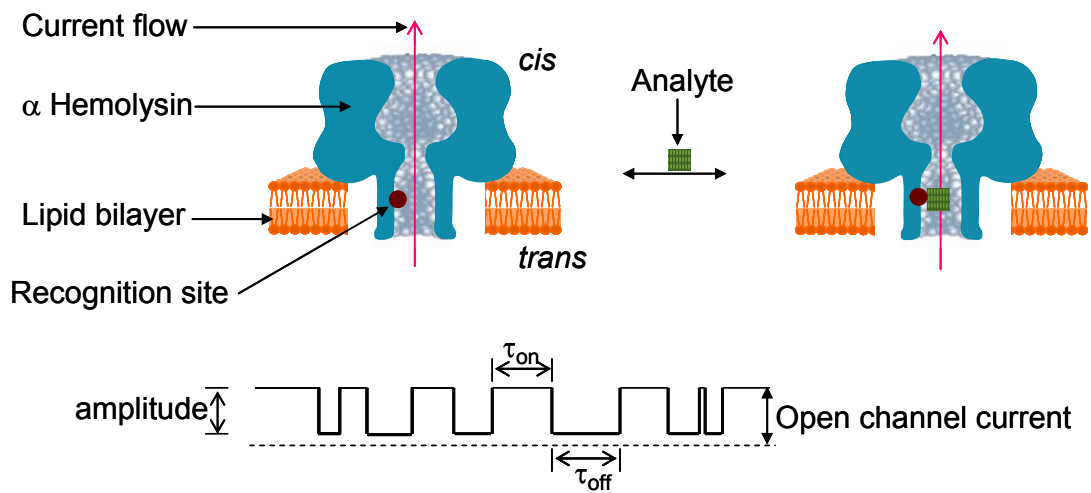


Figure 1.1 Schematic representation of stochastic sensing

The first experiment in this field was performed in 1970, where peptide antibiotic gramicidin formed an ion-conducting channel in a planar lipid bilayer.³ Currently, there are two prototypes of nanopore sensing systems, i.e., biological nanopore and synthetic nanopore.

1.2 Biological nanopore

This sensing system is borrowed from mother nature,⁴ which employs transmembrane protein ion channels embedded in lipid bilayers as sensor elements. Although numerous ion channels such as acetylcholine receptor,⁵ gramicidin,⁶ potassium channel (KcsA),^{7, 8} and porins of bacteria and mitochondria^{9,10} have been found in nature, the most widely used protein nanopore is α -hemolysin, since its open channel is quiet without transient background current modulations, and hence the α -hemolysin pore is an ideal sensor element for sensitive detection of trace amounts of analytes.

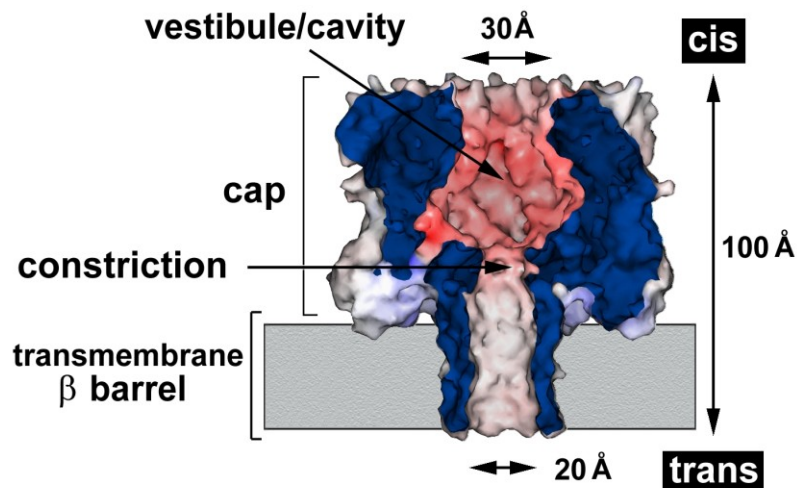


Figure 1.2 Structure and dimensions of α -hemolysin channel

The α -hemolysin is a spontaneous pore-forming toxin secreted by *Staphylococcus aureus*. The wild-type α -hemolysin forms a mushroom shaped, solvent-filled heptameric pore, which consists of seven identical subunits arranged around a central axis.¹¹ The diameter of the *cis* opening of the pore is ~ 30 Å, while that of the *trans* entrance is ~ 20 Å (Figure 1.2). The constriction of the α -hemolysin channel has a diameter of ~ 15 Å. Hence, molecules with a diameter smaller than ~ 15 Å can move through the 100 Å long channel.¹² Engineered versions of α -hemolysin protein pore have been used as stochastic sensing elements for the identification and quantification of a wide variety of substances,¹ including metal ions,^{13,14} anions,¹⁵ proteins,^{16,17} DNA,¹⁸⁻²¹ enantiomers,²² explosives,^{23,24} organic molecules²⁵ and reactive molecules.²⁶ Note that, in the nanopore stochastic sensing, the magnitude and the duration of the current modulations primarily depends on the migration rate of the analyte, which is governed by the diffusion, charge selectivity of the protein pore, size of the analyte, and the affinity between the analyte molecule

and the binding site of the pore.

1.3 Experimental details

1.3.1 Single-channel recordings

Protein ion channel-based stochastic sensing experiments involve the formation of a lipid bilayer (1,2-diphytanoylphosphatidylcholine) using the Montal-Mueller method²⁷ over a ~100-120 μm hole which is around the middle of a Teflon membrane, placed between two chamber compartments, as shown in Figure 1.3. In general, the *cis* compartment is grounded, and each compartment contains aqueous NaCl (1 M, 1.5 ml) solution, buffered with aqueous Tris·HCl (10 mM, pH 7.5), as the electrolyte. Then, α -hemolysin protein is added to the *cis* compartment. In this way, after insertion of a single α HL channel, the mushroom cap of the α HL channel would be located in the *cis* compartment, while the β -barrel of the α HL would insert into the lipid bilayer and connect with the *trans* of the chamber device. After insertion of the channel into the lipid bilayer, analytes can be added either from the *cis* or *trans* compartments depending on the nature of the protein pore. Currents are recorded with a patch clamp amplifier (Axopatch 200B, Molecular Devices; Sunnyvale, CA, USA). They are low-pass filtered with a built-in four-pole Bessel filter at 5 kHz and sampled at 25 kHz by a computer equipped with a Digidata 1440 A/D converter (Molecular Devices). To shield against ambient electrical noise, a metal box is used to serve as a Faraday cage, inside which the bilayer recording amplifying headstage, stirring system, chamber, and chamber holder are enclosed.

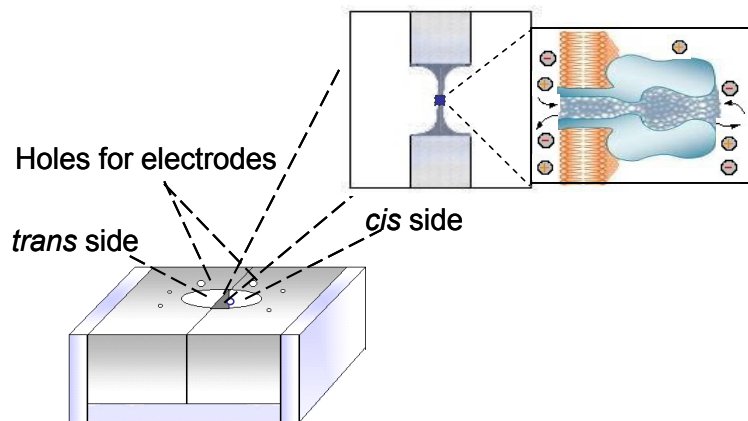
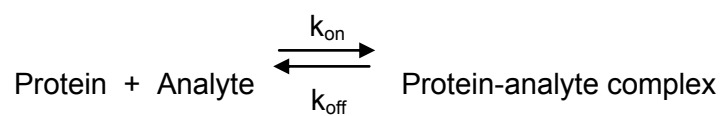


Figure 1.3 Schematic representation of the chamber

1.3.2 Data analysis

Data analysis is performed with pClamp software. Mean residence times (τ_{off} and τ_{on} values) for the analytes are obtained from dwell time histograms by fitting the distributions to single exponential functions by the Levenberg-Marquardt procedure. The conductance values are obtained from the amplitude histograms after the peaks were fit to Gaussian functions. The mean values of τ_{off} , and τ_{on} can be used further to obtain the kinetic and thermodynamic information of the interaction between the protein pore and the analyte via the following equations.



$$k_{\text{on}} = \frac{1}{\tau_{\text{on}}[A]}$$

$$k_{\text{off}} = \frac{1}{\tau_{\text{off}}}$$

$$K_f = \frac{k_{\text{on}}}{k_{\text{off}}}$$

$$\Delta G_f = -RT \ln K_f$$

Where, k_{on} = rate constant of protein-analyte complex formation

k_{off} = rate constant of protein-analyte complex dissociation

τ_{on} = mean residence time of the open state

τ_{off} = mean residence time of the bound state

[A] = analyte concentration

K_f = formation constant of protein-analyte complex

ΔG_f = change in Gibb's free energy of formation

R = universal gas constant

T = absolute temperature

1.4 Synthetic nanopore

The major hurdle in the transition of the protein pore technology to a deployable sensor is the lack of durability,¹ which is mainly attributed to the fragile lipid bilayer used for supporting the protein pore. Although the recent protein nanopore studies have demonstrated that a single α -hemolysin pore, in a planar phospholipid bilayer, could be sandwiched between two agarose layers which gel in situ and make a robust and portable single-channel chip, which may be transported, stored, and used repeatedly,²⁸ the currently available protein pore based

stochastic sensing has been confined to the laboratory research. Therefore, in order to make a deployable stochastic sensor device, there is a need for the construction of robust synthetic nanopores.

Several techniques have been used to make single nanopores on solid supports,²⁹ including ion or electron beams, soft lithography and LASER. Further, carbon nanotubes and hybrid systems have also been tried.² Currently, two of the most popular methods to construct synthetic nanopores are base etching of silicon wafers and track-etched conical nanopores in polymer membranes.²⁹ Although the synthetic nanopore approach has obtained considerable success, the difficulty and time consumption in fabrication, and most importantly, the lack of reproducibility has become the biggest hurdles to further advance the synthetic nanopore technique.

1.5 Nanopore stochastic sensing with ionic liquid supporting electrolytes

To date, nanopore stochastic sensing has typically been carried out in electrolyte solutions of 1M NaCl or 1M KCl. Although the detection of divalent metal ions such as Zn^{2+} , Cd^{2+} , and Co^{2+} has been achieved by using these common inorganic salts, high concentrations of these electrolytes would prevent the detection of monovalent species that are present in trace quantities. Further, the aqueous inorganic salt medium has limited the analysis to only water soluble analytes. Therefore, there is a need for the introduction of new background electrolytes which may permit the analysis of compounds that are difficult or even impossible to achieve in the NaCl or KCl solution. The unique cation / anion combinations reported for ionic liquids (ILs) make ideal candidates for novel electrolytes in the nanopore stochastic sensing. Although pure room temperature ILs are viscous materials with interesting

solvent properties,^{46,47} they are also finding use as nontraditional electrolyte solutions.

ILs are defined as salts, which melt at or below 100 °C.³⁰ If they are liquids at room temperature (~25 °C), they fall into the category of room temperature ILs.³¹ In almost all of the ILs, either the anion or the cation is an organic ion. Examples for such anions and cations are follows:

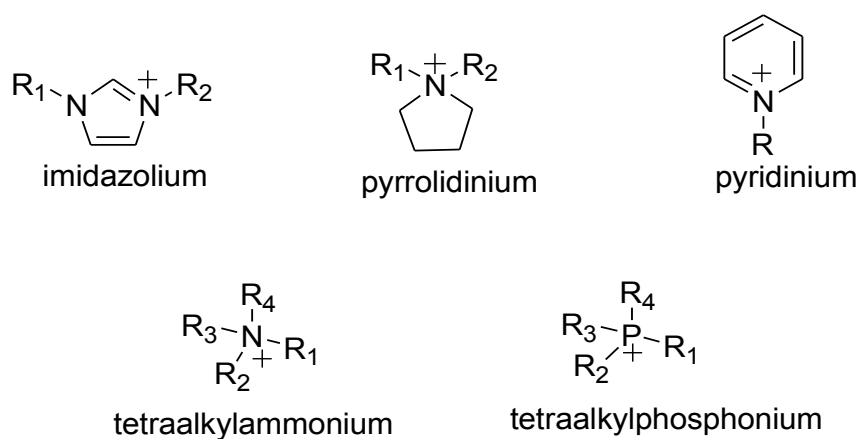


Figure 1.4 Structures of common cations

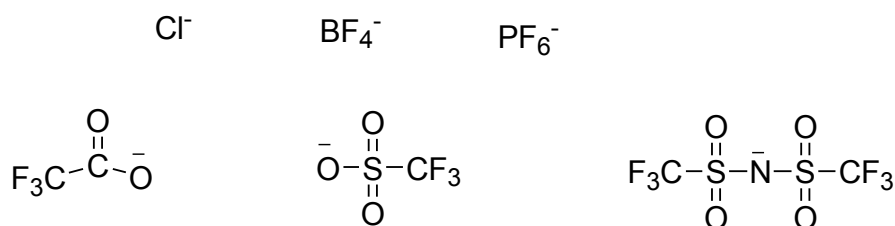


Figure 1.5 Structures of common anions

The low melting point of ILs is a result of relatively weak intermolecular forces (i.e. hydrogen bonding, dipole-dipole and London-dispersion) which arise from the lower symmetry, larger size of the ions and charge delocalization. Traditional ionic compounds are bound by strong electrostatic forces which makes them higher melting compounds. ILs have unique properties such as negligible vapor pressure, wide liquid ranges, electrical conductivity with wide electrochemical windows, wide range of viscosities, adjustable miscibility, and good thermal stability.³⁰ These properties can be tuned as desired by varying the cation and anion combinations. This widens the areas of applicability of ILs. The advent of ILs has led to their use in organic synthesis,³² catalysis,³³ separation,³⁴ extraction,³⁵ electrochemistry,³⁶ mass spectrometry and spectroscopy.³⁰ Indeed, it may be advantageous to implement ILs as background electrolytes for nanopore sensing, given their electric conductivity, wide electrochemical window, and solubility in water.⁴⁸

1.6 Ionic liquid based water quantitation using gas chromatography

The determination of water content in consumer products, such as foods and pharmaceuticals, and to industrial materials/products, like solvents, oil and paint, is of great importance. Indeed analytical testing for the presence and concentration of water is one of the most frequent, important and ubiquitous measurements made in modern industrial society. Thus a versatile and simple analytical technique for the accurate quantification of water is imperative. Due to the essentially universal presence of water, accurate, facile and sensitive techniques are needed. Though various techniques such as gravimetry,³⁷ Karl Fisher titration (KFT),^{38,39} gas chromatography,⁴⁰⁻⁴⁹ near IR spectrophotometry,^{40,50-52} solvatochromic sensing,⁵³ ¹⁹F-NMR spectroscopy,⁵⁴ isotope ratio mass spectrometry (IRMS),⁵⁵ and many more

have been reported in the literature, only few are accepted widely and used.

Currently, the most commonly used method for water analysis is KFT, which was first published in 1935 by the chemist, Karl Fischer.³⁸ In this titrametric method, I₂ is reduced to HI in the presence of water.⁴⁵

Despite the fact that this is a well established method, interference of side reactions,⁴⁵ reagent instability, sample insolubility⁵⁶ and pH issues⁴⁰ prevent it from being accepted as a universal method. Some KFT methodologies have been developed in an attempt to overcome these issues.^{39,45,56} However, many issues still remain, not the least of which is that there is residual water in most KFT reagents.

Another applied method for water detection is based on gas chromatography (GC). It has proven to be useful tool for the analysis of a vast majority of samples with low to moderate boiling points and high volatilities. The separation is achieved by the differences in partitioning of the analytes, between the stationary phase and the gaseous mobile phase. GC is a rapid, sensitive, efficient, cost effective and user friendly technique.

Early attempts using gas chromatography were mainly based on packed (molecular sieves) columns, involving both direct detection by thermal conductivity detector (TCD)^{43-45,47,49} and indirect detection (i.e. reacting water with calcium carbide to convert to acetylene) by flame ionization detection (FID).⁴¹ Peak asymmetry,⁴⁰ poor sensitivity, adsorption of water by the stationary phase,⁴³ overlapping of the water peak by other larger peaks, and the inability to detect higher amounts of water⁴⁰ delayed its practical applications. Attempts to eliminate peak asymmetry,^{40,57}

using wide-diameter open tubular columns⁴² and capillary columns⁴⁶ showed some success. The unique nature of ILs including; high thermal stabilities,⁵⁸ variable polarities³⁰ and exceptional stability to water and oxygen make them excellent choices as stationary phases for this methodology. As will be shown, open tubular capillary columns, coated with specific IL stationary phases (developed for water analysis) can tremendously increase the sensitivity and reliability of this technique. In this study, the absolute water content in 50 different solvent samples was determined and the quantification has been carried out by using either acetone or acetonitrile as internal standards (IS).

1.7 Organization of dissertation

The first portion of this dissertation (Chapters 2-5) will focus on the stochastic sensing technique. Specifically, Chapter 2 involves the analysis of peptides in a traditional NaCl electrolyte solution. Chapters 3 through 5 discuss advances made by the introduction of IL as an advantageous supporting electrolyte for stochastic nanopore sensing technique. Lastly, Chapter 6 concentrates on the IL based water quantitation using capillary GC.

CHAPTER 2

STOCHASTIC SENSING OF PEPTIDES IN AN ENGINEERED PROTEIN CHANNEL

2.1 Introduction

A nanopore sensor works by monitoring the ionic current modulations induced by the passage of analytes of interest through a single pore, most often, the α -hemolysin (α HL)¹⁴ protein channel, at a fixed applied potential. In this way, the concentration of the analyte can be obtained by the frequency of occurrence ($1/\tau_{on}$) of the recorded blockage events, while the mean dwell time (τ_{off}) of the analyte coupled with the extent of current blockage (amplitude) allows to determine its identity. The resolution and sensitivity of stochastic detection is largely dependent on the nature of the protein pores and the experimental conditions. Cassette or site-directed mutagenesis is commonly used as a versatile means to modify the biological protein pores with a variety of new functional groups to regulate the translocation of target analytes,⁵⁹ whereas the experimental parameters, including pH, temperature, ionic strength, and applied potential, also affect the molecular transport and possibly other dynamic factors associated with channel performance.^{15,60-63}

Nanopore technology has been used to identify and quantify a variety of analytes including cations,¹³ organic molecules,²³ proteins,¹⁶ chemical warfare agents,⁶⁴ and DNA.^{18,65,66} The translocation of polypeptides through nanopores has also been investigated.⁶⁷⁻⁷¹ However, the currently available nanopore technology does not have the single-amino acid resolution that enables the detection of short peptides, differentiation of peptide molecules that differ slightly in composition,

peptide sequencing, and even simultaneous quantification of peptide mixtures. It should be noted that, peptides play important roles in a variety of physiological processes in living systems. Accordingly, assay of these biologically active molecules are of paramount importance in diagnostics and therapeutics.⁷²⁻⁷⁴ For example, it is known that neurodegenerative dementias including Alzheimer's disease and Parkinson's disease are characterized by the aggregation and deposition of amyloid-based peptides as pathological lesions in brain.⁷⁵⁻⁷⁷ The inhibition of amyloid aggregation and the reduction of the amyloid neurotoxicity could be achieved by using small peptide molecules, e.g., tetrapeptide endomorphin-2 (YPFF).⁷⁸ A variety of methods have been developed for the detection and/or characterization of peptides, including optical detections, mass spectrometry, capillary electrophoresis, nuclear magnetic resonance and high-performance liquid chromatography.⁷⁹⁻⁸⁴ Nanopore sensors should be useful for the detection of these biomolecules given that analytes are detected under physiological conditions and no complicated sample pretreatment procedures⁸⁵ required in stochastic sensing.¹

In this work, we first performed systematical studies of the kinetics of peptide-protein interactions to examine how the length and structure of peptides affect their interaction with a protein pore modified with an aromatic binding site. Then, the effect of wild-type and modified protein pores on peptides' translocation was further investigated. Furthermore, to show the sensor application of the nanopores, a series of short peptides, including those differing by a single amino acid, was examined with a properly engineered α HL channel. Moreover, the viability of utilizing the modified protein pores for the simultaneous detection of peptide mixtures and even peptide sequencing was investigated.

2.2 Experimental methods

2.2.1 Reagents

Peptides, including amyloid- β peptide (10-20) with a sequence of YEHHQKLVFF ($A\beta$ -11 or YF-11), YYYYYY (Y6), YPFF, YPWG, YFF, YPF, and WW, were purchased from American Peptide Company, Inc. (Sunnyvale, CA). Other peptides such as YPWF, YWPF, YPFW, and PYWF were obtained from Biomatik Corporation (Wilmington, DE). All of these peptides did not contain any protecting groups at the N- or C-terminus and were supplied in lyophilized form. The purity of these peptides was greater than 95% as verified by high-performance liquid chromatography and mass spectrometry. All the peptides were dissolved in HPLC-grade water. With the exception of the stock solutions of YF-11 and Y6, which were prepared at concentrations of 0.5 mM, all the stock solutions of other peptides were prepared at 1.0 mM each. All these peptide solutions were kept at $-80\text{ }^{\circ}\text{C}$ before and after use. 1,2-Diphytanoylphosphatidylcholine was obtained from Avanti Polar Lipids (Alabaster, AL). Teflon film was purchased from Goodfellow (Malvern, PA). All other reagents were purchased from Sigma (St. Louis, MO).

2.2.2 Preparation and formation of protein pores

Mutant α HL M113Y, M113F and M113F/K147N/T145F (2FN) genes were constructed by site-directed mutagenesis (Mutagenex, Piscataway, NJ) with a WT α HL gene¹¹ in a T7 vector (pT7- α HL). Wild-type α HL and mutant α HL monomers were first synthesized by coupled *in vitro* transcription and translation (IVTT) using the *E. Coli* T7 S30 Extract System for circular DNA from Promega (Madison, WI). Subsequently, they were assembled into homoheptamers by adding rabbit red cell

membranes and incubating for 1~2 h.⁸⁶ The heptamers such as (WT)₇, (M113F)₇, and (M113F)₇(K147N)₇(T145F)₇ [(2FN)₇] were purified by SDS-polyacrylamide gel electrophoresis and stored in aliquots at -80°C.⁸⁷

2.2.3 Electrical recording

A bilayer of 1,2-diphytanoylphosphatidylcholine was formed on an aperture (150 μm) in a Teflon septum (25 μm thick) that divided a planar bilayer chamber into two compartments, *cis* and *trans*. The formation of the bilayer was achieved by using the Montal-Mueller method,²⁷ and monitored by using a function generator (BK precision 4012A; Yorba Linda, CA, USA). In most cases, the lifetime of the bilayer is at least three hours even after insertion of an αHL pore. The experiments were performed under a series of symmetrical buffer conditions with a 2.0 mL solution comprising 1M NaCl, and 10 mM Tris-HCl (pH 7.5) at 22 ± 1 °C. Unless otherwise noted, the αHL protein was added to the *cis* compartment, which was connected to “ground”, while the peptide was added to the *trans* compartment. In such a way, after insertion of a single αHL protein channel, the mushroom cap of the αHL channel would be located in the *cis* compartment, while the β-barrel of the αHL would insert into the lipid bilayer and connect with the *trans* side of the chamber device. The final concentration of the αHL proteins was 0.2–2.0 ng·mL⁻¹. Currents were recorded with a patch clamp amplifier (Axopatch 200B, Molecular Devices; Sunnyvale, CA, USA). They were low-pass filtered with a built-in four-pole Bessel filter at 5 kHz and sampled at 50 kHz by a computer equipped with a Digidata 1322 A/D converter (Molecular Devices).

2.2.4 Data analysis

Conductance values were obtained from the amplitude histograms after the peaks were fit to Gaussian functions. The values of τ_{on} (the inter-event interval) and τ_{off} (the residence time) for the peptides were obtained from dwell time histograms by fitting the distributions to single exponential functions by the Levenberg-Marquardt procedure.¹⁷ Kinetic constants were calculated by using $k_{off} = 1/\tau_{off}$, $k_{on} = 1/(C\tau_{on})$, $K_f = k_{on}/k_{off}$, and $\Delta G_f = -RT\ln K_f$, where C is the concentration of the peptide. Each current trace was recorded at least 2 min and repeated at least 3 times. With the exception to amyloid- β peptide (10-20), for which 350 - 500 events were recorded in each of the single channel recording experiments, between 3000 and 10000 events were collected in each of the single channel recording experiments with other peptides. The event residual current can be obtained by: $I_r = I_o - I_b$, where I_r , I_o , and I_b is the residual current, open channel current, and current blockage amplitude, respectively. The charge selectivity of a protein pore or the permeability ratios (P_{Na^+}/P_{Cl^-}) can be calculated by using the Goldman-Hodgkin-Katz equation⁸⁸ as follows;

2.2.5 Activities of NaCl used in buffers

The mean activity coefficient of NaCl can be given by^{89, 90}

$$\ln \gamma_{NaCl} = f^\gamma + 2IB_{MX} + (3/2)I^2C_{MX}^\phi + I^2B'_{MX}$$

Where,

$$f^\gamma = -A_\phi \left[\frac{I^{1/2}}{1 + bI^{1/2}} + (2/b) \ln(1 + bI^{1/2}) \right]$$

$$B_{MX} = \beta_{MX}^{(0)} + \beta_{MX}^{(1)} g(\alpha I^{1/2})$$

$$B'_{MX} = \beta_{MX}^{(1)} g'(\alpha I^{1/2}) / I$$

$$g(x) = 2[1 - (1+x)e^{-x}] / x^2$$

$$g'(x) = -2[1 - (1+x+0.5x^2)e^{-x}] / x^2$$

$$(A_\phi = 0.3921, b = 1.2, \alpha = 2, C_{NaCl}^\phi = 0.00127, \beta_{NaCl}^{(0)} = 0.0765, \beta_{NaCl}^{(1)} = 0.2664)$$

Here, I is the ionic strength of the solution: $I = \frac{1}{2} \sum_i m_i z_i^2$, where m is the mass molarity of NaCl.

2.2.6 Ion selectivity of α HL pores

The charge selectivity of a pore can be calculated by using the Goldman-Hodgkin-Katz equation⁸⁸:

$$\frac{P_{Na^+}}{P_{Cl^-}} = \frac{[\alpha_{Cl^-}]_t - [\alpha_{Cl^-}]_c e^{V_r F / RT}}{[\alpha_{Na^+}]_t e^{V_r F / RT} - [\alpha_{Na^+}]_c}$$

where α_M is the activity of ion M, subscripts c and t represent *cis* and *trans* sides of the bilayer, V_r is the reversal potential, F the Faraday constant, and R the gas constant. For the measurement of reversal potential V_r , single-channel currents were recorded under asymmetric conditions with a 2.0 mL solution comprising 1M NaCl,

and 10 mM Tris-HCl (pH 7.5) (*cis*), and a 2.0 mL solution comprising NaCl (0.2 M), 10 mM Tris-HCl (pH 7.5) (*trans*). Then, V_r was obtained by a polynomial fitting of the current-voltage (I-V) curve near zero current, in which the I-V data were recorded from voltage ± 20 mV to ± 120 mV.

2.2.7 Estimate of debye length

The Debye length can be estimated by $l_D^2 = \epsilon \epsilon_0 RT / (2F^2 C)$, where C is the salt concentration of the buffer, F the Faraday constant, R the gas constant, while ϵ ($\epsilon = 80$) and ϵ_0 ($\epsilon_0 = 8.85 \times 10^{-12}$ F/m) are relative dielectric constant of water and the absolute dielectric constant of vacuum, respectively.⁹¹ It should be mentioned that the mean activities of NaCl solution were used for the calculation of the Debye length.

Table 2.1 Mean activities of 0.2 M and 1.0 M NaCl solutions at 22 ± 1 °C.

NaCl (mol·L ⁻¹)	I (mol·Kg ⁻¹)	f'	$g(x)$	$g'(x)$	B	B'	$\ln \gamma$	γ	α
0.2	0.201	-0.3956	0.5629	-0.1550	0.2265	-0.2054	-0.3128	0.7314	0.1470
1	1.0371	-0.7015	0.2911	-0.1607	0.1541	-0.0412	-0.4243	0.6542	0.6785

2.2.8 Molecular graphics

The models of amyloid- β peptide (10-20) and the mutant α HL proteins were produced with PyMol (0.99, DeLano Scientific, Palo Alto, CA.)

2.3 Results and discussion

2.3.1 The Effect of structures of peptides on binding affinities

Fundamental studies on molecular transport through transmembrane channels or pores have suggested that binding interactions occurring in a channel play a significant role in facilitating or retarding the translocation of molecules through the pores.^{69, 92, 93} However, it remains unclear how the structure of the transported molecule and the residues of the binding sites lining the lumen of the pores influences the binding affinity, thus resulting in the change in the residence time and blockage amplitude of the compound in a protein pore. To address this issue, a series of peptides consisting of mainly aromatic amino acids and with various lengths was utilized to examine the length and side chain-dependent noncovalent interactions in a (M113Y)₇ pore, which contains an aromatic binding site with seven aromatic Tyr side chains (Figure 2.1). In general, hydrophobic interactions can also occur in the (M113Y)₇ protein pore, although the designed binding between the peptides and the protein in this experiment is predominantly due to the aromatic interaction.

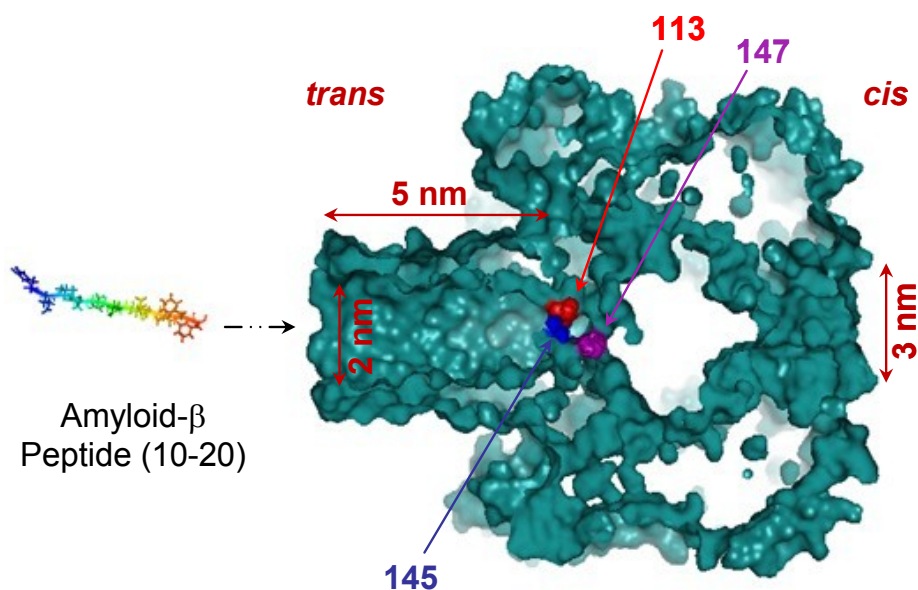


Figure 2.1 Molecular graphics representation of the staphylococcal α HL protein pore and relative size of the amyloid- β peptide (10-20).

Figure 2.2 shows the typical electrical recordings of a variety of peptides with different lengths ranging from 11 (YF-11) to 2 (WW), and Figure 2.3 the obtained current signatures (i.e., dwell time and amplitude). It can be seen that in general, both the event mean dwell time and the current blockage amplitude increased with the increase in the length of the peptide (Figure 2.2). As shown in Figure 2.3, statistical analysis from the current traces showed that with an increase in the peptide length, the blockage amplitudes increased from 8.3 ± 0.6 pA (for peptide WW) to 36.3 ± 0.6 pA (for peptide YF-11), whereas the mean durations of events dramatically increased from 0.27 ± 0.02 ms (WW) to 143 ± 8 ms (YF-11).

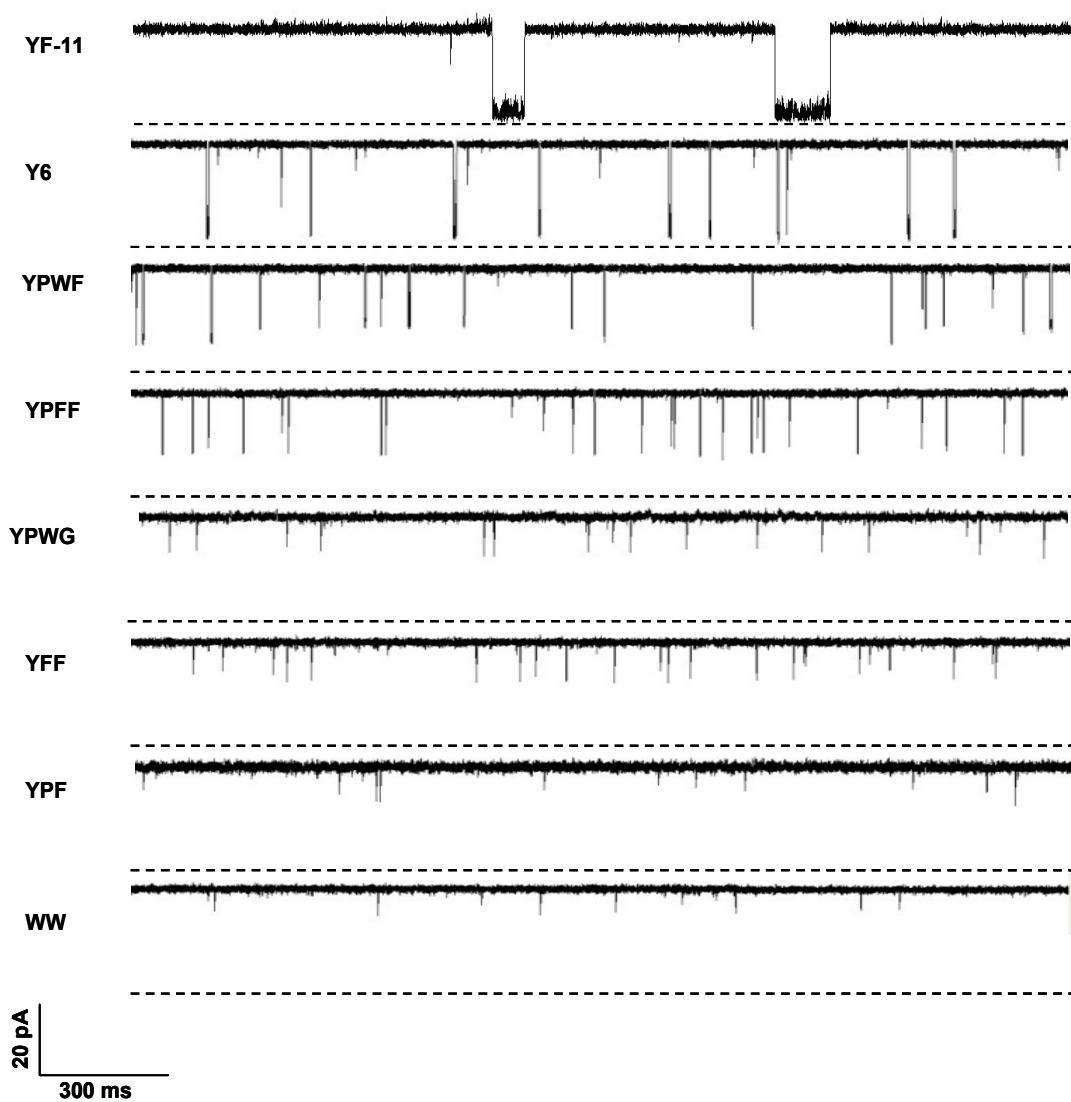


Figure 2.2 Representative single-channel traces showing the effect of peptide length and structure on the transport of peptides through a single (M113Y)₇ pore.

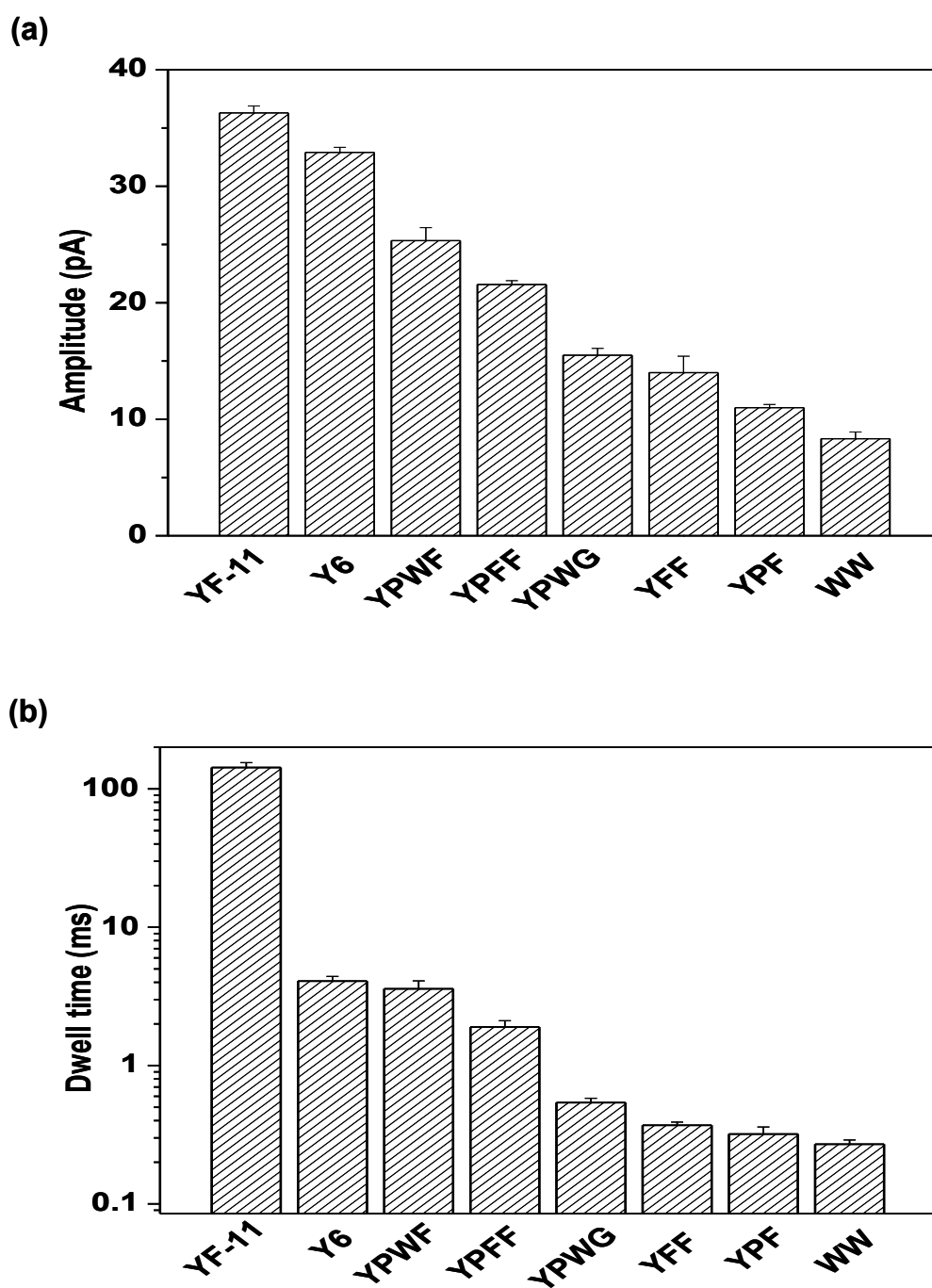


Figure 2.3 Effect of peptide length and structure on the transport of peptides through a single (M113Y)₇ pore. (a) Current blockage amplitudes; and (b) Event mean dwell times.

As a result, the dissociation rate constants k_{off} decreased by 522 fold (from $3.67 \pm 0.22 \times 10^3 \text{ s}^{-1}$ to $7.02 \pm 0.38 \text{ s}^{-1}$) (Table 2.2). In contrast, the association rate constants k_{on} decreased by 17.7 fold (from $2.04 \pm 0.14 \times 10^6 \text{ M}^{-1}\cdot\text{s}^{-1}$ to $1.15 \pm 0.08 \times 10^5 \text{ M}^{-1}\cdot\text{s}^{-1}$). Note that the values of k_{on} for dipeptides, tripeptides, and tetrapeptides did not differ significantly, but then decreased rapidly with the increase in the peptide length. This finding is not unreasonable considering that long peptides diffuse more slowly than short peptides. Furthermore, with the increase of the peptide length, it will be more difficult for long peptides to enter the pore from the bulk solution due to a larger steric effect. It is clear that the overall reaction formation constants $K_f (= k_{\text{on}}/k_{\text{off}})$, and hence the binding affinities of various peptides to the (M113Y)₇ protein pore, are largely dependent upon the dissociation rate constants rather than association rate constants (Table 2.2). It should be noted that, the translocation times of YFF, YPF, and WW derived in this experiment were too short to be adequately resolved at the currently used filtering frequency of 5 KHz. However, these dwell time and amplitude values (which were uncorrected for missed peptide events) might be useful for qualitative determination of the relationship between the event signature and peptide length.⁹⁴

Table 2.2 Kinetic and thermodynamic constants of the non-covalent interactions between various peptides and the (M113F)₇ pore.

Peptide	k _{off}	std	k _{on}	std	K _f	std
KF	7.02	0.38	1.15·10 ⁵	807.47	16420.86	865.61
Y6	246.18	19.34	1.34·10 ⁶	1.65·10 ⁵	5522.94	1146.26
YPWF	282.84	40.10	5.93·10 ⁶	7.00·10 ⁵	21507.23	5328.14
YPPF	531.36	60.71	7.60·10 ⁶	1.32·10 ⁶	14290.30	1980.10
YPWG	1850.44	154.07	4.54·10 ⁶	8.48·10 ⁵	2467.62	489.10
YFF	2690.91	163.29	6.37·10 ⁶	3.21·10 ⁵	2375.73	263.65
YPF	3149.27	435.24	2.29·10 ⁶	1.06·10 ⁵	732.63	63.10
WW	3661.14	218.83	2.04·10 ⁶	8.18·10 ⁴	557.28	10.95

In addition to the length of the peptide, our experimental results demonstrated that the composition of the peptide would also affect the event dwell time and amplitude. For example, the dwell time and amplitude of YPWF were 3.59 ± 0.51 ms, 25.3 ± 1.1 pA, respectively, while those of YPWG were 0.54 ± 0.04 ms, 15.5 ± 0.6 pA, respectively. As a result, the formation constant increased by 8.7 fold (from $2.47 \pm 0.49 \times 10^3 \text{ M}^{-1}$ to $2.15 \pm 0.53 \times 10^4 \text{ M}^{-1}$) when YPWF was tested instead of YPWG. Note that these two peptides differed by only one amino acid. Since the (M113Y)₇ protein pore used in the experiment contains an aromatic binding site, it is not unreasonable that the aromatic amino acids in a peptide have stronger binding affinities to the pore than other types of amino acids (e.g., hydrophobic and charged), thus contributing more to the overall event dwell times and amplitudes. Take peptides YPWF and YPWG for example, Tyr (Y), Trp (W), and Phe (F) are aromatic amino acids and hence are primarily responsible for the produced event

signatures in the (M113Y)₇ pore, while Pro (P) and Gly (G) played smaller roles. Since YPWF has more aromatic amino acids than YPWG, YPWF produced a larger event dwell time and blocking amplitude. Similarly, in the case of YPF and YFF, since F is an aromatic amino acid, while P is a hydrophobic residue, YFF would have a higher binding affinity to the (M113Y)₇ protein pore than YPF. This hypothesis is confirmed by our experiment result, where the formation constant ($2.38 \pm 0.26 \times 10^3 \text{ M}^{-1}$) of YFF was 3.2 fold larger than of YPF ($7.33 \pm 0.63 \times 10^2 \text{ M}^{-1}$). Further experiment showed that the W component in a peptide causes a stronger aromatic interaction with (M113Y)₇ pore than the F amino acid, as the observed formation constant for YPWF ($2.15 \pm 0.53 \times 10^4 \text{ M}^{-1}$) was 1.5 fold larger than that of YPFF ($1.43 \pm 0.20 \times 10^4 \text{ M}^{-1}$). This difference in the binding strength may be attributed to the change in the van der Waals volumes of amino acids ($V_W (227.8 \text{ \AA}^3) > V_F (189.9 \text{ \AA}^3)$).⁹⁵ The observation is similar to those made for the binding of 2, 4, 6-trinitrotoluene to the aromatic amino acid side chains in the (M113F)₇ and (M113W)₇ pores, in which donor-acceptor aromatic interactions occurred.²³ The combined results suggest that it is possible to estimate the binding affinity of the biomolecule to a specific nanopore from the composition and the structure of the amino acids present in a peptide.

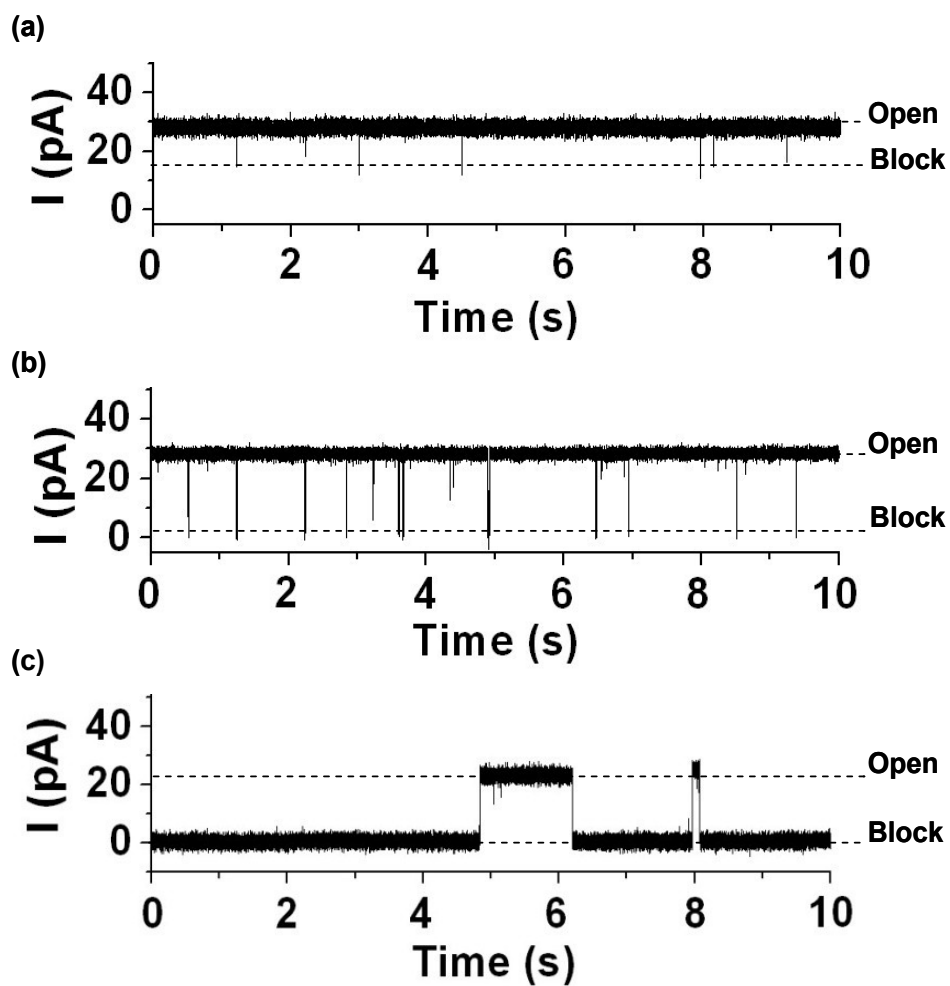


Figure 2.4 Effect of structure of protein pores on peptide translocation. Typical single-channel recording traces: (a) $(WT)_7$, (b) $(M113F)_7$, and (c) $(2FN)_7$, showing the interaction between peptide Y6 and three different protein pores.

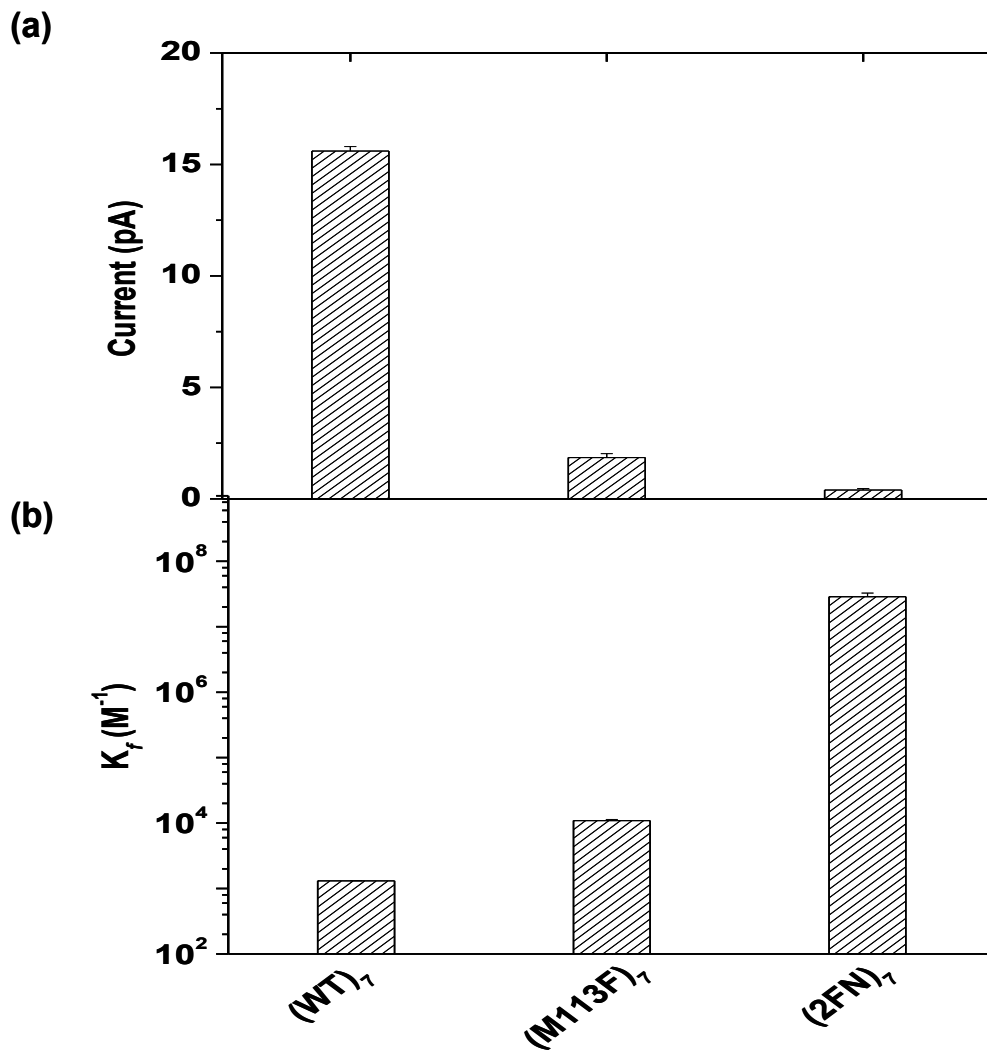


Figure 2.5 The interaction between peptide Y6 and three different protein pores; (a) event residual currents; and (b) formation constants

To evaluate the effect of genetically engineered protein pores on peptide translocation, three α HL pores, including wild type (WT)₇, as well as mutants (M113F)₇ and (2FN)₇ (Figure 2.1) were used. Figures 2.4 and 2.5 shows the electrical recording traces as well as residual current and mean dwell time plots for

peptide Y6 in the three pores. Y6 produced short duration and small current blockage events in the (WT)₇ α HL protein (Figure 2.4), probably due to the weak hydrophobic interactions occurred between the peptide and the pore. In contrast, with the introduction of aromatic side chains into the lumen of the (WT)₇ α HL protein at positions 113 and 145, longer dwell time and larger current blockage events were observed for Y6 in the (M113F)₇ and (2FN)₇ pores. The event residual currents obtained for (WT)₇, (M113F)₇, and (2FN)₇ were 15.6 ± 0.2 pA (i.e. 48% of channel block), 1.8 ± 0.2 pA (94% of channel block), and 0.4 ± 0.1 pA (98% of channel block), respectively. Due to the additional aromatic interactions, the formation constants of Y6 with the (M113F)₇ and (2FN)₇ pores, i.e., $1.09 \pm 0.05 \times 10^4$ M⁻¹ and $2.87 \pm 0.40 \times 10^7$ M⁻¹, respectively, were 8.3 fold and 2.19×10^4 fold larger than that of Y6 in the (WT)₇ pore ($1.3 \pm 0.1 \times 10^3$ M⁻¹). Similar phenomena were also found in the experiments with the peptide YFF in the (WT)₇, (M113F)₇, and (2FN)₇ pores (Figure 2.6). It should be noted that, since the peptide YFF bound to the (WT)₇ pore much more weakly than Y6, YFF did not produce observable current modulation events in the (WT)₇ protein. In contrast, YFF events were observed in both the mutant (M113F)₇ and (2FN)₇ pores due to the aromatic interactions occurred. Furthermore, the current blockage amplitude, event frequency, and dwell time were larger in the (2FN)₇ pore than those in the (M113F)₇ pore. These results suggest that the functional groups engineered inside a protein pore are responsible for the affinities between peptide and protein, thus predominantly determining the sensitivity and the resolution of stochastic nanopore detection. Thus, it is possible to rationally design site-specific protein pores with a variety of non-covalent bonding sites to detect various target analytes.

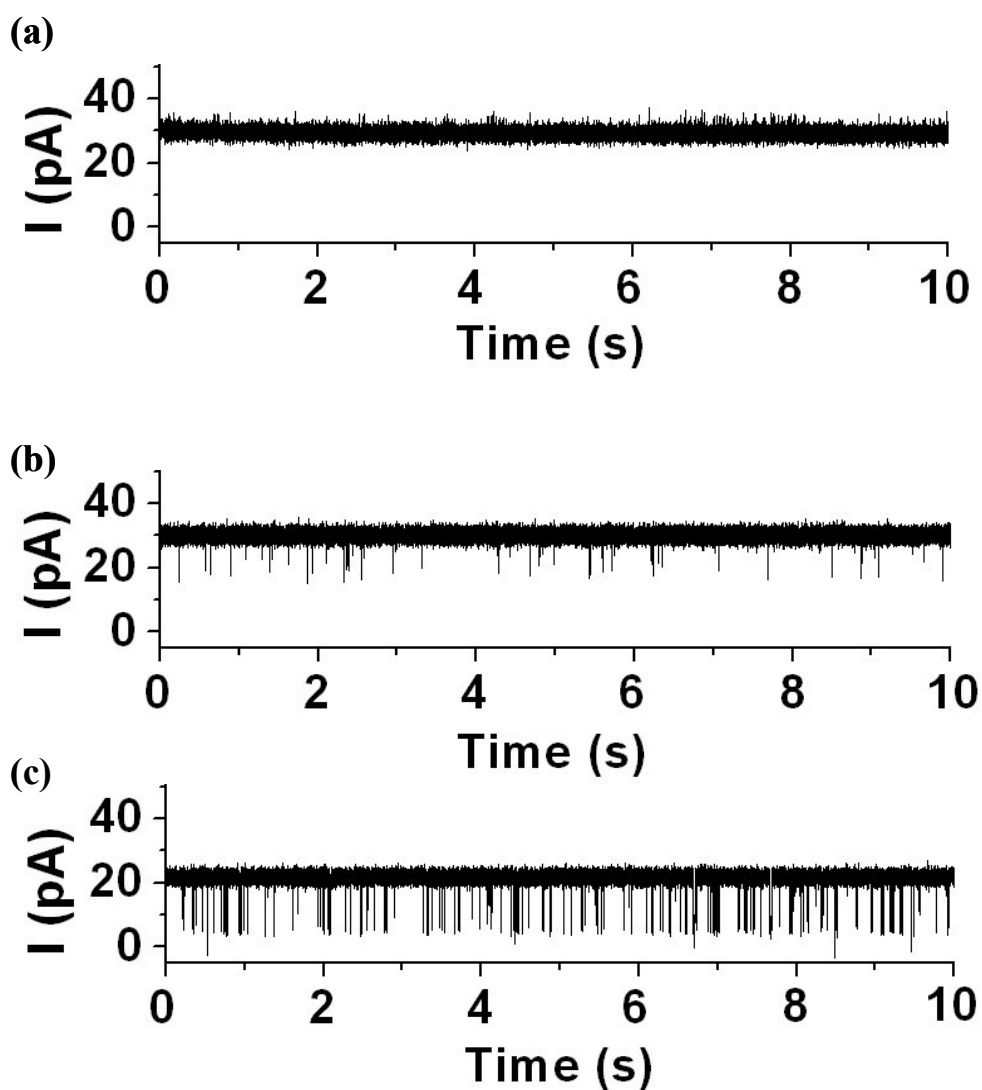


Figure 2.6 Representative single-channel recordings, showing the effect of engineered protein pores on the peptide transport. (a) $(WT)_7$; (b) $(M113F)_7$; and (c) $(2FN)_7$.

As discussed above, the sensitivity for the detection of a target peptide can be improved by the introduction of functional groups inside the lumen of a protein channel. However, it is still unclear how the side chain change and/or the conformational change in a protein channel kinetically affect the solvent flow and the

diffusion of target molecules upon application of a transmembrane field. To address this issue, the charge selectivities or permeability ratios ($P_{\text{Na}^+}/P_{\text{Cl}^-}$) of the above-mentioned protein pores have been examined. It should be noted that, charge selectivity of a protein pore is largely dependent upon the dimension of the pore and the spatial distribution of charges at the entrance to and within the lumen of the channel.⁹⁶ It was found that the charge selectivities for (WT)₇, (M113F)₇, and (2FN)₇ were 0.80 ± 0.02 , 0.74 ± 0.03 , and 0.64 ± 0.01 , respectively (Table 2.3). These results suggest that all the protein pores used in our experiments are anion selective so that they preferentially allow the anions to pass by the pores. It can be seen that the ion selectivities of (M113F)₇ and (2FN)₇ pores decreased by 7.5% , and 20.0%, respectively, compared to that of the unmodified WT α HL pore. It should be mentioned that the lower the $P_{\text{Na}^+}/P_{\text{Cl}^-}$ value, the higher the anion selectivity and the narrower the protein pore.^{88, 97} In this case, a decreased transport of analytes and water coupled with ions is responsible for a larger mean residence time inside the pores.^{93, 98} It is well known that in the WT α HL pore, the narrowest diameter in the constriction area is ~ 14 Å near Met-113,¹¹ excluding Debye length (~ 3.7 Å, in 1M NaCl buffer) close to the wall of the channel.⁶³ It is not unreasonable that the structure modification of the α HL pore may alter the size of its constriction area, thus resulting in a change in the ion selectivity, since the van der Waals volumes^{59,95} of the amino acid residues lining the lumen of the α HL pores are in the order of $V_{(\text{WT})_7} < V_{(\text{M113F})_7} < V_{(\text{2FN})_7}$. This interpretation can be further supported by the single channel recording experiments, where the open channel conductance values obtained for the proteins (M113F)₇ (710 ± 9 pS) and (2FN)₇ (558 ± 16 pS) were decreased by 5.3% and by 25.6%, respectively, compared with that of the (WT)₇ pore (750 ± 12 pS). The decreased percentages in the open channel conductances are in

agreement with the changes in the ion selectivities of three protein channels. Therefore, our results demonstrate that the property (e.g., channel conductance and the charge selectivity) of a protein pore as well as the binding affinity of a peptide to the pore can be altered by modifying the side chains along the entrance or the lumen of the constriction area in a predictable manner.

Table 2.3 Charge selectivities of α HL pores. Single-channel currents were recorded under asymmetric conditions: 1 M NaCl, 10 mM Tris-HCl (pH 7.5) (*cis*), and 0.2 M NaCl, 10 mM Tris-HCl (pH 7.5) (*trans*).

α HL Proteins	V_r /mV	P_+/P_-
(WT) ₇	-3.69 ± 0.44	0.80 ± 0.02
(M113F) ₇	4.75 ± 0.35	0.74 ± 0.03
(2FN) ₇	7.31 ± 0.31	0.64 ± 0.01

2.3.2 Effects of peptide concentration and applied voltage on the binding kinetics

Our experiments with the peptide YFF in two different protein pores (Figure 2.7) showed that the mean dwell times of YFF in a specific protein pore were almost unchanged with an increase in the peptide concentration. This suggests that the binding affinity occurring in a protein pore is specific for a particular peptide in favor of the noncovalent interactions, in such a way that the identity of the peptide could be distinguished. The experimental results (Figure 2.8) demonstrated that the event frequency ($1/\tau_{on}$) was linearly related to the concentration of the peptide, thus providing a basis for quantifying these biomolecules. Further, the voltage dependence of the peptide in the (M113F)₇ pore regarding the residence

time and binding frequency was also investigated, and we found that the voltage effect was not significant (Figures 2.6c and 2.6d). This suggests that the binding frequency for aromatic-aromatic interactions is largely dependent on the dose response, rather than on voltage effect due to no net charge posed onto the peptide chain or the protein pore. However, the mean duration value for YFF in the (2FN)₇ protein pore slightly decreased with an increase in the applied potential. We attribute this observation to the rather different nature of the protein pores that work as selective filters, which give rise to different kinetic solvent flow associated with voltage-dependent electrophoresis through the pores.⁹⁹ In our case, the pore (2FN)₇ has a smaller constriction area and a higher anion selectivity than the (M113F)₇ protein, resulting in a solvent flow toward the binding site that would be enhanced and quickly weakened by flow away from it under a high voltage. However, in a larger pore like (M113F)₇, the electroosmotic solvent is hardly influenced because of the relatively symmetric transport arisen from the weak binding interactions, despite the asymmetric channel potential and analyte diffusion. This consideration is in accordance with the situation that the single molecule is bound by the binding site, thus its escape is faster to the closest side.⁹²

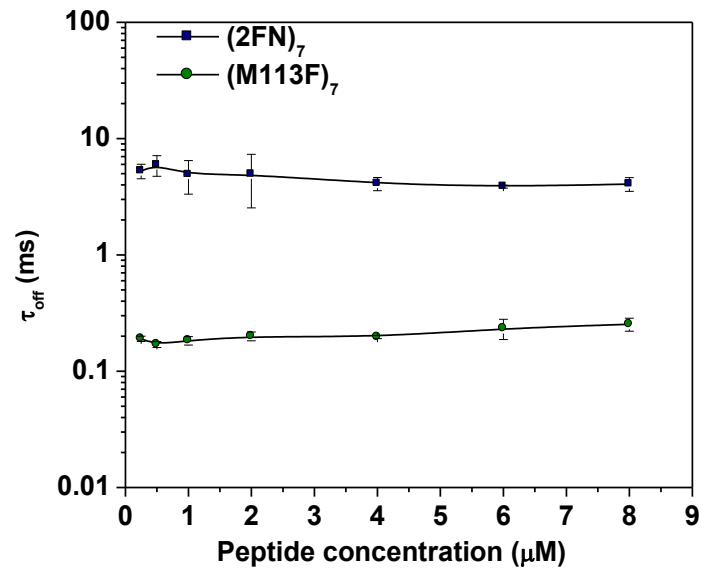


Figure 2.7 The effect of peptide concentration on the residence time of binding events.

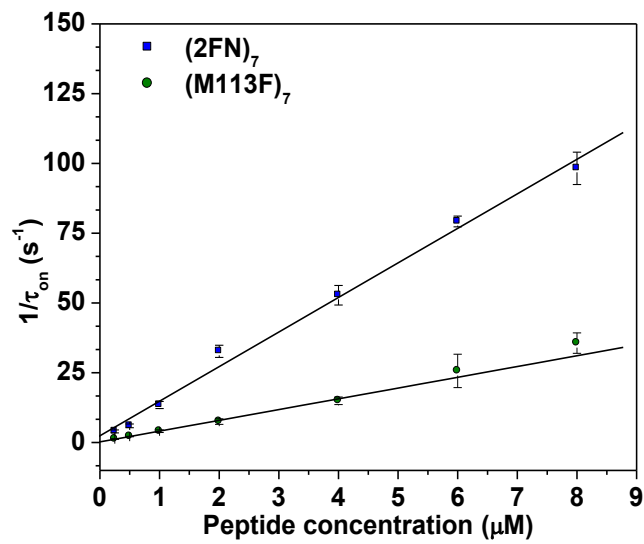


Figure 2.8 The effect of peptide concentration on the frequency of binding events.

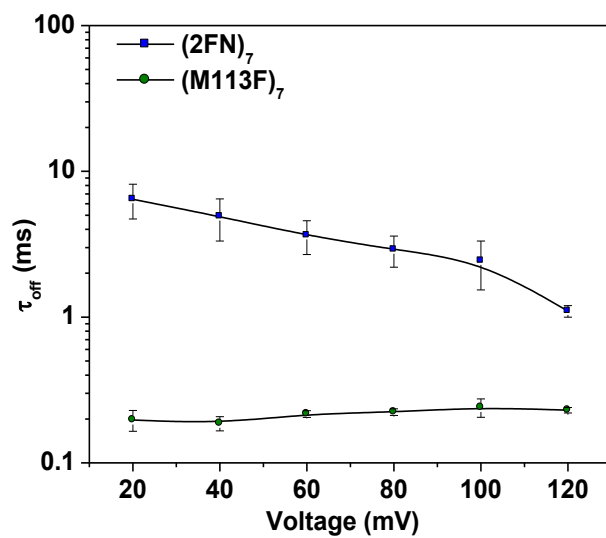


Figure 2.9 The effect of the applied voltage on the residence time of binding events.

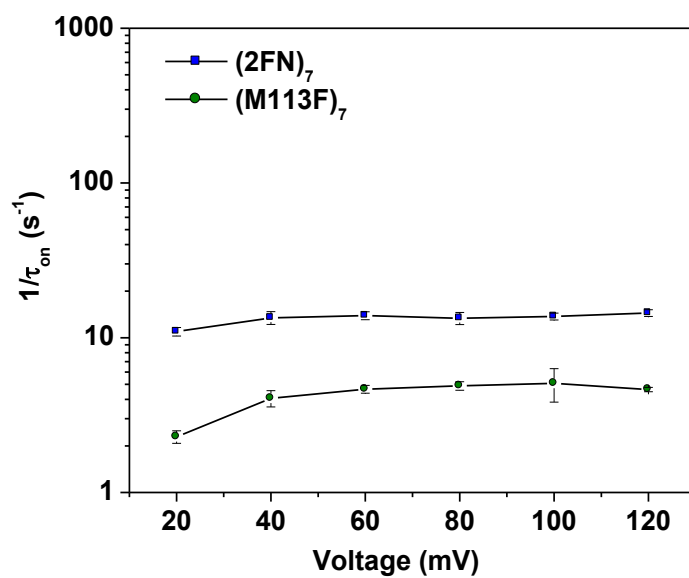


Figure 2.10 The effect of the applied voltage on the frequency of binding events.

2.3.3 Application of peptide-protein pore interaction for peptide detection

Our experimental results demonstrate that the resolution and the sensitivity for peptide detection could be significantly improved by using the protein pore with a properly engineered binding site(s). Furthermore, the length and the structure of peptides would affect their translocation in the modified protein pore. Thus, different peptides, including those differing by a single amino acid, might show different characteristic “fingerprints” (represented by event dwell time and/or amplitude), and hence could be differentiated (Figures 2.2 and 2.3). To explore the feasibility of utilizing a single pore for the detection of a target peptide or even simultaneous quantification of multiple peptide components, as present in complex biological systems, a series of experiments was performed using the (M113F)₇ pore. Note that the availability of a high-throughput method for multi-analyte detection would have enormous implications in fields such as proteomics, genomics, and metabolomics. As shown in Figure 2.11a, when only peptide Y6 was present in the solution, a major amplitude peak at 2.7 ± 0.1 pA appeared in the amplitude histogram. When the peptides YPFW, YWPF, and YPWG were further added to the same solution, one by one, their characteristic amplitude peaks could be observed at 14.1 ± 0.1 pA, 21.0 ± 0.1 pA, and 25.6 ± 0.1 pA, respectively (Figures 2.7b-2.7d). Furthermore, we found that the mean dwell time for each peptide in the mixture was in agreement with that of the individual peptide standard alone (e.g., 1.19 ± 0.08 ms for a solution containing a single YPFW standard, and 1.25 ± 0.13 ms for YPFW present in the mixture). Thus, the identity of a particular peptide component in the mixture can be inferred from the mean residence time and/or amplitude of a single peptide standard (Figure 2.3).

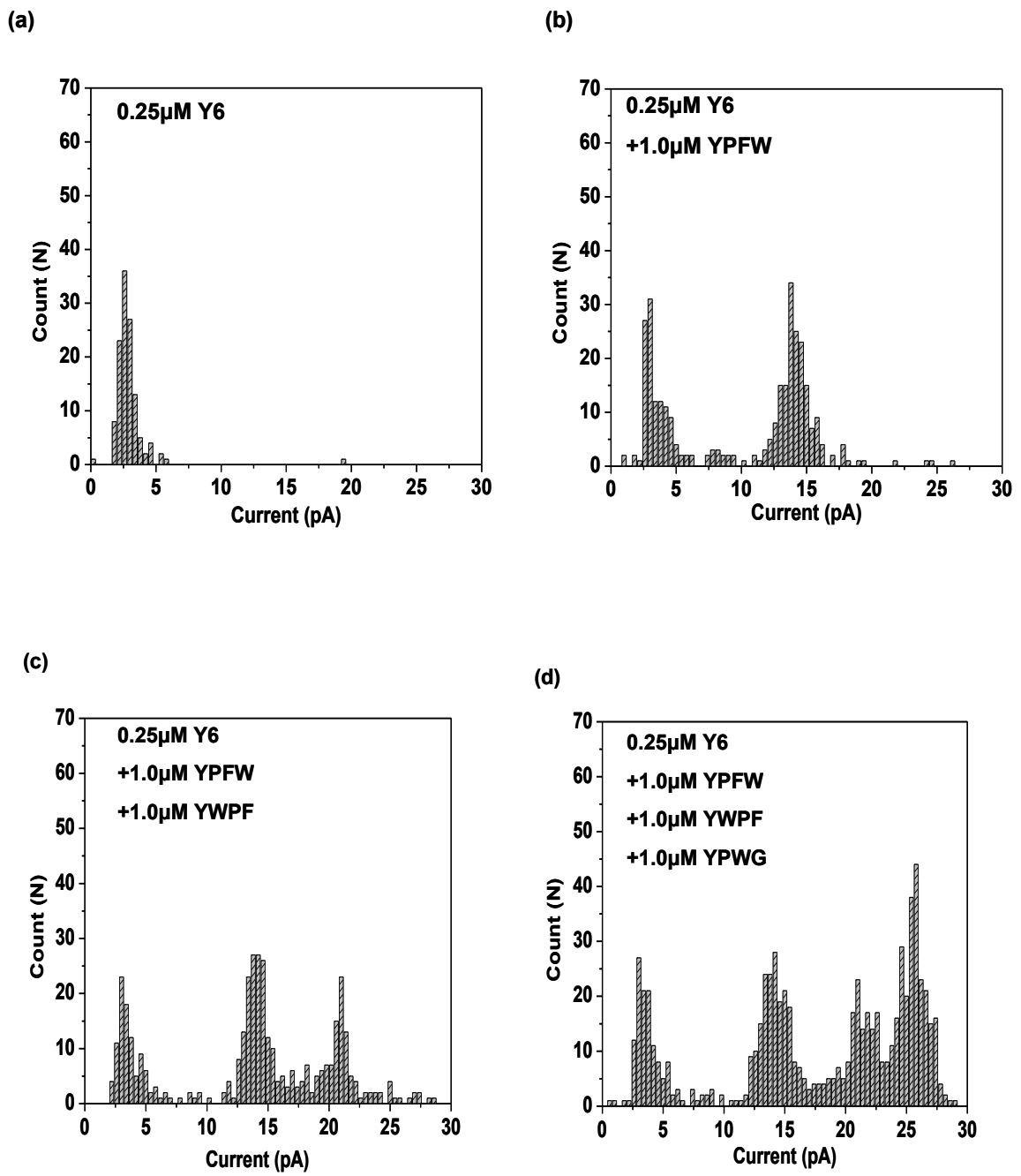


Figure 2.11 Simultaneous detection of a mixture of peptides.

Event histograms of (a) peptide Y6; (b) a two-peptide mixture containing Y6 and YPFW; (c) a mixture of three peptides containing Y6, YPFW and YWPF; (d) a mixture of four peptides containing Y6, YPFW, YWPF and YPWG.

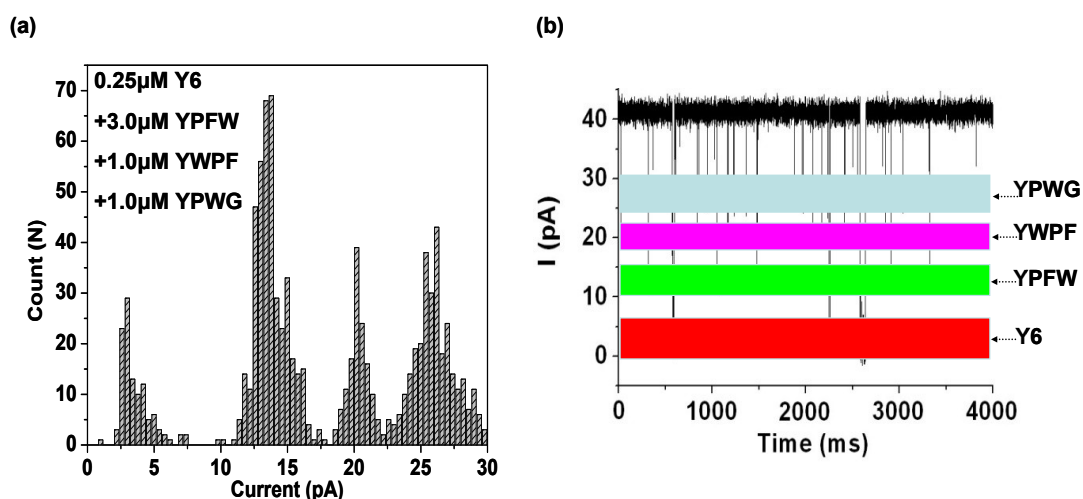


Figure 2.12 (a) a mixture of Y6, YPFW, YWPF and YPWG, where the concentration of YPFW was three times larger than that of (2.9d); and (b) the corresponding representative single-channel current trace of (2.9d), in which the individual Y6, YPFW, YWPF and YPWG events were arrow-marked at different levels.

In addition to identifying multiple peptides by using a single mutant pore, the concentration of each peptide component in the mixture can also be simultaneously quantified. It should be noted that, the overall frequency of all the current blockage events produced by a mixture of peptides is the sum of the frequencies of each individual component peptide. For example, the overall event frequency $f_{(T)}$ of a four-peptide mixture (containing Y6, YPFW, YWPF, and YPWG) can be expressed as follows:

$$f_{(T)} = f_{(1)} + f_{(2)} + f_{(3)} + f_{(4)}$$

where $f_{(1)}$, $f_{(2)}$, $f_{(3)}$, and $f_{(4)}$ are the event frequencies for each individual peptide Y6, YPFW, YWPF, and YPWG, respectively. As shown in Figures 2.7d and 2.7f, the

value of $f_{(1)}$ could be calculated from the event dwell time $\tau_{on(1)}$ using the equation: $f_{(1)} = 1/\tau_{on(1)}$, where $\tau_{on(1)}$ could be obtained from the event dwell time histogram which is consisted of events only with residual currents less than 7.0 pA. To obtain $f_{(2)}$, we need to first select and analyze the events with residual currents less than 17 pA to obtain the event mean interval duration ($\tau_{on(1,2)}$) and frequency ($f_{(1,2)}$) for Y6 and YPFW. Then, $f_{(2)}$ could be calculated by using the equation $f_{(2)} = f_{(1,2)} - f_{(1)}$. Similarly, event frequencies for YWPF, and YPWG, i.e., $f_{(3)}$, and $f_{(4)}$, can be sequentially obtained. Our experiments showed that the presence of other peptides in the sample solution would not affect the event frequency of a target peptide significantly. For example, the event frequency of a single peptide Y6 standard at a concentration of 0.25 μM was $0.73 \pm 0.06 \text{ s}^{-1}$, while that of Y6 in the four-peptide mixture $0.71 \pm 0.18 \text{ s}^{-1}$. Furthermore, in the case that the concentration of YPFW was increased from 1 μM to 3 μM (Figure 2.11d and 2.12a), we found that its experimental event frequency increased $297 \pm 16 \%$. This suggests that the concentration of a particular peptide component in the mixture can be inferred from the dose response curve of a single peptide standard (Figure 2.8).

Another significant example is that the effect of structure of proteins as well as the effect of peptide length and structure on peptide-protein interaction could be employed to fine tune the sensitivity of nanopore sensor. As shown in Figures 2.8a-2.8c, both peptides YFF and YPF produced events with a wide range of amplitudes in the (M113F)₇ pore, and could not be simultaneously detected since their events were overlapped. In order to detect such short peptides simultaneously, mutant protein pores with a much stronger binding affinity to the peptides than the (M113F)₇ protein should be employed. Under identical experimental conditions, the events of these

two peptides (YFF and YPF) were distributed in a much narrow region in the (2FN)₇ protein pore due to the significantly enhanced binding interactions between the peptides and the pore. Their events showed distinct well-defined current blockage peaks at 6.6 ± 0.1 pA, and 10.4 ± 0.1 pA, respectively, thus permitting the two-peptide mixture (YFF and YPF) to be simultaneously detected (Figures 2.8d-2.8e). It could be visualized that, different protein pores should be used in the analysis of peptides with various lengths. In general, wild type α HL could be used for the detection of long peptides, while the single mutant protein pore (such as (M113F)₇) would be more appropriate for the quantification of relatively shorter peptides (Figures 2.2 and 2.5). If long aromatic peptides (e.g., much longer than 12-mer) are analyzed with the (M113F)₇ pore, all of them will produce events with quite large dwell time and almost full current block, and hence will be extremely difficult to be differentiated. In terms of very short peptides, specifically designed multiple mutants should be used instead.

An important finding of the peptide-protein interaction is that an appropriately engineered protein pore could be used to discriminate peptide sequences, thus offering the potential for peptide or protein sequencing. As shown in Figure 2.15a, the blockage residual currents for peptides PYWF, YPWF, YWPF, and YPFW in the (M113F)₇ pore are -14.7 ± 0.5 pA, -13.9 ± 0.1 pA, -11.8 ± 0.4 pA, and -9.7 ± 0.2 pA, respectively, at an applied potential of -40 mV. The mean dwell times for the above mentioned peptides were 0.69 ± 0.09 ms, 0.57 ± 0.02 ms, 0.82 ± 0.02 ms, and 1.19 ± 0.08 ms, respectively (Figure 2.15b). Thus, the four peptides with the same length and composition but different sequences could be differentiated from their quite different current signatures.

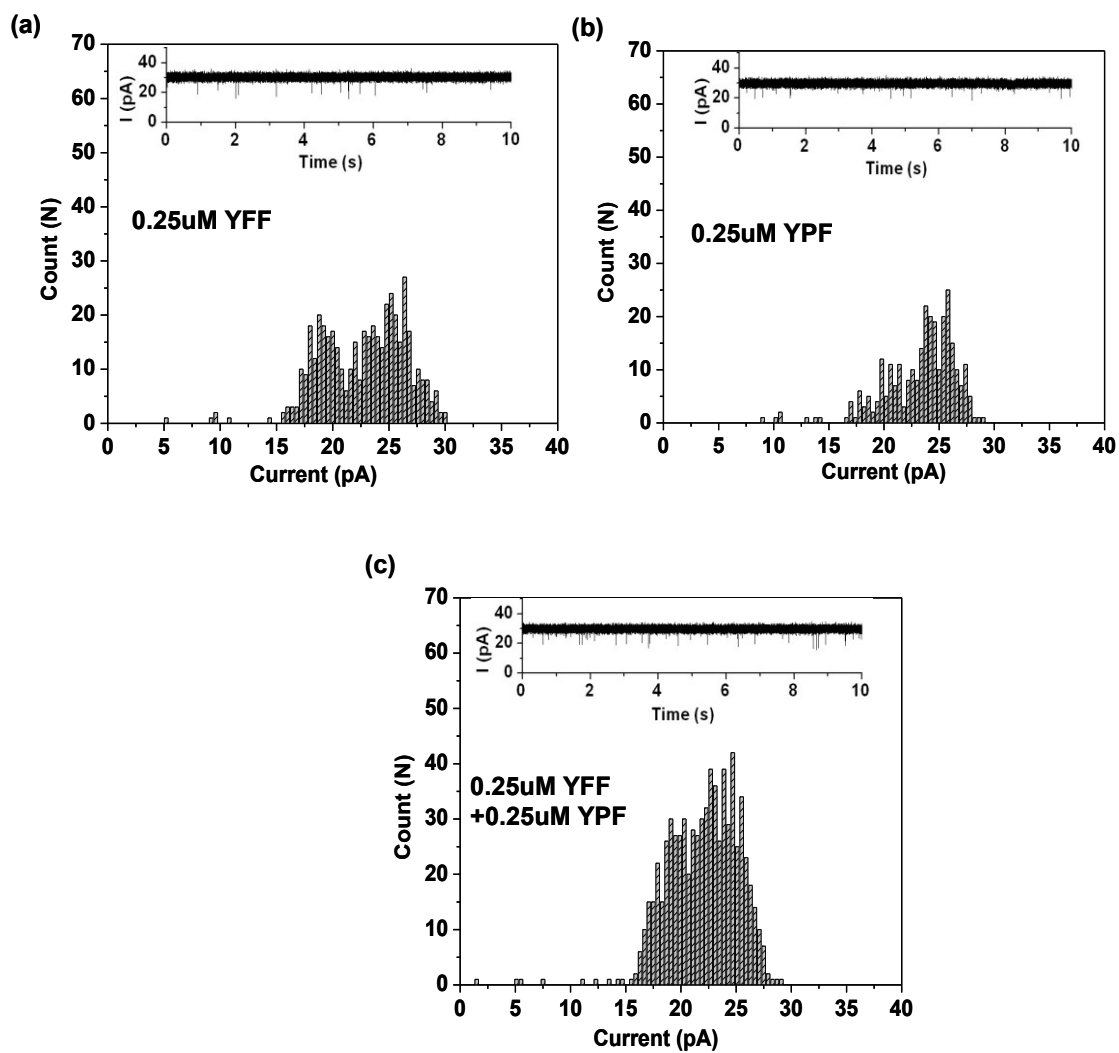


Figure 2.13 Simultaneous detection of a two-peptide mixture in the $(M113F)_7$ pore. Event histograms of (a) YFF, (b) YPF, and (c) a mixture of YFF and YPF.

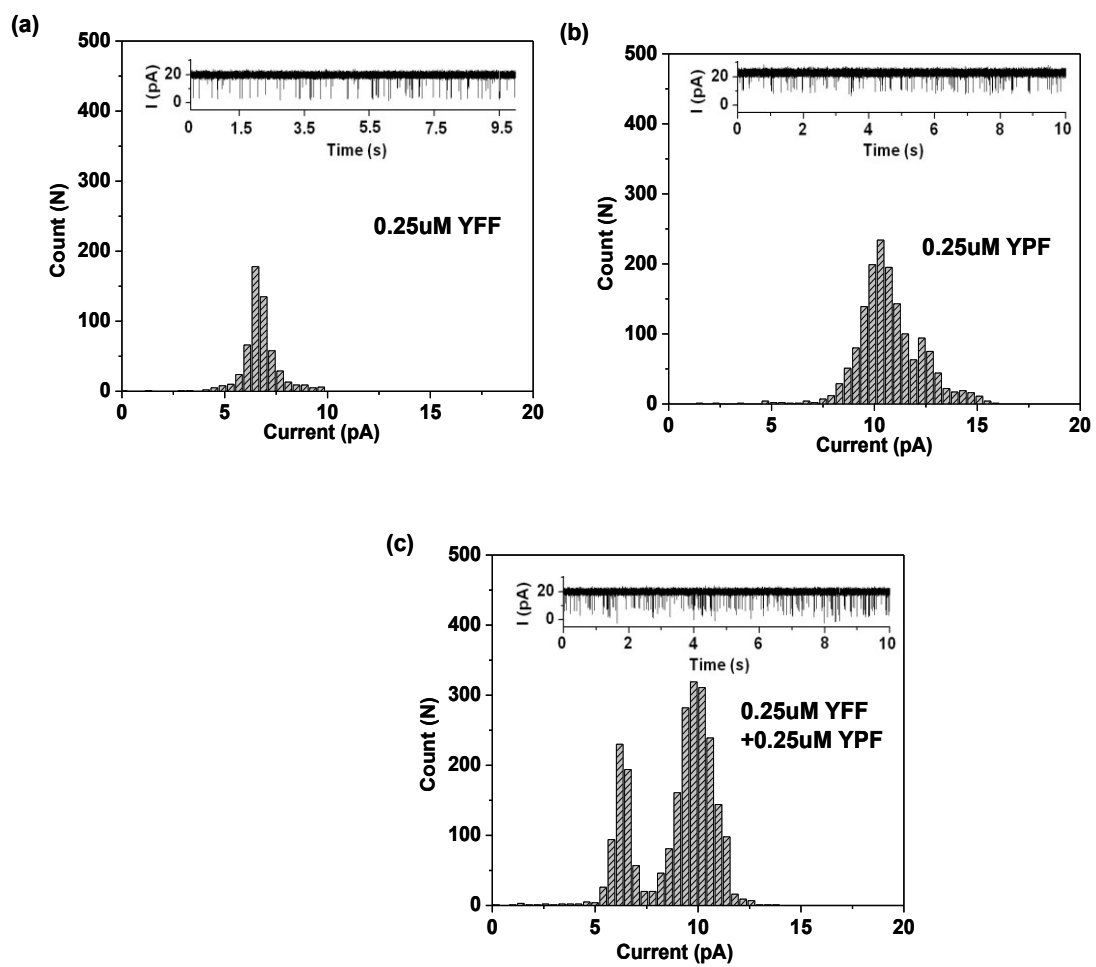


Figure 2.14 Simultaneous detection of a two-peptide mixture in the $(2FN)_7$ pore. Event histograms of (a) YFF, (b) YPF, and (c) a mixture of YFF and YPF.

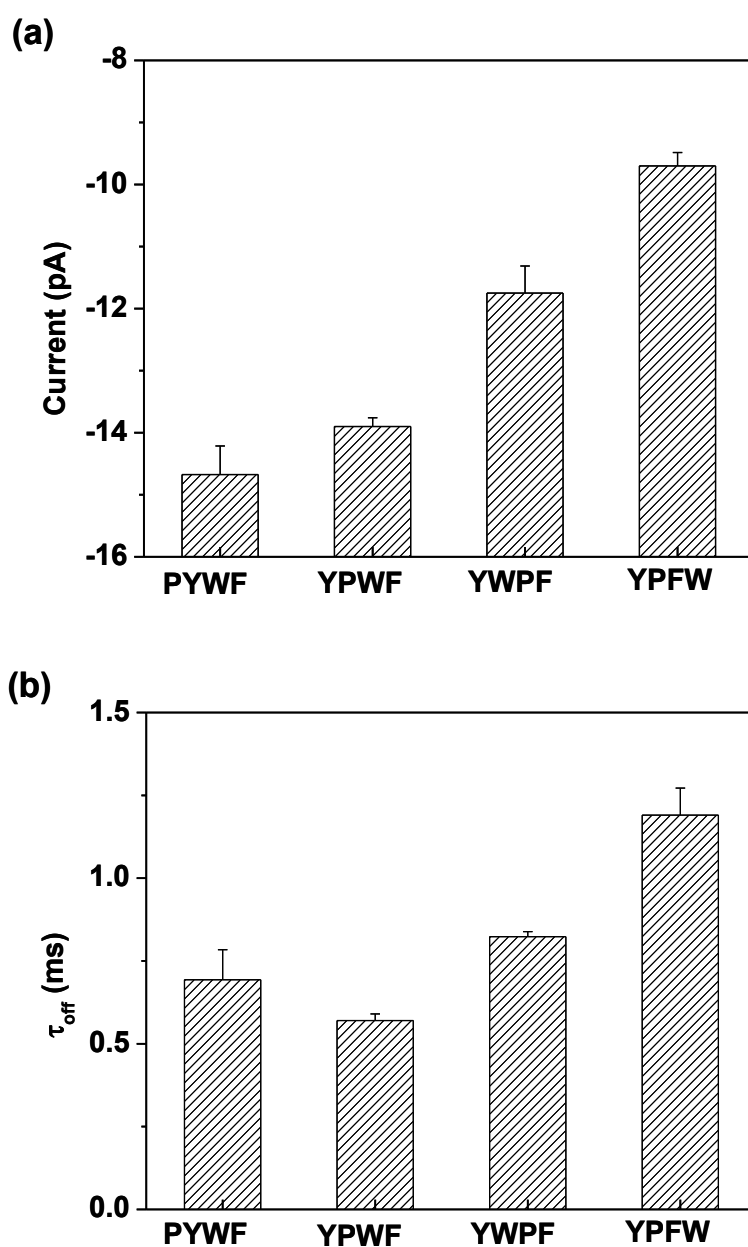


Figure 2.15 Differentiation of peptide sequences. (a) Event residual currents; and (b) Mean dwell times.

+40mV

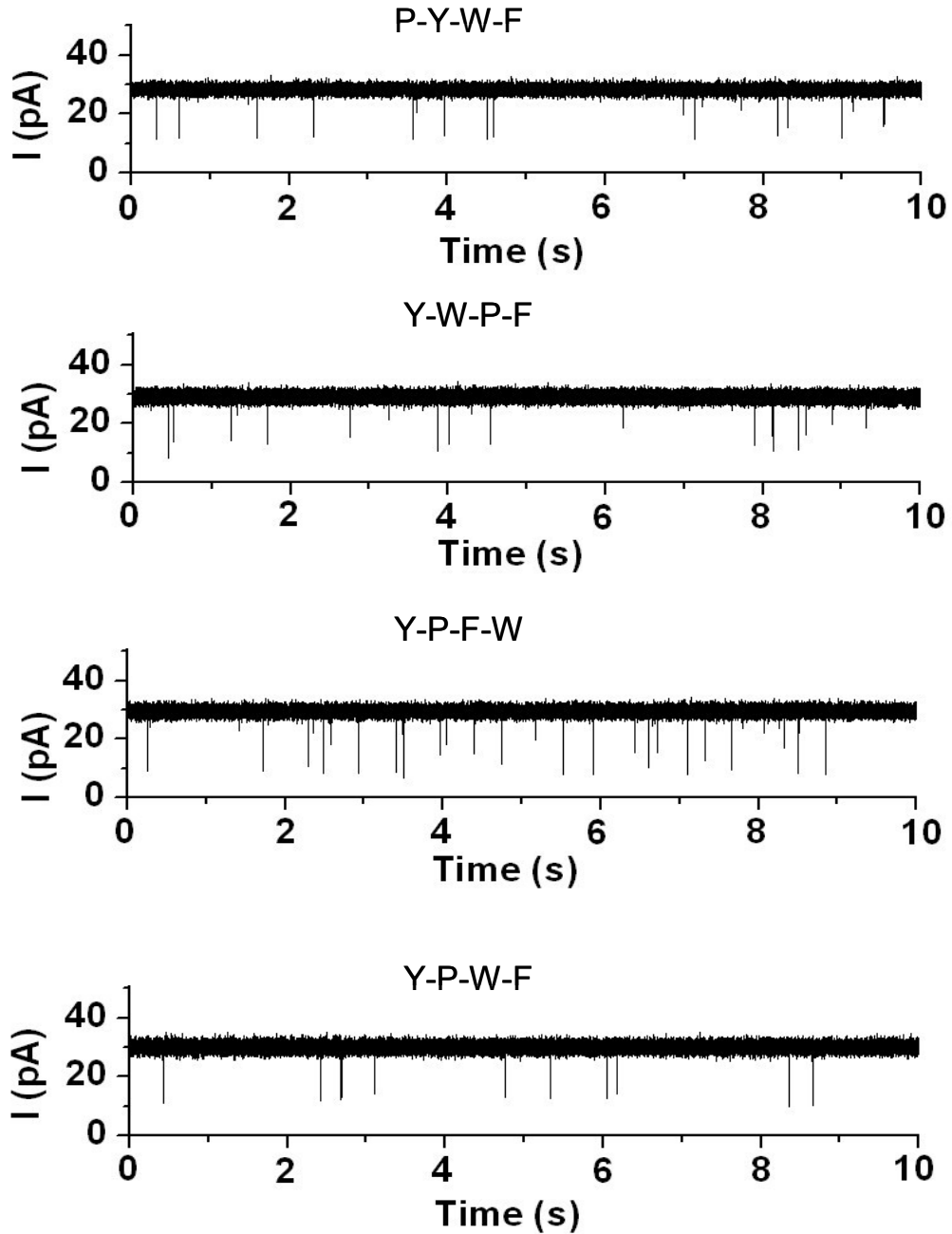


Figure 2.16 Typical single-channel recordings, showing the detection of a series of peptides with the same length and amino acid composition but different sequences in positive voltage bias.

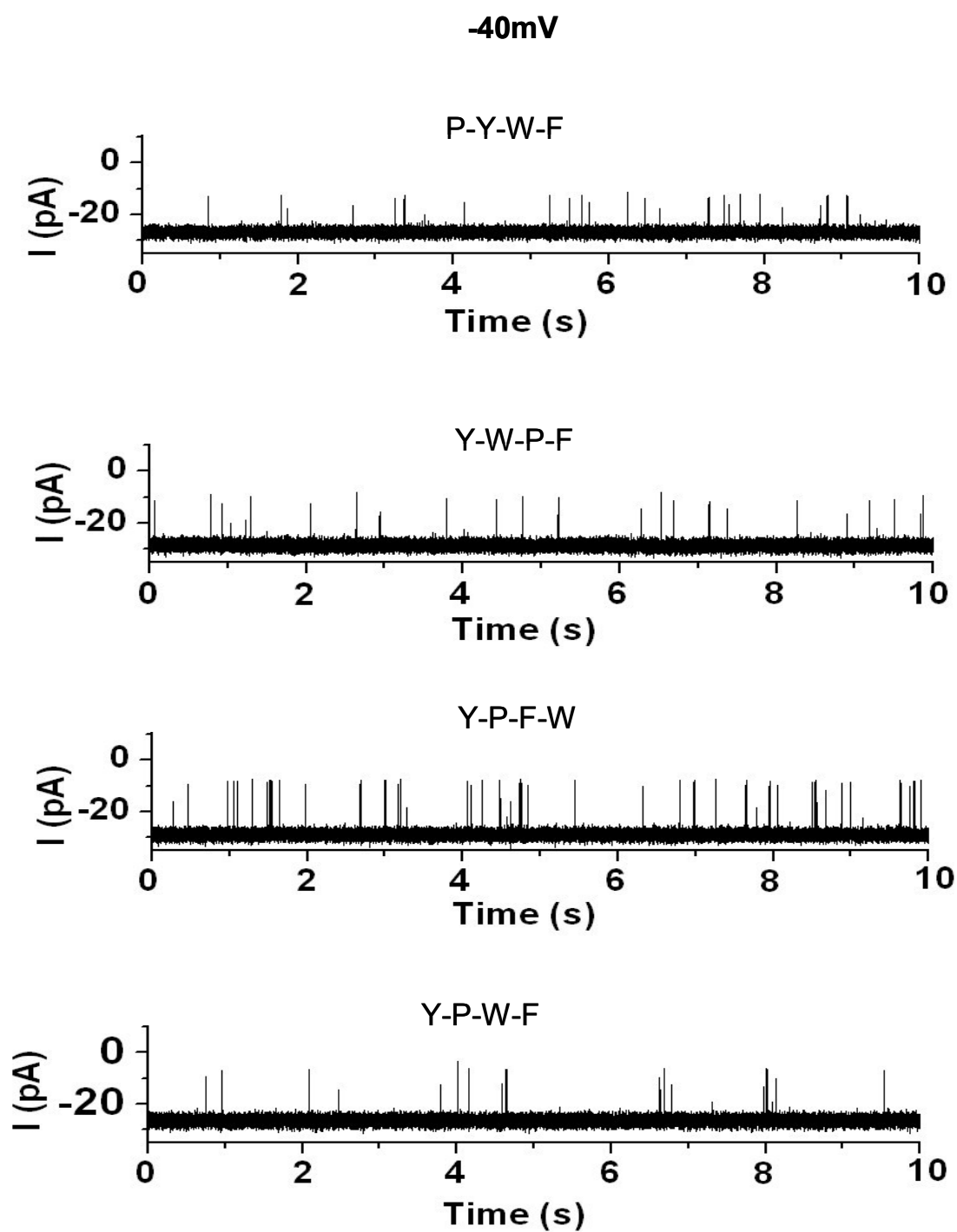


Figure 2.17 Typical single-channel recordings, showing the detection of a series of peptides with the same length and amino acid composition but different sequences in negative voltage bias.

2.4 Conclusions

In this work, we systematically investigated the translocation of aromatic, short oligopeptides through protein pores. With more aromatic binding sites engineered inside the lumen of the protein pore, a decrease in the open channel conductance and a decrease in the permeability ratio ($P_{\text{Na}^+}/P_{\text{Cl}^-}$) were observed. This leads to a stronger binding affinity between peptides and the pore, and hence an improved sensitivity of the nanopore stochastic sensor. Thus, modification of protein pores with a variety of new functional groups offers the potential to significantly prolong the translocation of peptides through the protein channels, enabling us to obtain more detailed structure and kinetic information involving molecular transport. The effect of structure and length of the peptides, as well as the nature of the protein pore could be employed to design effective sensors for peptides with various lengths. With a properly engineered protein pore, a series of short peptides, including those differing by only an amino acid were successfully differentiated. The feasibility of utilizing the engineered protein pore for simultaneous detection of a mixture of peptides and even differentiation of peptide sequences were further demonstrated.

Given the capability of a properly engineered protein pore to differentiate the sequences of short peptides, this rapid protein pore-based peptide sensing method might offers the potential to be further developed as a novel protein sequencing technique. For example, after cleavage of long peptide or protein molecules into short fragments by enzymatic digestion or chemical cleavage, the peptide/protein fragments can be analyzed with engineered protein pores. Thus, the identities (e.g., structure and sequence) of these short peptides can be determined from their characteristic current signatures in the pore. Indeed these studies are currently in

progress. It should be mentioned that one limitation hindering the application of this method for extended usage is the fragility and the long-term stability of the lipid bilayer. This disadvantage could be overcome by in situ sandwiching a single α HL pore into two agarose gel layers, making a robust and portable single-channel chip,²⁸ or employing a glass nanopore membrane.¹⁰⁰

CHAPTER 3

NANOPORE STOCHASTIC DETECTION OF A LIQUID EXPLOSIVE COMPONENT AND SENSITIZERS USING BOROMYCIN AND AN IONIC LIQUID SUPPORTING ELECTROLYTE

3.1 Introduction

Nanopore stochastic sensing is currently an active research area, as a highly-sensitive, rapid and multi-functional sensing system.¹ This method employs a planar lipid bilayer and single-channel recording. Individual binding events can be detected as current modulations. The genetically engineered versions of α -hemolysin (α HL)¹¹ have been used as stochastic sensing elements for the identification and quantification of a wide variety of substances including: anions,¹⁵ organic molecules,²⁵ explosives,²³ enantiomers,²² proteins,¹⁶ DNA,²⁰ and reactive molecules.²⁶ Nanopore stochastic sensing has shown that divalent metal ions such as Zn(II), Co(II) and Cd(II) could be identified using a mutant α HL pore containing histidine residues.¹³ However, it has not yet been employed to detect monovalent cations and amine type liquid explosives components. In large part this limitation can be attributed to the high salt concentrations employed by the nanopore stochastic sensing methods which are necessary to produce the open channel currents to be monitored. Typically 1 M NaCl or KCl electrolyte solutions are needed for nanopore stochastic sensing and this high background prevents trace amounts of such cations from being detected. Since each analyte produces a characteristic signature, the sensor element itself need not be highly selective and multiple analytes can be quantitated simultaneously using a single sensor element, as long as the sensor itself

can provide enough resolution. Further, the most recent protein nanopore studies have demonstrated that a single α HL pore, in a planar phospholipid bilayer, could be sandwiched between two agarose layers which gel in situ and make a robust and portable single-channel chip, that may be transported, stored, and used repeatedly.²⁸

Due to the recent development of liquid explosives as integral components of some terrorist attacks, interest in their facile detection has escalated. Most of the time, liquid explosives are binary mixtures where either one or both components are liquids.¹⁰¹ Since the two individual components alone are nonexplosives, they can be transported easily, and without being noticed.¹⁰¹ Nanosensors have the potential to be developed as an effective platform to detect the explosives.¹⁰² Hydrazine is a component of the liquid explosive, Astrolite, which is widely and not too precisely referred to as the world's most powerful non-nuclear explosive.¹⁰¹ Diethylamine, triethylamine and morpholine are liquid explosive sensitizers for nitromethane.¹⁰¹ The identification of amine type liquid explosive components and the associated sensitizers are possible only because of the advances we have made in the detection of monovalent cations, e.g., potassium and ammonium, which play important roles in biological metabolic/catabolic processes and can be of environmental interest.

Here, we report a rapid and sensitive stochastic nanopore sensing method for the detection of liquid explosive components. Indeed this is the first time monovalent cations have been detected using the stochastic sensing technique. It should be noted that numerous other techniques have been developed for the detection of ammonium,¹⁰³⁻¹⁰⁹ potassium,¹¹⁰⁻¹¹⁵ hydrazine,¹¹⁶⁻¹²⁴ diethylamine,¹²⁵ triethylamine,¹²⁶ and morpholine.^{127,128} However, no single method could detect all of these

components.

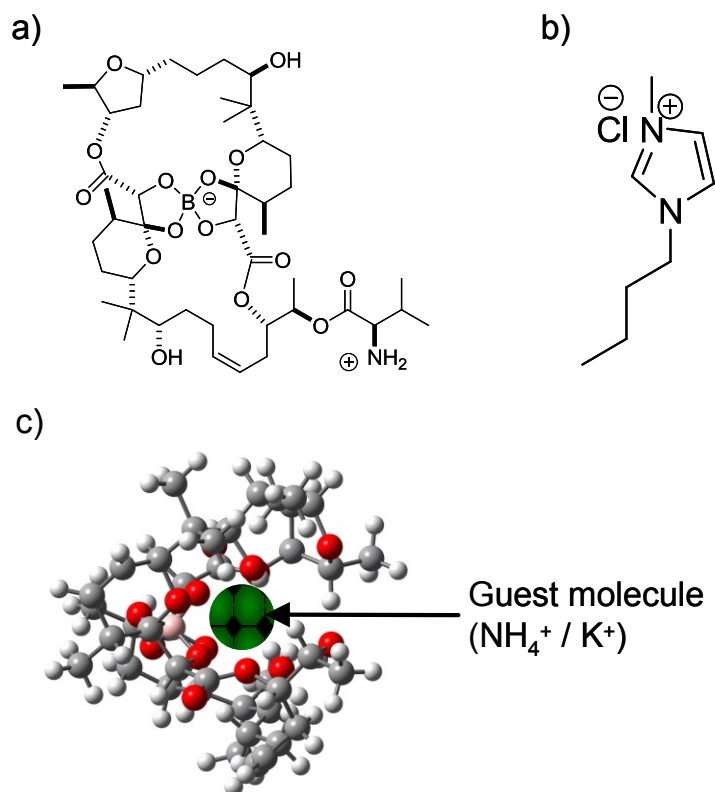


Figure 3.1 a) Structure of boromycin, b) structure of BMIM-Cl, and c) complexation of guest molecule with boromycin.

In order to detect the above analytes for the first time, via a nanopore stochastic sensing format, boromycin^{129,130} (Figure 3.1a) was used as a molecular adaptor and a dissolved ionic liquid (IL) was used as the supporting electrolyte. Boromycin is a macrodiolide Böeseken complex containing a D-valine ester, and is produced via fermentation by a strain of *Streptomyces antibioticus*.¹³⁰ The cleft formed by the boromycin structure can accommodate monovalent cations such as potassium, ammonium, amine compounds, etc (Figure 3.1c).

3.2 Experimental section

3.2.1 Materials

NaCl (99.0%), KCl (99.0-100.5%), and acetonitrile were purchased from EMD Chemicals Inc. (Darmstadt, Germany), and all the other reagents were obtained from Sigma-Aldrich (St. Louis, MO).

The IL, butylmethylimidazolium chloride [BMIM-Cl] was synthesized as follows. 1 molar equivalent of 1-methylimidazole and 1.1 molar equivalents of 1-chlorobutane were heated and stirred at 60 °C for 24 hrs. The resulting IL was dissolved in water and excess starting material was extracted with ethylacetate eight times. Water was then removed with a rotary evaporator.

All the analytes (triethylammonium chloride, diethylammonium chloride, and 4-(2-chloroethyl)morpholine hydrochloride, hydrazine dihydrochloride, tetramethylammonium chloride, KCl, and NH₄Cl) were dissolved in HPLC-grade water (ChromAR, Mallinckrodt chemicals), while boromycin was prepared by dissolving it in acetonitrile. The concentrations of the stock solutions were 1 M for analyte and 2.5 mM for boromycin, respectively. To obtain the analyte-boromycin complex, boromycin and the analyte was premixed and incubated for 30 mins. The mixture contained 1.25 mM analyte, and 12.5 μM boromycin unless otherwise noted (in the simultaneous analysis experiment, the analyte concentrations were in the micromolar range). The both electrolyte solutions, i.e., 1 M NaCl and 1 M BMIM-Cl, were prepared in HPLC-grade water, buffered with 10 mM HEPES (pH = 6.9).

The wild-type α HL monomer was first synthesized by coupled *in vitro* transcription and translation (IVTT) using the *E. Coli* T7 S30 Extract System for Circular DNA from Promega (Madison, WI). Subsequently, they were assembled into homoheptamers by adding rabbit red cell membranes and incubating for 1 h.⁸⁶ The heptamers were purified by SDS-polyacrylamide gel electrophoresis and stored in aliquots at -80°C.

3.2.2 Methods

A bilayer of 1,2-diphytanoylphosphatidylcholine (Avanti Polar Lipids; Alabaster, AL, USA) was formed on an aperture (150 μ m) in a Teflon septum (25 μ m thick; Goodfellow, Malvern, PA, USA) that divided a planar bilayer chamber into two compartments, *cis* and *trans*. The formation of the bilayer was achieved by using the Montal-Mueller method,²⁷ and monitored by using a function generator (BK precision 4012A; Yorba Linda, CA, USA). The experiments were performed using two different electrolytes, comprising either 1 M NaCl or 1 M BMIM-Cl with 10 mM HEPES (pH 6.9) at 22 ± 1 °C. The α HL protein (with the final concentration of 0.2–2.0 ng·mL⁻¹) was added to the *cis* compartment, which was connected to “ground”, while the analyte was added to the *trans* compartment. In such a way, after insertion of a single α HL channel, the mushroom cap of the α HL channel would be located in the *cis* compartment, while the β -barrel of the α HL would insert into the lipid bilayer and connect with the *trans* of the chamber device. The applied potential was -80 mV or -100 mV as noted. Currents were recorded with a patch clamp amplifier (Axopatch 200B, Molecular Devices; Sunnyvale, CA, USA). They were low-pass filtered with a built-in four-pole Bessel filter at 2 kHz and sampled at 10 kHz by a computer equipped with a Digidata 1440 A/D converter (Molecular Devices). To shield against

ambient electrical noise, a metal box was used to serve as a Faraday cage, inside which the bilayer recording amplifying headstage, stirring system, chamber, and chamber holder were enclosed.

Data were analyzed with the following software: pClamp 10.0 (Molecular Devices) and Origin 6.0 (Microcal, Northampton, MA). Conductance values were obtained from the amplitude histograms after the peaks were fit to Gaussian functions. Mean residence times (τ values) for the analytes were obtained from dwell time histograms by fitting the distributions to single exponential functions by the Levenberg-Marquardt procedure. Between 570 and 2608 events were recorded in each of the single channel recording experiments with monovalent cations as well as amine type liquid explosive components and the associated sensitizers.

Conductivity measurements were determined at 22 ± 1 °C by Waterproof EC/TDS/°C/NaCl conductivity meter (Hanna Instruments Inc., Woonsocket, RI). Kinematic viscosities were obtained using Cannon-Manning Semi-Micro capillary viscometer (State College, PA) at 22 ± 1 °C. All the results were reported as mean values \pm standard deviation.

3.2.3 Results and discussion

Since organic cations (e.g., tetraalkylammonium salts) have been used to estimate the diameters of protein ion channels,^{131,132} the feasibility of employing tetramethylammonium chloride (TMA) as the background electrolyte to overcome the interference of NaCl and KCl was investigated. Before using it as the background electrolyte, it was tested as an analyte. TMA produced an interfering signal for the detection of the target analytes, thereby confirming that it cannot be used as the

background electrolyte for these applications (Figure 3.2).

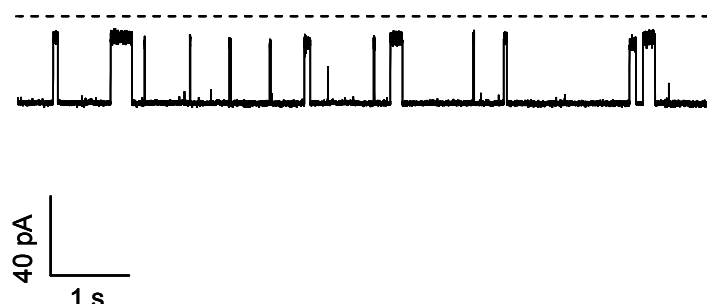


Figure 3.2 Typical single channel current recording traces for the detection of tetramethylammonium chloride.

We believed that the unique cation / anion combinations reported for some ILs might make ideal supporting electrolytes in nanopore sensing. Although pure room temperature ILs are viscous materials with interesting solvent properties,^{34,133} they are also finding use as non-traditional electrolyte solutions. Indeed, they may be advantageous given their electric conductivity, wide electrochemical window, and solubility in water.¹³⁴ After examining several different ILs, including butylmethylimidazolium chloride [BMIM-Cl], butylmethylimidazolium tetrafluoroborate [BMIM-BF₄], and tetrakis(hydroxymethyl)phosphonium chloride [P(CH₂OH)₄-Cl]; BMIM-Cl (Figure 3.1b) was chosen as an electrolyte for use in our single-channel recording experiments. The other ionic liquids could not yet be obtained in sufficiently high purity so as to produce unambiguous results. To investigate the effect of the IL as supporting electrolyte, two experiments were performed at -80 mV: one in 1 M NaCl; and the other in 1 M BMIM-Cl solution. The wild-type α HL protein was added to the *cis* compartment, while boromycin was added to the *trans* compartment. In such a way, after the insertion of a single α HL channel, the

mushroom cap of the α HL channel would be located in the *cis* compartment, while the β -barrel of the α HL would insert into the lipid bilayer and connect with the *trans* of the chamber device (see supporting information for more detail). As shown in Figures. 3.3a and 3.3b, the open channel conductance of the α HL protein was 638 ± 12 pS, and the event mean dwell time was 3.29 ± 0.15 ms in NaCl. In contrast, those values were 450 ± 12 pS, and 8.54 ± 0.04 ms, respectively, in BMIM-Cl. Thus, a smaller (29% decrease) open channel conductance and a larger (2.6-fold increase) event mean dwell time (and hence a higher sensor resolution or sensitivity) were observed in the BMIM-Cl versus the NaCl solution. To address the differences in open channel conductance and in event dwell times between in NaCl solution and in BMIM-Cl solution, the conductivity and viscosity were measured for both electrolytes. The conductivity and viscosity for 1 M NaCl solution were 81.6 mS/cm, and 1.438 mm²/s, respectively, while those of 1 M BMIM-Cl solution were 49.9 mS/cm, and 2.464 mm²/s, respectively. Therefore, with the change of the electrolyte from NaCl to BMIM-Cl, the conductivity of the bulk solution decreased by 39%, while the viscosity increased by 71%. Hence, the extent of decrease (i.e., 29%) in our experimental open channel conductance was somewhat in agreement with that (i.e., 39%) in the measured conductivities of the bulk solutions (note that conductance is proportional to the conductivity, i.e., $G \propto \kappa$).⁶³ This 10% difference may be due to the difference of ionic flow between the bulk solution and the nanopore. On the other hand, when the BMIM-Cl solution was used instead of NaCl, the percentage of the increase (i.e., 160%) in the experimental event mean dwell times was much larger than the 71% increase in the viscosities of the bulk solutions.

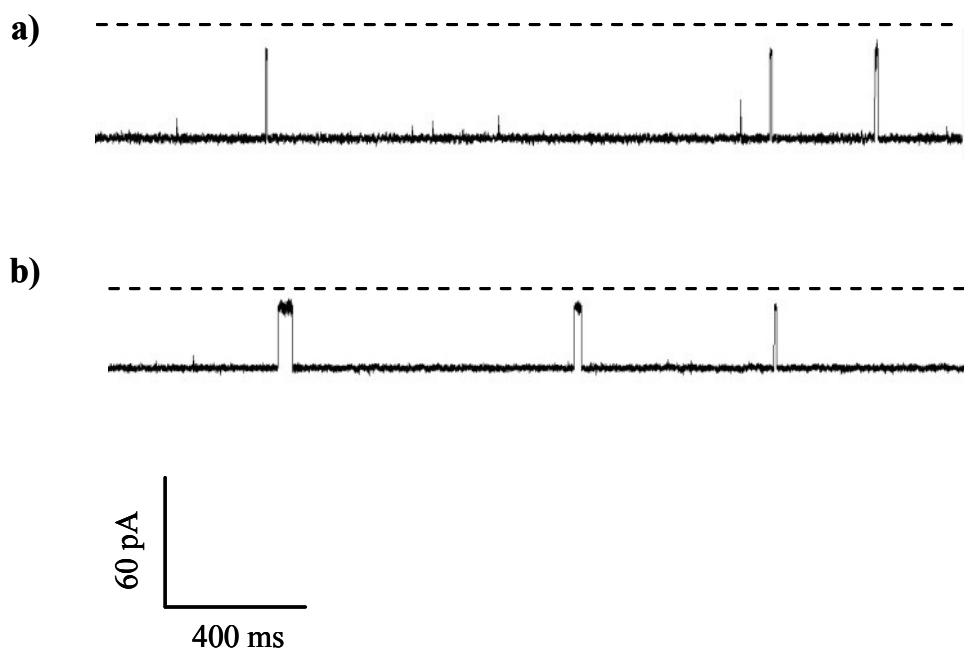


Figure 3.3 Typical single channel current recording traces of boromycin in (a) 1 M NaCl (aq); and (b) 1 M BMIM-Cl (aq).

3.2.3.1 Theoretical explanation for open channel current and dwell time change

According to the Nernst-Einstein equation,¹³⁵ the molar conductivity of an electrolyte (λ) is related to the diffusion coefficients of its ions (D) as:

$$\lambda = z^2 D F^2 / RT$$

where z is the number of charges on ions, F is the Faraday constant, R is the gas constant, and T is absolute temperature.

The diffusion coefficient of an ion is related to the viscosity of the medium (η) through the Stokes-Einstein equation:¹³⁵

$$D = kT / 6\pi\eta a$$

where k is the Boltzmann constant, and a is the hydrodynamic radius of the ion.

The combination of these two expressions provides the final expression of conductivity:

$$\lambda = z^2 F^2 k / R 6\pi\eta a$$

Therefore, the conductivity of an electrolyte solution is inversely proportional to both the viscosity of the medium and the hydrodynamic radius of the ion. However, the higher viscosity of BMIM-Cl dramatically decreases its conductivity by counteracting the size effect. As a result of these combined effects of size and viscosity, a smaller open channel current is observed in ionic liquid containing solutions than in NaCl solutions.

Since the identical analyte and pore were used in both conditions, specifically, in the experiments with both the NaCl solution and the BMIM-Cl solution as the electrolytes, the dwell time of the boromycin events depends primarily on the migration rate of the analyte as well as the binding affinity between boromycin and the α HL pore. The former can be primarily governed by the diffusion and charge selectivity of the pore. The effect of diffusion can be attributed using the above Stokes-Einstein equation. According to the equation, the only variable which governs the diffusion is viscosity, because all the other factors can be considered as identical in both systems.

Since the characteristic time for a molecule to diffuse the 10 nm length pore such as α HL is 50–500 ns,¹³⁶ the relatively small change in the viscosity of the medium could not explain the observed large boromycin residence time. Therefore, it is more likely that the electrolyte change may significantly affect the charge selectivity⁶³ and the binding of boromycin to the pore. It should be noted, our experiments showed that the values for both reversal potentials and streaming potentials of the wild-type α HL protein were different in BMIM-Cl and NaCl solutions (data not shown). However, due to the lack of data for the activity coefficient of BMIM-Cl solution, the actual charge selectivity of the pore could not be obtained. It was reported that the change of the charge selectivity of a protein pore could be reflected from streaming potential and reversal potential.⁶³ Thus, different streaming potential and reversal potential values obtained in NaCl and BMIM-Cl solutions suggests that the charge selectivities of the α HL protein pore are different in these two electrolyte solutions.

The effect of applied potential on the interaction between the potassium-boromycin or ammonium-boromycin complex and the WT α HL pore was investigated to find the optimum experimental voltage. The event dwell times of these host-guest complexes first increased and then decreased significantly with the increase of the applied voltage (Figure 3.4). In contrast, the event dwell times of the boromycin host remained almost unchanged. The reason is that after the zwitterionic boromycin is complexed with either potassium or ammonium, the host-guest complex is positively charged. The voltage dependent phenomenon is well known for charged species in nanopores.¹⁵ Further experiments were performed at -100 mV, since the highest dwell time was observed at this voltage.

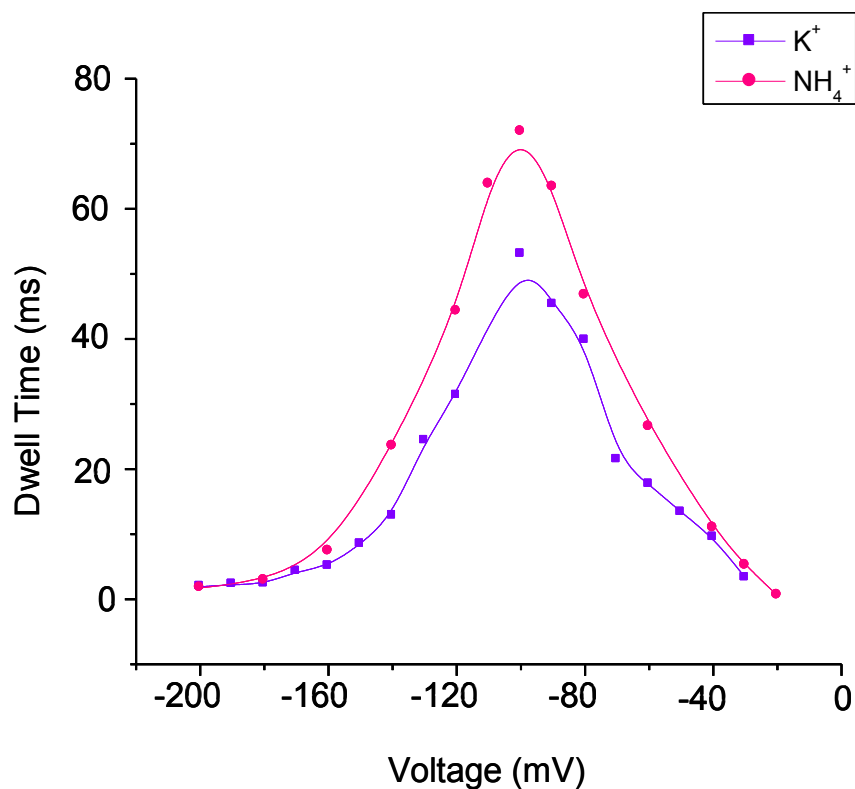


Figure 3.4 The effect of applied potential on the detection of mono-valent cations.

Because this study employs a positively charged host-guest complex (as mentioned above), chloride salts of targeted analytes were used for the detection. Therefore, hydrazine dihydrochloride (HZ), triethylammonium chloride (TEA), diethylammonium chloride (DEA), and 4-(2-chloroethyl)morpholine hydrochloride (CM) were chosen as analytes. However, recent studies have shown that uncharged amines also can complex with boromycin,¹³⁰ and hence, there is a possibility to detect even neutral amines.

In the absence of analytes, only the signals for the host boromycin molecules could be identified, and have a dwell time of 8.54 ± 0.04 ms. However, in the presence of cations, in addition to the relatively short boromycin events, either much longer dwell times or significantly smaller current blockage events were observed (Figures 3.5 and 3.6), which may be attributed to the analyte-boromycin complex. For example, at -100 mV, TEA-boromycin, DEA-boromycin, CM-boromycin and HZ-boromycin complexes produced events with mean dwell times at 60.6 ± 1.9 ms [the number of repeat experiments (n) = 7], 40.5 ± 0.5 ms (n = 4), 34.7 ± 0.6 ms (n = 4), and 1.71 ± 0.06 ms (n = 6), respectively, thus providing the accurate differentiation of these liquid explosive components (Figures. 3.5a – 3.5d). It should be mentioned that the ammonium-boromycin complex produced events with a mean dwell time at 75.0 ± 1.6 ms (n = 3), while the events of potassium-boromycin complex had a mean dwell time at 52.1 ± 0.7 ms (n = 3). Note that in determining the dwell times for TEA-boromycin, DEA-boromycin, CM-boromycin, ammonium-boromycin and potassium-boromycin complexes, the events which were lower than 20 ms were ignored whereas in HZ-boromycin complex analysis, events larger than 6 ms were ignored to minimize the interference from uncomplexed boromycin signal. Hence, not only is there no interference from either potassium or ammonium when analyzing for these liquid explosives and their sensitizers, (Figs. 3.5e and 3.5f), but these monovalent cations are also easily distinguished from one another via their dwell times.

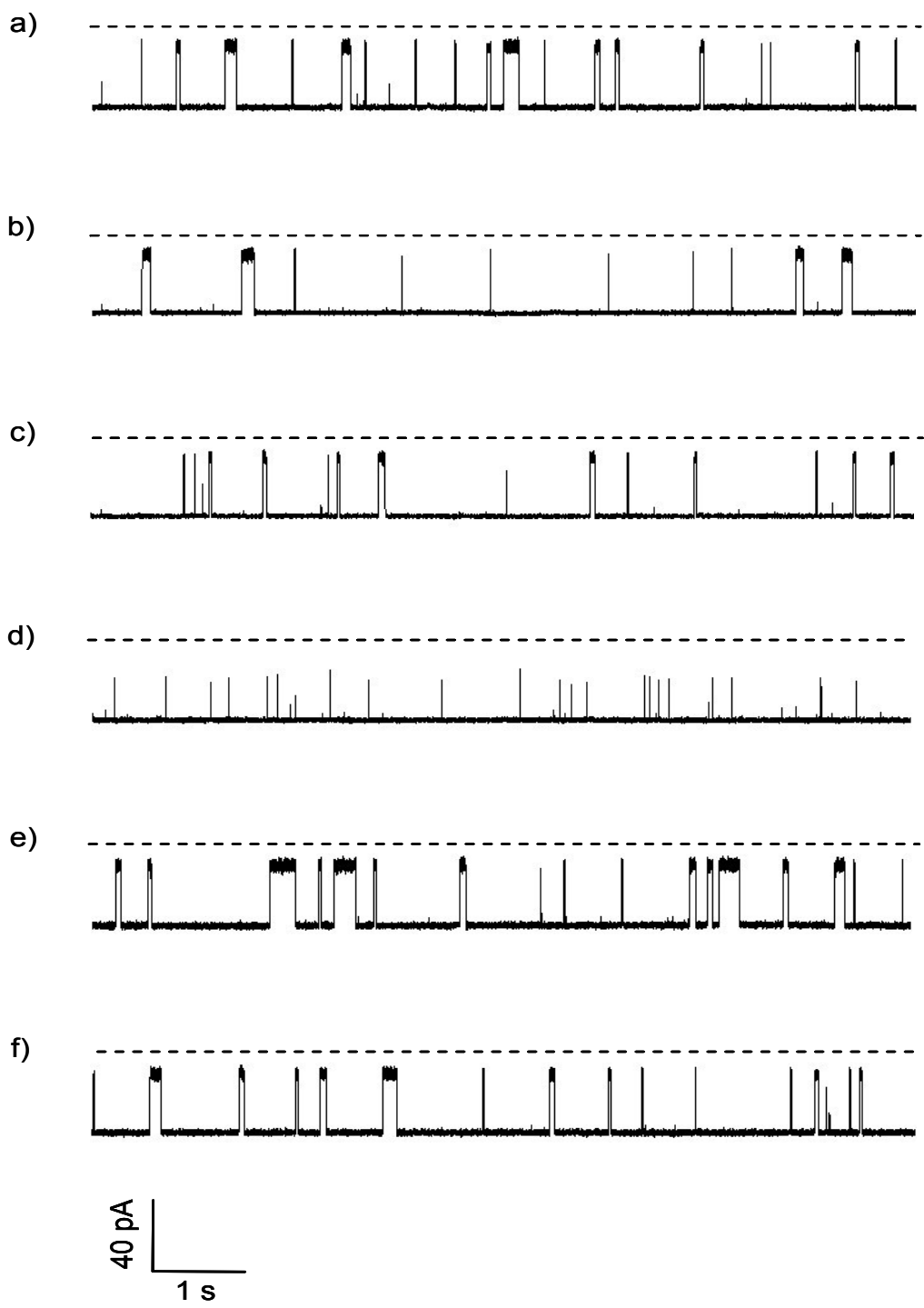


Figure 3.5 Typical single channel current recording traces showing the stochastic sensing of analytes in 1M BMIM-Cl solution and using boromycin as a host. a) TEA, b) DEA, c) CM, d) HZ, e) NH_4^+ , and f) K^+ .

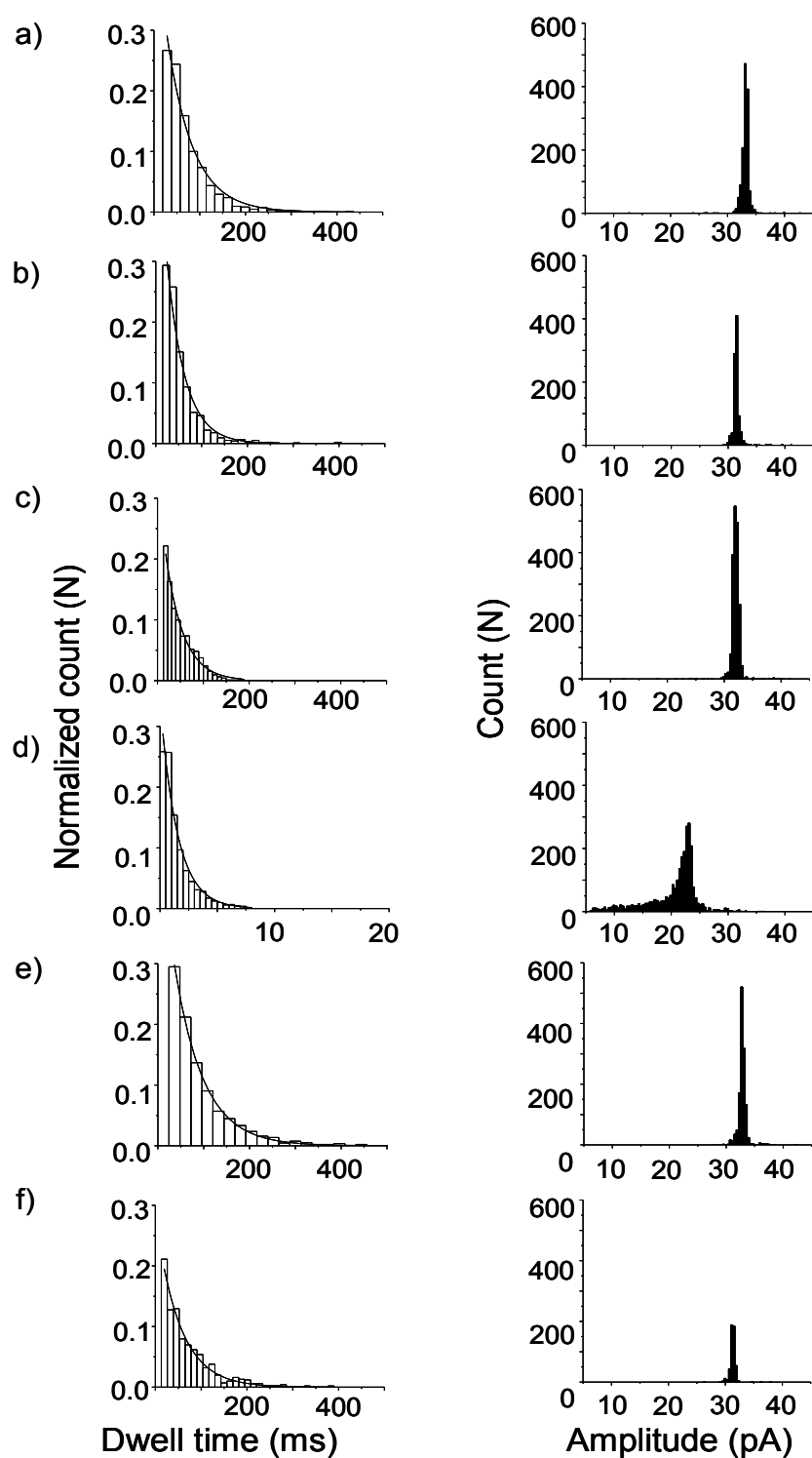


Figure 3.6 Stochastic sensing of analytes in 1M BMIM-Cl solution and using boromycin as a host. (*Left*) Dwell time histograms. (*Right*) Amplitude histograms. a) TEA, b) DEA, c) CM, d) HZ, e) NH_4^+ , and f) K^+ .

Table 3.1 The dwell time and amplitude values for analyte-boromycin complexes.

Analyte	$\tau_{\text{off}} \pm \text{std}$ (ms)	Amplitude \pm std (pA)
TEA	60.6 ± 1.9	33.7 ± 0.4
DEA	40.5 ± 0.5	33.6 ± 0.8
CM	34.7 ± 0.6	33.5 ± 1.2
HZ	1.71 ± 0.06	22.6 ± 0.7
NH ₄ ⁺	75.0 ± 1.6	33.7 ± 0.2
K ⁺	52.1 ± 0.7	33.6 ± 0.3

Although amplitude (Table 3.1) does not provide enough resolution to differentiate among the liquid explosive sensitizers or potassium and ammonium, it could be used conveniently to distinguish HZ (the component of liquid explosive astrolite) from liquid explosive sensitizers and monovalent cations. For example, for simultaneous differentiation and quantification, the same wild-type α HL protein pore was used to test the TEA-HZ-boromycin mixture (Figure 3.7). When HZ-boromycin (100:1 mixture) was present in solution, a major amplitude peak at ~ 22.5 pA appeared in the amplitude histogram (Figure 3.8a), while that of TEA-boromycin (100:1 mixture) complex appeared at ~ 33 pA (Figure 3.8b). When TEA-HZ-Boromycin (1:1:2) mixture was added to the solution, both HZ-boromycin and TEA-boromycin peaks could be identified (Figure 3.8c). When TEA-HZ-Boromycin (0.5:1.5:2) mixture was used, an increase in the HZ-boromycin peak area could be observed (Figure 3.8d). However, TEA-boromycin peak area remained almost unchanged probably due to the effect of free boromycin (note that both TEA-

boromycin and free boromycin have the same amplitude). The free boromycin signal did not appear in the HZ-boromycin mixture because it contained 100 times more HZ than boromycin, thus allowing almost all the boromycin to be complexed. By varying the ratio of the TEA-HZ-boromycin mixture to be analyzed, from (1:1:2) to (0.5:1.5:2), it can be seen that the HZ concentration was increased by 50%. The experimentally calculated HZ-Boromycin event frequency ($1/\tau_{on}$) was increased by 50.1% ($n=3$), which is in good agreement with the standard test mixtures. Further, the event dwell times for the HZ-boromycin in the above TEA-HZ-boromycin mixtures were 1.72 ms, and 1.74 ms, respectively (note that the dwell time for HZ alone was 1.71 ± 0.06 ms in the presence of boromycin). This confirms the accurate identification of HZ even in the presence of TEA. Moreover, TEA could be detected as low as $3.125 \mu\text{M}$.

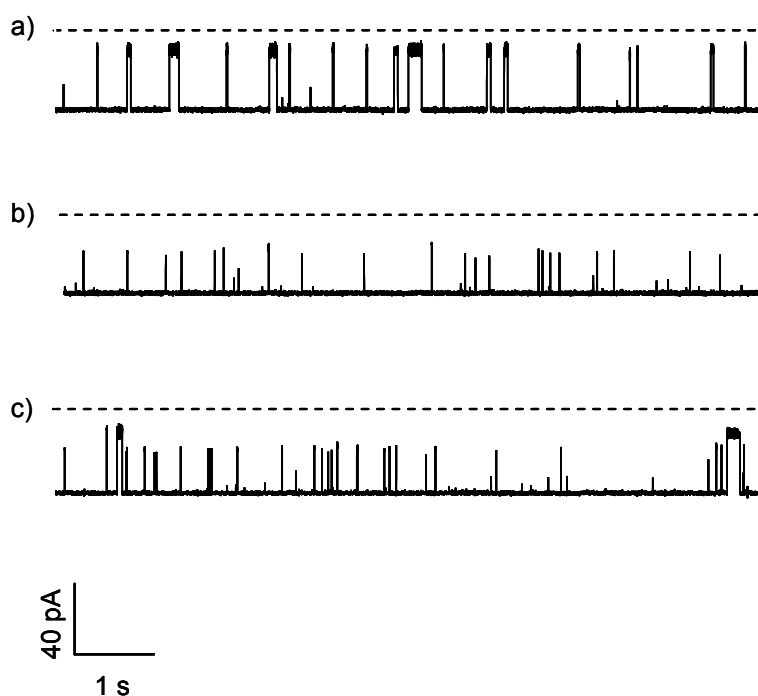


Figure 3.7 Typical single channel current recording traces for the simultaneous detection of TEA and HZ in 1 M BMIM-Cl (aq). a) Boromycin + TEA; b) boromycin + HZ; and c) boromycin + HZ + TEA.

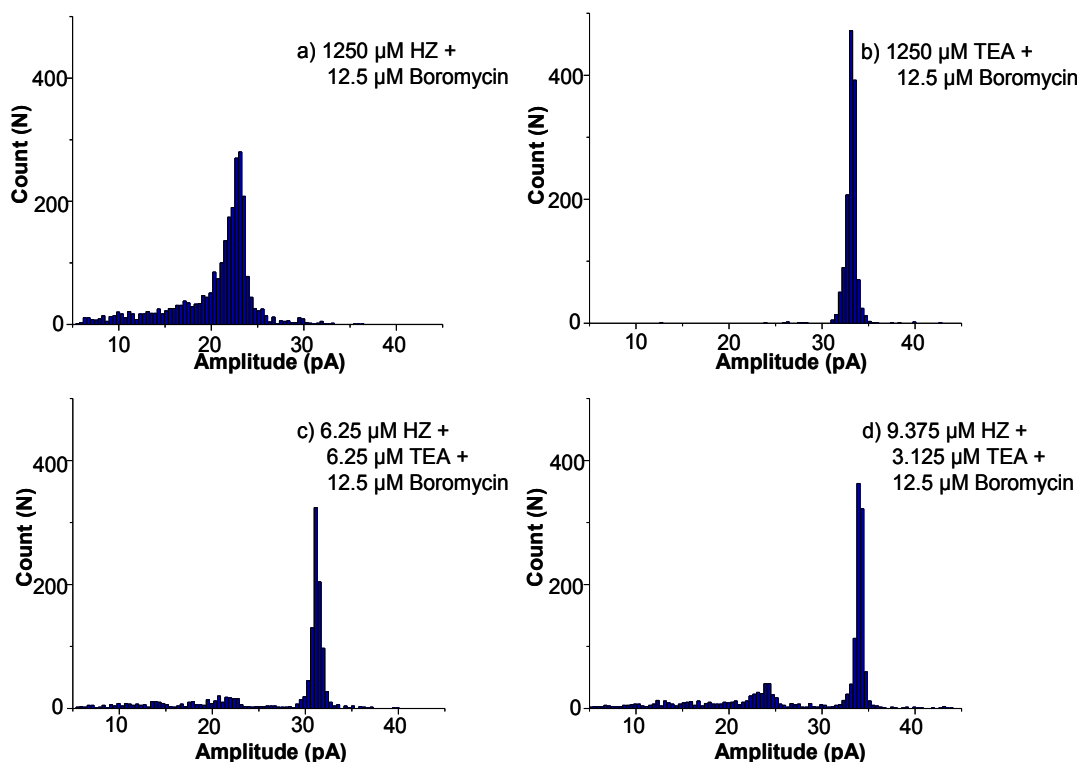


Figure 3.8 Amplitude histograms for simultaneous detection of TEA and HZ.

In conclusion, ILs have been successfully introduced as advantageous supporting electrolytes in nanopore technology for the first time. They permit the analysis of compounds that are difficult or even impossible to achieve in NaCl or KCl solution, e.g., in the analysis of compounds that are insoluble in water but soluble in ionic liquids and/or their solutions, and in situations where NaCl or KCl interfere with analyte detection. Furthermore, the nanopore sensor sensitivity was enhanced in solutions of BMIM-Cl as compared to NaCl solutions of the same concentrations. In addition, the novel selector, boromycin, works extraordinarily well in these solutions. Hence, our nanopore system could be used as a rapid and sensitive approach to screen certain liquid explosives and their sensitizers, since the different signatures

permit convenient differentiation and even simultaneous detection. Further studies on the effect of other multifunctional ionic liquid solutions^{58,137-139} of increased concentrations and even with pure ionic liquids are currently in progress.

CHAPTER 4

SLOWING DNA TRANSLOCATION THROUGH NANOPORES USING A SOLUTION CONTAINING ORGANIC SALTS

4.1 Introduction

Development of a high-throughput and cost-effective DNA sequencing method provides invaluable information on the biological and biomedical fields and also makes vital contributions to many areas of high priority research such as forensics, archeology, and anthropology.^{140,141} Although significant reductions in DNA sequencing costs have been achieved in the past 25 years, fundamentally different approaches will be required to drastically reduce the cost and increase the speed of routine complete genome sequencing.¹⁴¹ Among the various DNA sequencing methods under development, the nanopore approach has emerged as one of the most promising technologies to achieve the “\$1000 genome” goal set by the U.S. National Institutes of Health.^{141,142} In the nanopore method, single-stranded DNA (ssDNA) molecules are electrophoretically driven through a nanochannel, and the discrimination of polynucleotides might be achieved based on their different current signatures, represented by residence times and/or current blockage amplitudes in the pore.⁶⁵ However, one of the major hurdles of utilizing nanopores to sequence ssDNA molecules is that DNA polymers translocate through the nanopore very rapidly.¹⁴³ For instance, the translocation rate of polydeoxycytosine was $\sim 1 \mu\text{s}/\text{base}$, whereas that of polydeoxyadenine was $\sim 3 \mu\text{s}/\text{base}$.¹⁸ This rate requires a high temporal resolution for the accurate detection of single bases, which cannot be provided by the currently available single-channel recording technique.¹⁴² To increase the nanopore resolution

for nucleotide differentiation, many attempts have been made to slow down DNA translocation. It has been shown that a decrease in the experimental temperature allowed ssDNA molecules to be electrophoretically driven through the pore more slowly.^{18,144} Further, DNA translocation could be manipulated by changing the applied potential.¹⁴⁵ Other approaches include sequence-specific detection of individual DNA strands,²⁰ formation of DNA-hemolysin rotaxane,¹⁴⁶ differentiation of nucleotide bases in a host β -cyclodextrin compound,¹⁴⁷ and immobilization of DNA polynucleotides with streptavidin.¹⁴⁸ In addition, it was reported that the detection of DNA sequences could be achieved by using an alternating electric field in a nanopore capacitor.¹⁴⁹

In this study, we investigate the feasibility of utilizing aqueous solutions of ionic liquids to slow ssDNA translocation in the α -hemolysin pore. The study of ionic liquids is currently an active research area. They have been used in various applications, including organic synthesis,³² extraction,¹⁵⁰ separation,^{33,34} catalysis,³³ and electrochemical studies.³⁶ In previous work, a solution containing ionic liquid butylmethylimidazolium chloride (BMIM-Cl) was used as a supporting electrolyte in the nanopore stochastic detection of liquid explosives and monovalent cations.²⁴ The results suggested that the use of BMIM-Cl solution instead of the commonly used NaCl/KCl solutions could improve nanopore resolution.

4.2 Experimental methods

4.2.1 Materials and reagents

ssDNA samples, including (dA)₂₀, (dC)₂₀, (dT)₂₀, (dCdT)₁₀, and (dC)₁₀(dT)₁₀, were purchased from Integrated DNA Technologies, Inc. (Coralville, IA). Lipid 1,2-

diphytanoylphosphatidylcholine was obtained from Avanti Polar Lipids (Alabaster, AL). Teflon film was purchased from Goodfellow (Malvern, PA). All of the other reagents including butylmethylimidazolium chloride (BMIM-Cl) and tetramethylammonium chloride (TMA-Cl) were purchased from Sigma Aldrich. All the ssDNA polymers were dissolved in HPLC-grade water (ChromAR, Mallinckrodt Baker). The concentrations of the stock solutions were 4 mM for each of the DNA samples. All the three electrolyte solutions used in this work, i.e., 1 M BMIM-Cl, 1 M TMA-Cl, and 1 M NaCl, were prepared in HPLC-grade water and buffered with 10 mM Tris (pH) 6.0). Preparation and formation of wild-type and mutant protein pores has been described elsewhere.¹⁵¹ Briefly, the mutant RHL M113F gene was constructed by site-directed mutagenesis. Then, the wild-type and mutant M113F RHL monomer were first synthesized by coupled in vitro transcription and translation (IVTT) using the *E. coli* T7 S30 Extract System for Circular DNA from Promega (Madison, WI). Subsequently, they were assembled into homoheptamers by adding rabbit red cell membranes and incubating for 1 h. The heptamers were purified by SDS-polyacrylamide gel electrophoresis and stored in aliquots at -80 °C.

4.2.2 Planar bilayer experiments

The single-channel recording procedure has been described elsewhere.¹⁵² Briefly, a Teflon septum was used to divide the planar bilayer chamber into two compartments, cis and trans. A lipid bilayer of 1,2-diphytanoylsn- glycerol-3-phosphocholine was formed on the aperture in the Teflon film by using the Montal-Mueller method.²⁷ The experiments were carried out under symmetrical buffer conditions with a 2.0 mL solution comprising 1 M BMIM-Cl, and 10 mM Tris · HCl (pH 6.0) at 22 ± 1 °C unless otherwise stated.

Both the α HL protein (with the final concentration of 0.2-2.0 ng \cdot mL⁻¹) and the ssDNA sample were added to the cis chamber compartment, which was connected to “ground”. The applied potential was +120 mV. Currents were recorded with a patch clamp amplifier (Axopatch 200B, Axon instruments, Foster City, CA). They were low-pass filtered either with an external fourpole Bessel filter at 30 kHz and sampled at 125 kHz or with a built-in four-pole Bessel filter at 10 kHz and sampled at 20 kHz by a computer equipped with a Digidata 1440 A/D converter (Molecular Devices). The final concentrations of ssDNA samples were 10 μ M each for the experiments performed at the 30 kHz filter, while those were 4 μ M each for the experiments carried out at the 10 kHz filter. At least three separate experiments were carried out for each DNA sample.

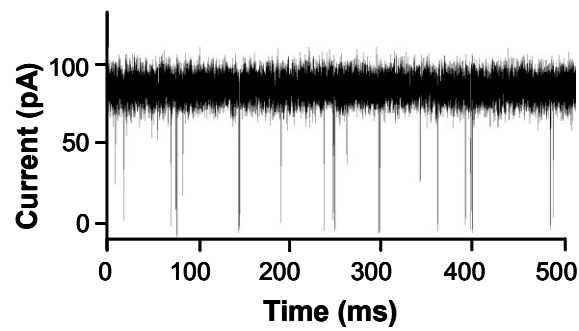
4.2.3 Data analysis

Only the events with at least 70% of full blockage were included in the analysis. It is believed that the events with the blockage amplitudes less than 70% of the open channel current are not associated with the translocation of ssDNA polymers through the α HL pore but instead may be caused by collision with the pore opening or residence only in the channel vestibule.¹⁵³ Two significantly different types of events were observed for DNA’s transit in the α HL pore in the BMIM-Cl solution, short-lived events with mean residence times of \sim 50-100 μ s and long-lived events with mean residence times of milliseconds or larger. Data were analyzed with the following software: pClamp 10.0 (Molecular Devices) and Origin 6.0 (Microcal, Northampton, MA). Conductance values were obtained from the amplitude histograms after the peaks were fit to Gaussian functions. Mean residence time (τ_{off}) values of the short-lived events were obtained from the dwell time histograms by

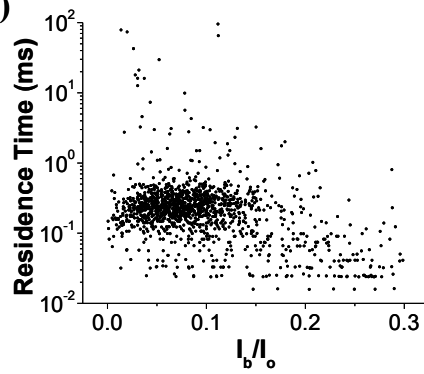
fitting the distributions to Gaussian functions,¹⁸ while those of the long-lived events were obtained by fitting the dwell time distributions to single exponential functions by the Levenberg-Marquardt procedure.⁶⁹ It should be noted that the dwell time histograms of the short-lived events could also be fitted to single exponential functions by using larger bin widths, and we found that the mean τ_{off} values obtained using these two different approaches were not significantly different. To obtain the mean residence times of the long-lived events for (dA)₂₀, (dT)₂₀, (dCdT)₁₀, and (dC)₁₀(dT)₁₀, the events with duration less than 1 ms were not included, while in the analysis of (dC)₂₀ events with duration less than 0.5 ms were ignored to minimize the potential interference from the short event signals. Between 1330 and 20,000 events were recorded in each of the single channel recording experiments performed at the 30 kHz filter, while between 280 and 10,000 events were collected in each of the single channel recording experiments carried out at the 10 kHz filter. All the results were reported as mean values \pm standard deviation.

To obtain the streaming potentials¹⁵⁴ of protein pores, singlechannel current recording experiments were performed under asymmetric conditions. The cis chamber compartment contained a 2.0 mL solution comprising either 1 M NaCl or 1 M BMIMCl, 10 mM TrisHCl (pH 6.0), while the trans compartment contained 2.0 mL of the same buffer solution plus 1 M urea. Streaming potential $\Delta\phi$ for the protein pore was obtained by linearly fitting the I - V curves, which were recorded from ± 5 to ± 50 mV.

a)



b)



c)

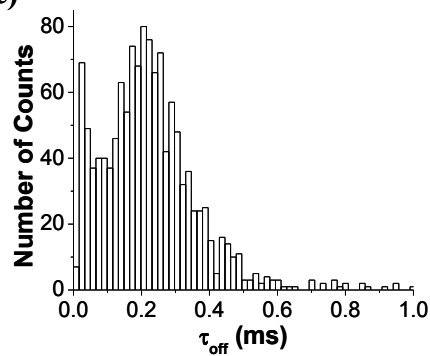


Figure 4.1 Translocation of (dA)₂₀ in the mutant (M113F)₇ α HL pore in 1M NaCl solution.

(a) Representative single channel current recording trace; (b) scatter plot of event amplitude vs. residence time; and (c) event residence time histogram.

4.3 Results and discussion

To investigate the effect of the ionic liquid solution on DNA translocation, the initial experiment was performed at +120 mV with (dA)₂₀ in the mutant α -hemolysin (α HL) (M113F)₇ pore and using a 1 M BMIM-Cl solution as the supporting electrolyte. The current was low-pass filtered with a four-pole Bessel filter at 30 kHz and sampled at 125 kHz. As a control, the experiment was repeated under the same conditions with the exception that NaCl was substituted for BMIM-Cl as the background electrolyte. The (M113F)₇ protein was constructed by replacing the Met residues at position 113 of the wild-type (WT) α HL with Phe amino acids, and has been shown to provide an enhanced resolution for peptide detection compared with that observed with the WT α HL pore.¹⁵¹ The experimental results showed that in 1 M NaCl solution, (dA)₂₀ produced only a major type of rapid translocation events, although these events could be separated into two subgroups (Figure 4.1). The mean residence times for the two subgroup events were $190 \pm 20 \mu\text{s}$ and $40 \pm 5 \mu\text{s}$, respectively (Figure 4.1). These events might be attributed to the translocation of (dA)₂₀ in two different orientations, 5'-first and 3'-first. Note that the observation of two subgroup translocation events with different residence times has been previously reported by Kasianowicz and co-workers in the experiment with the translocation of 210-nt-long poly[U] through the WT α HL channel.⁶⁵ Hence, the translocation velocity of (dA)₂₀ in the mutant (M113F)₇ α HL pore are not significantly different from those well-documented values obtained for the translocation of polydeoxyadenine through the WT α HL pore.^{18, 144} Similar to the observation made for the translocation of polynucleotides through the WT α HL channel,⁶⁵ events with much longer residence times at milliseconds or larger were also occasionally observed for (dA)₂₀ in the (M113F)₇ α HL pore (Figure 4.1). These events are believed to be caused by the

tangling of polynucleotides to the α HL channel.⁶⁵

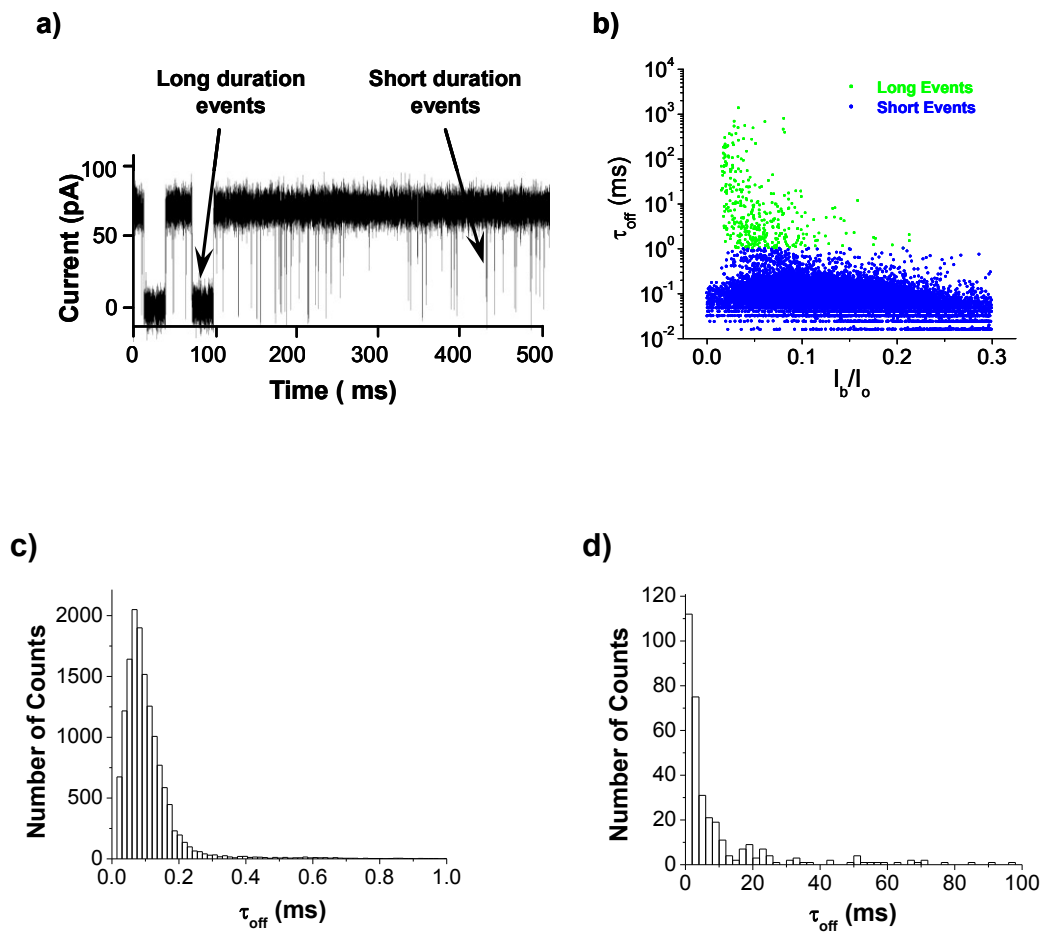


Figure 4.2 Translocation of (dA)₂₀ in the mutant (M113F)₇ α HL pore in 1M BMIM-Cl solution.

(a) Representative single channel current recording trace; (b) scatter plot of event amplitude vs. residence time; (c) residence time histogram of short-lived events; and (d) residence time histogram of long duration events.

In contrast, in 1 M BMIM-Cl solution two major types of current blockage events were observed for $(dA)_{20}$ (Figure 4.2). One type of events shows a small mean residence time ($\tau_{\text{off-short}}$) and a wide range of current blockage amplitudes (from ~70% to almost full channel blockage), while the other type of events presents a narrow range of current blockage amplitudes and a large mean duration value ($\tau_{\text{off-long}}$) but with a broad distribution of residence times. The mean $\tau_{\text{off-short}}$ and $\tau_{\text{off-long}}$ values were $78 \pm 5 \mu\text{s}$, and $3.93 \pm 0.12 \text{ ms}$, respectively. Since the risetime ($\approx 0.33/f_c$) is $\sim 11 \mu\text{s}$ at 30 kHz,¹⁵⁵ the vast majority of the rapid DNA translocation events should have been detected under the experimental conditions employed in this work. It should be mentioned that these long-lived current modulations occurred very frequently (at ~ 5 events per second), although they only accounted for a small portion ($\sim 2.5\%$) of the total current blockages. In part, this was attributed to a ~ 2 fold increase in the frequency of the $(dA)_{20}$ events when the electrolyte BMIM-Cl was substituted for NaCl. In addition, we noticed that with the change of the electrolyte from 1 M NaCl to 1 M BMIM-Cl the current value of the open state of a single αHL (M113F)₇ channel decreased from 90 ± 4 to $62 \pm 5 \text{ pA}$ at +120 mV. The extent of decrease (i.e., 31%) in our experimental open channel conductance was in agreement with that (i.e., 39%) in the measured conductivities of the bulk solutions (note that the conductivities of 1 M NaCl and 1 M BMIM-Cl solutions were 81.6 and 49.9 mS/cm, respectively²⁴).

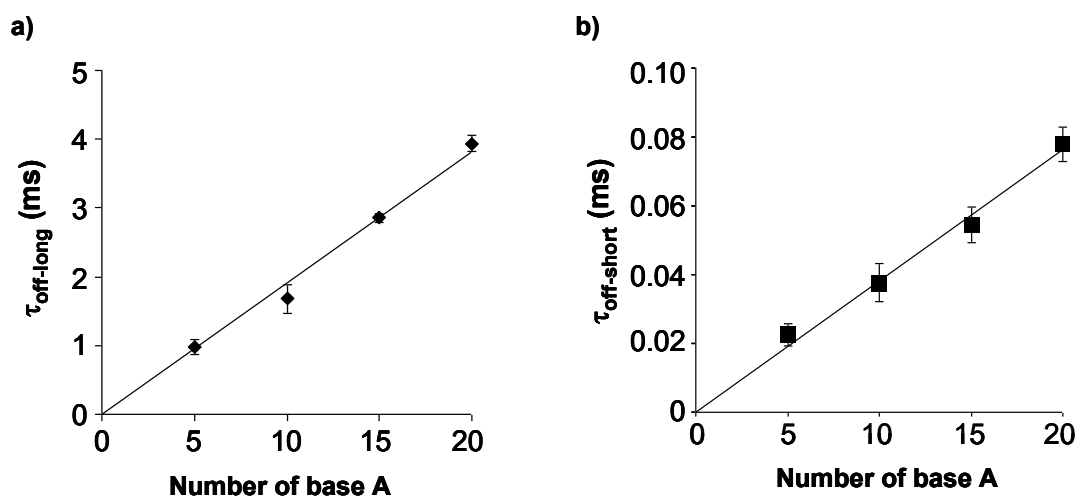


Figure 4.3 Effect of DNA length on the mean residence time of (a) long-lived events; and (b) short-lived events, suggesting that the long duration events are caused by DNA's threading through the α HL pore.

To investigate whether these long-live events are caused by $(dA)_{20}$'s threading through the α HL pore or rather they are attributed to the sticking of these DNA polymers to the channel, a series of polydeoxyadenine polymers with different lengths were examined with the mutant α HL (M113F)₇ protein channel in 1 M BMIM-Cl solution. Our experimental results show that with an increase in the DNA length the mean residence time of the long-lived events increased linearly (Figure 4.3a). This suggests that these long-lived events were not due to the tangling of the $(dA)_{20}$ molecule to the channel or binding of one or more bases of the polymer to the protein pore for long periods of time with intermittent short periods of rapid translocation but rather caused by the slower translocation of the DNA molecule as a whole. And hence, the long duration events are suitable for the analysis of the length and structure of a polynucleotide molecule.

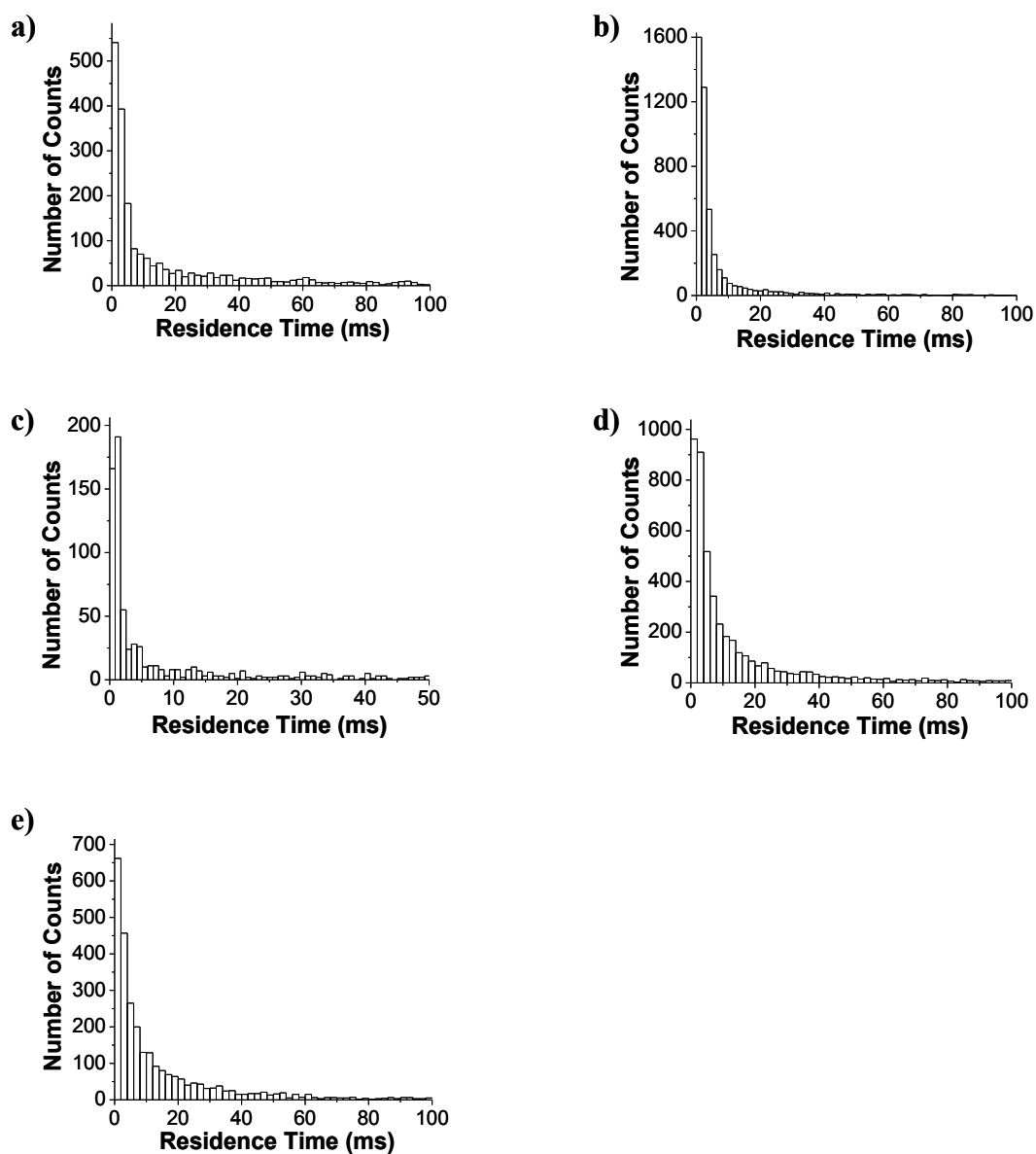


Figure 4.4 Event dwell time histograms of (a) $(dA)_{20}$; (b) $(dT)_{20}$; c) $(dC)_{20}$; (d) $(dC)_{10}(dT)_{10}$; and (e) $(dCdT)_{10}$.

In terms of the short-lived events, we noticed that $(dA)_5$ (with a mean $\tau_{\text{off-short}}$ value of 22.5 (3.1 μs) was still in the linear range of the plot of the event residence time versus DNA length (Figure 4.3b). In contrast, a linear relationship between

the event residence time and polymer length was observed only when DNA polymers longer than ~12 bases were electrophoretically driven through the WT RHL pore in the KCl solution.^{144,145} Therefore, this suggests that the use of ionic liquid solutions coupled with the engineered protein pores provides a potential means to improve the resolution of the nanopore to the nucleotide differentiation, especially in the analysis of short DNA polymers.

It should be noted that such long duration translocation events of polydeoxyadenine have not been previously reported,¹⁸ although (dT)₅₀ produced events with duration at ~3.7 ms in the WT α HL pore in 1 M KCl solution.¹⁵³ In this work, we focus on the pertinent long residence time events and investigate whether they can be employed to differentiate between various nucleotides. The large duration events have a significant advantage over the short-lived events since high measurement bandwidths are not necessary and hence significantly reduced measurement noise could be achieved. For this purpose, five ssDNA samples, including (dA)₂₀, (dC)₂₀, (dT)₂₀, (dCdT)₁₀, and (dC)₁₀(dT)₁₀, were examined with the same mutant (M113F)₇ pore in the BMIM-Cl solution at a filter frequency of 10 kHz and sampled at 20 kHz. As was found for (dA)₂₀, all of the four additional DNA molecules produced large residence time events (Figure 4.4). The mean residence times and amplitudes of these long-lived events for the five different DNA samples are summarized in Table 4.1. The translocation rates for various DNA polymers (201 μ s/base for (dA)₂₀, 98 μ s/base for (dC)₂₀, 150 μ s/base for (dT)₂₀, 256 μ s/base for (dCdT)₁₀, and 320 μ s/base for (dC)₁₀(dT)₁₀) obtained were ~2 orders of magnitude larger than the well-documented rates of ~1-3 μ s/base with the translocation of 100-mer DNA polymers through the WT RHL channel in the KCl solution at room temperature.^{18,144} This clearly shows that the use of BMIM-Cl solution instead of

NaCl/KCl solutions significantly slows DNA translocation and provides a much enhanced resolution/sensitivity. This increased nanopore resolution coupled with the different event blockage amplitudes produced by different nucleotides (Table 4.1) permits the convenient differentiation between the five DNA molecules examined.

To further document the utilization of ionic liquid solutions as an effective means to slow the translocation of DNA polymers in nanopores, the WT α HL pore was used instead of the mutant (M113F)₇ protein to examine the same series of DNA samples in 1 M BMIM-Cl solution. Similar to the observation made for the DNA translocation through the (M113F)₇ pore in the BMIMCl solution, all the five tested DNA samples produced long duration events (Figure 4.5). The mean residence times and amplitudes of these long-lived events for the five different DNA samples are summarized in Table 4.2.

Table 4.1 The mean residence times and current blockage amplitudes of five ssDNA samples in the (M113F)₇ protein pore.

ssDNA sample	Residence Time (ms)	Residual Current (pA)	Current Blockage (%)
(dA) ₂₀	4.02 ± 0.17	2.9 ± 0.2	95.3 ± 0.4
(dC) ₂₀	1.96 ± 0.22	7.0 ± 0.4	88.7 ± 0.6
(dT) ₂₀	3.00 ± 0.25	2.8 ± 0.2	95.4 ± 0.3
(dCdT) ₁₀	5.13 ± 0.91	4.0 ± 0.3	93.6 ± 0.5
(dC) ₁₀ (dT) ₁₀	6.40 ± 0.19	4.9 ± 0.2	92.2 ± 0.4

Table 4.2 The mean residence times and current blockage amplitudes of five ssDNA samples in the wild-type α HL protein channel.

ssDNA sample	Residence Time (ms)	Residual Current (pA)	Current Blockage (%)
(dA) ₂₀	2.37 ± 0.20	2.8 ± 0.2	95.6 ± 0.3
(dC) ₂₀	1.65 ± 0.23	4.1 ± 0.3	93.5 ± 0.4
(dT) ₂₀	2.17 ± 0.10	0.8 ± 0.1	98.6 ± 0.1
(dCdT) ₁₀	3.00 ± 0.20	1.3 ± 0.1	98.0 ± 0.2
(dC) ₁₀ (dT) ₁₀	4.79 ± 0.71	3.3 ± 0.3	94.8 ± 0.5

Although the residence time values were smaller than those obtained in the (M113F)₇ protein pore, the translocation rates of various polynucleotides at 82.5-240 μ s/base were still \sim 102 fold larger than those in KCl or NaCl solutions. The difference in the residence times for the DNA translocation through two different protein pores may be attributed to the change in the van der Waals volumes of amino acids at position 113 of the α HL channels (V_M (124 \AA^3) < V_F (135 \AA^3)).²⁷ All together, these results suggest that the BMIM-Cl solution is essential to obtaining the long duration DNA events in the α HL pore, while mutant protein pore plays a smaller role.

The significant increase in the residence time of DNA translocation in the ionic liquid BMIM-Cl solution over the NaCl/KCl solution might be attributed to several

possible reasons, for example, the changes in the viscosity of the medium and in the charge selectivity of the pore. Under a specific applied voltage bias, for example, +120 mV in this work, the DNA translocation process is mainly determined by the interaction of the polynucleotides and the α HL pore, and the migration rate of the nucleotide molecules. The latter is primarily dependent on the diffusion of the polymer and the charge selectivity of the pore. Our previous research showed that the viscosity of the BMIM-Cl solution was only 71% greater than that of the NaCl solution.²⁴ Hence, the change in the viscosity of the medium could not explain the observed large DNA residence times¹⁵⁶ (note that the diffusion coefficient of an ion is inversely related to the viscosity of the medium). On the other hand, the actual charge selectivity of the pore could not be obtained due to the lack of data for the activity coefficient of BMIM-Cl solution. However, our experiments showed that, when BMIM-Cl solution was used instead of NaCl, the values for the streaming potentials in both the WT and mutant (M113F)₇ α HL pores reduced significantly (Figure 4.6). For example, in 1 M NaCl solution the streaming potentials in the wild-type and mutant (M113F)₇ α HL pores were -3.00 ± 0.10 and -4.20 ± 0.35 mV, respectively (Figure 4.7). In contrast, in 1 M BMIM-Cl, those values were -1.41 ± 0.22 and -1.43 ± 0.24 mV, respectively (Figure 4.8). It should be noted that a smaller streaming potential of the pore indicates a more even transport of solvent by cations and anions, leading to a drop in the preferential charge selectivity to either cation or anion.⁶³ Thus, our results suggest that the weakly anion selective WT or mutant (M113F)₇ α HL pore in the NaCl/KCl solution is becoming more neutral in the BMIM-Cl solution.

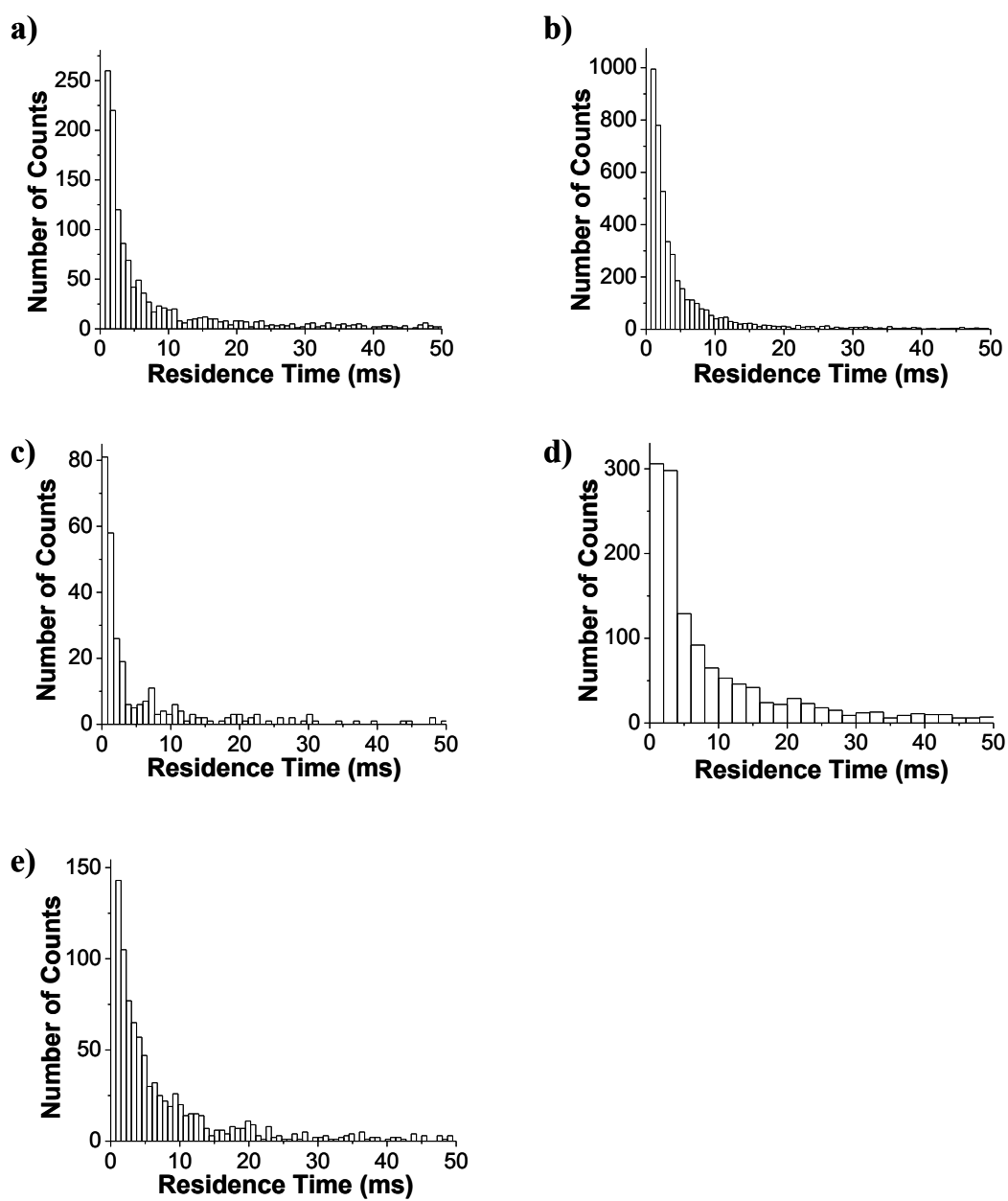


Figure 4.5 Event dwell time histograms of (a) $(dA)_{20}$; (b) $(dT)_{20}$; (c) $(dC)_{20}$; (d) $(dC)_{10}(dT)_{10}$; and (e) $(dCdT)_{10}$.

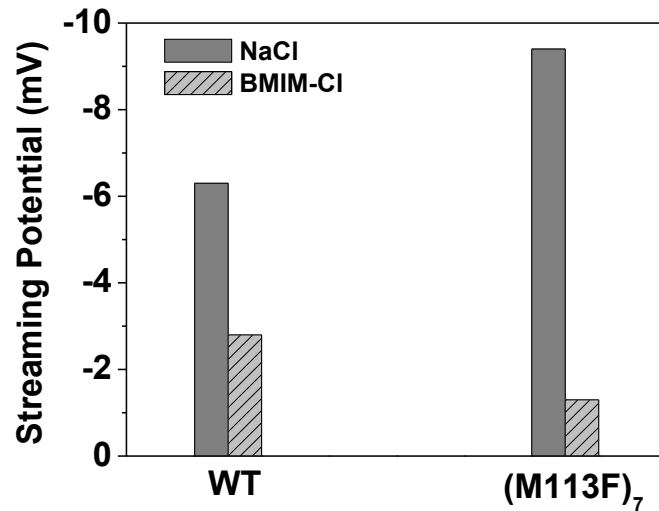


Figure 4.6 The mean residence times and current blockage amplitudes of five ssDNA samples in the wild-type α HL protein channel.

However, previous work suggests that although the frequency of DNA translocation events could be significantly affected by the charge selectivity of a protein pore, the translocation time is not greatly altered.³⁰ In addition, the constant impact of the charge selectivity of the protein pore on molecular transport (e.g., the event residence time)^{59, 63} could not explain our observation that the long-lived events only accounted for a small portion of the total events. Contrary to the observation that poly(dA) translocates through the α HL pore more slowly than poly(dCdT) in the KCl solution,¹⁴⁴ the residence time of (dCdT)₁₀ events were larger than that of (dA)₂₀ with the BMIM-Cl solution. This suggests that the interaction between nucleotides and the protein pore could be significantly influenced by the presence of the imidazolium cation.

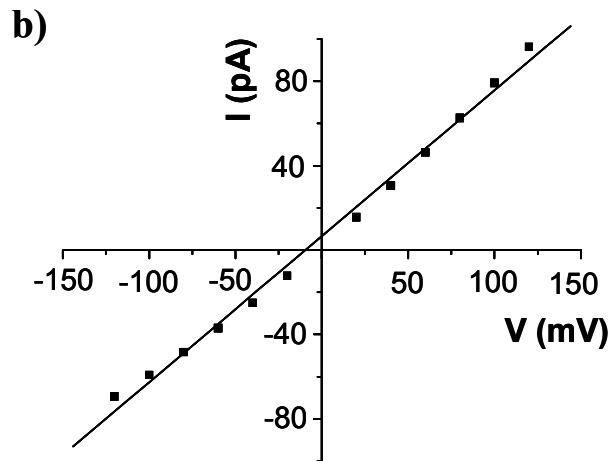
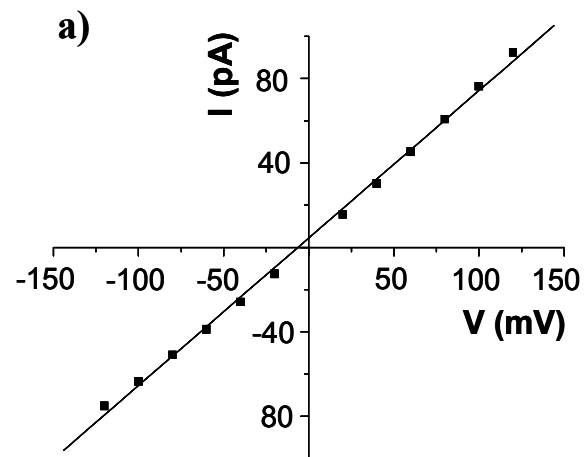


Figure 4.7 Determination of the streaming potentials of α HL channels in NaCl solution.

I-V curves for the (a) wild-type and (b) mutant (M113F)₇ α HL protein pores based on recordings made with *cis*: 1 M NaCl, 10 mM Tris-HCl (pH 6.0); *trans*: the same buffer solution as *cis* plus 1 M urea. Streaming potentials obtained were -6.3 mV, and -9.4 mV for the wild-type and mutant (M113F)₇ α HL pores, respectively.

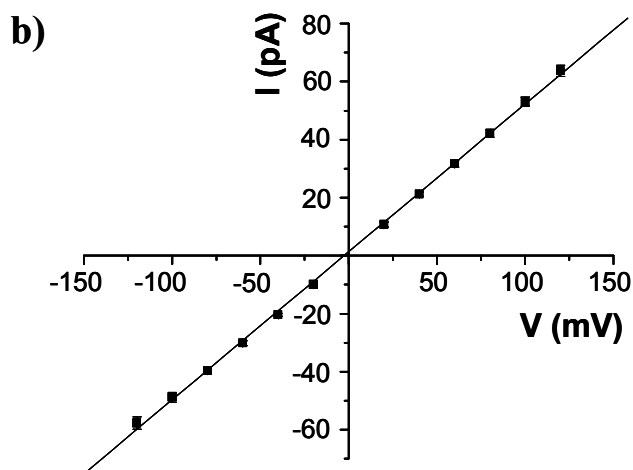
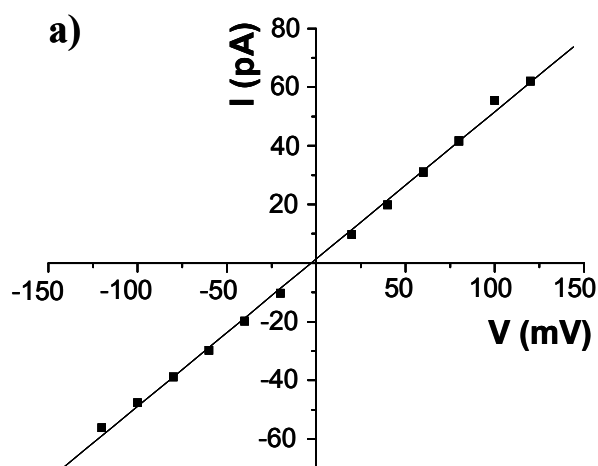


Figure 4.8 Determination of the streaming potentials of α HL channels in BMIM-Cl solution.

I-V curves for the (a) wild-type and (b) mutant (M113F)₇ α HL pores based on recordings made with *cis*: 1 M BMIM-Cl, 10 mM Tris·HCl (pH 6.0); *trans*: the same buffer solution as *cis* plus 1 M urea. Streaming potentials obtained were -2.8 mV, and -1.3 mV for the wild-type and mutant (M113F)₇ α HL pores, respectively.

It is known that the diameter of the constriction region of the α HL pore is only slightly larger than the diameter of a ssDNA polymer.¹⁵⁷ Thus, in order for a ssDNA

molecule to translocate through the α HL pore, the counterions need to be squeezed in the narrow water-filled space surrounding the DNA.¹⁵⁸ Compared with the naked K^+ (radius, 1.33 Å) or Na^+ (radius, 0.97 Å),¹⁵⁹ the bulky $BMIM^+$ (length, 11.0 Å; width, 5.8 Å)¹⁶⁰ is much larger. Furthermore, recent studies have suggested that the interaction between $BMIM^+$ and DNA is very strong, so much so that DNA could be extracted by ionic liquid $BMIM-PF_6$ solution.¹⁶¹ The strong interaction between $BMIM^+$ and DNA might be attributed to the interaction of the bulky organic $BMIM^+$ and P-O bonds of phosphate groups in the DNA molecule,¹⁶¹ and/or the electrostatic interaction between $BMIM^+$ and DNA.¹⁶² Therefore, it is not unreasonable that it would be much more difficult to squeeze DNA molecules through the narrow α HL pore in $BMIM-Cl$ than in KCl or $NaCl$ solution. Considering that the long-lived $(dA)_{20}$ events only accounted for 2.5% of the total events and the significant difference in the residence times of two types of events, it is likely that the large duration events were attributed to the threading of the DNA- $BMIM^+$ complex through the pore. In contrast, the short-lived events were due to the translocation of uncomplexed DNA molecules or the rapid entrance/exit of the DNA- $BMIM^+$ complex at the cis opening of the channel (e.g., the DNA- $BMIM^+$ complex enters the vestibule, moves toward the β -barrel but does not traverse through the limiting aperture, but instead retracts backward to the cis side and exits). We are leaning toward the latter interpretation of the short-lived events. Further experiments are required to resolve the origin of these events.

To further demonstrate the bulky cation effect on DNA translocation, $(dA)_{20}$ was examined with the $(M113F)_7$ pore using other common organic salt solutions, and the same prolonged DNA translocation phenomenon was observed. For example, in a solution containing 1 M tetramethylammonium chloride the mean

residence time of $(dA)_{20}$ in the $(M113)_7$ α HL pore was ~ 4.1 ms (Figure 4.9).

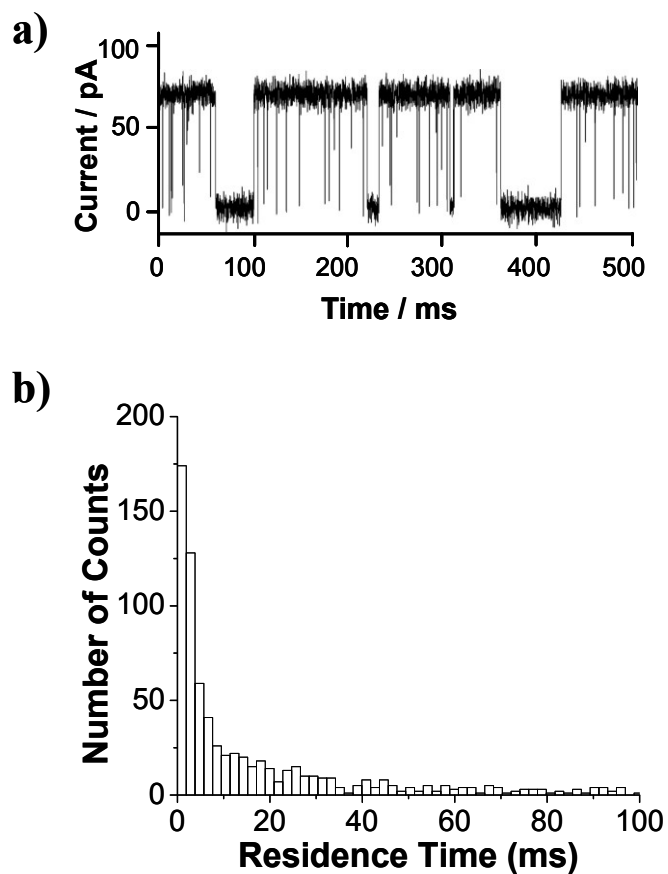


Figure 4.9 Translocation of $(dA)_{20}$ in the mutant $(M113F)_7$ α HL pore in 1 M tetramethylammonium chloride solution.

(a) Representative single channel current recording trace, and (b) dwell time histogram of long duration events.

4.4 Conclusions

In summary, we have demonstrated that by using electrolyte solutions that contain organic salts instead of NaCl/KCl, a ~2 order of magnitude reduction in the velocity of DNA translocation through protein pores can be achieved. Compared with other physical conditions, such as temperature, ionic strength, viscosity, etc.,¹⁶³ the effect of organic salts on DNA translocation was far more significant. It is likely that the strategy used in this work could be employed together with other experimental conditions by synthetic nanopores^{66,164,165} to substantially decrease the rapid DNA translocation velocity. Further experimental, theoretical, and computational research is necessary to understand and clarify how the organic salt solutions slow down the DNA translocation in the nanopores.

CHAPTER 5

LIGAND GATED α -HEMOLYSIN CHANNEL, TRIGGERED BY PH EFFECT

5.1 Introduction

Transmembrane protein ion channels (or pores) play an important role in selectively transporting molecules and ions essential for various signaling, physiological, and metabolic activities. In such a process, the protein pore acts as a signal transducer that senses chemical and physical stimuli, leading to the opening and closing of an ion channel⁸⁸ (also known as gating). Gating may be reversible or irreversible depending upon the intra/extracellular environment.^{166,167} Numerous pH gated,¹⁶⁶ voltage-gated,^{168,169} mechanical gated,^{158,170} and ligand gated^{88,171-173} ion channels have been found in nature. Gated channels offer the potential as a useful tool for controlled drug delivery.¹⁷¹

Stochastic sensing has provided a unique platform for probing such channel gating studies that might have potential applications in medicine, fuel cell, and analytical chemistry.¹⁷⁴ Both biological ion channels embedded in planar lipid bilayers and artificial nanopores fabricated in solid state membranes have been used as stochastic sensor elements to detect analytes at the single molecule level. When individual molecules pass through a nanometer-sized pore at a fixed applied potential bias, the modulations of the ionic current flowing through the pore can be detected as random events.² This approach reveals both the identity and the concentration of an analyte: the former by its characteristic current signature, typically the residence time (τ_{off}) of the analyte coupled with the extent of the channel blockage (amplitude), and

the latter from the frequency of occurrence ($1/\tau_{on}$) of the current modulations. Since each analyte produces a characteristic signature, the sensor element itself does not need to be highly selective, and multiple analytes can be quantitated simultaneously using a single sensor element, as long as the sensor itself can provide enough resolution. The most widely used sensor element in stochastic sensing is a single transmembrane protein α -hemolysin (α HL) pore, which has a ~ 3 nm diameter *cis* entrance and ~ 2 nm diameter *trans* opening.¹¹ The constriction of the α HL channel has a diameter of ~ 1.4 nm. The genetically engineered versions of α HL have been used as stochastic sensing elements for the detection of a wide variety of substances such as: organic molecules,²⁵ anions,¹⁵ cations,¹³ explosives,^{23,24} enantiomers,²² reactive molecules,²⁶ proteins,^{16, 17} DNA,^{20,21,146} peptides¹⁵¹ and their cleavage products.¹⁷⁵

In our previous study, we have successfully introduced ionic liquid solutions as advantageous supporting electrolytes to the nanopore technology.²⁴ Specifically, the use of butylmethylimidazolium chloride (BMIM-Cl) solution instead of the commonly used NaCl/KCl solution as a supporting electrolyte enhances the nanopore resolution, and also permits the analysis of ions and molecules, (e.g., liquid explosives and mono-valent cations¹⁹) that are difficult or even impossible to achieve in the inorganic salt solution. Here, we report that ionic liquid tetrakis(hydroxymethyl)phosphonium chloride [P(CH₂OH)₄-Cl] solution can induce gating for the α HL channel. Further, the opening and closing of the α HL pore is regulated by the pH of the solution.

5.2 Experimental section

5.2.1 Materials

Except that bis-tetrakis(hydroxymethyl)phosphonium sulfate [$\text{P}(\text{CH}_2\text{OH})_4\text{-SO}_4$] was obtained from TCI Chemicals Inc (Portland, OR), all the other reagents, including $\text{P}(\text{CH}_2\text{OH})_4\text{-Cl}$ were obtained from Sigma-Aldrich (St. Louis, MO).

All the electrolyte solutions, i.e., 1 M $\text{P}(\text{CH}_2\text{OH})_4\text{-Cl}$, 1 M $\text{P}(\text{CH}_2\text{OH})_4\text{-SO}_4$, 1 M BMIM-Cl, 1 M NaCl, and 1 M Bis-Tris methane were prepared in HPLC-grade water unless otherwise stated, and buffered with either 10 mM citric acid/sodium citrate buffer (pH range = 3.0 – 6.2) or 10 mM NaH_2PO_4 (pH range: $\text{pK}_1 = 1.7\text{-}2.9$, $\text{pK}_2 = 5.8\text{-}7.2$, $\text{pK}_3 = 11.3\text{-}13.3$). A stock solution of 4 mM β -cyclodextrin (βCD) was also prepared in HPLC-grade water (ChromAR, Mallinckrodt chemicals), and was used as the analyte of this study.

The wild-type αHL monomer was first synthesized by coupled *in vitro* transcription and translation (IVTT) using the *E. Coli* T7 S30 Extract System for Circular DNA from Promega (Madison, WI). Subsequently, they were assembled into homoheptamers by adding rabbit red cell membranes and incubating for 1 h⁸⁶. The heptamers were purified by SDS-polyacrylamide gel electrophoresis and stored in aliquots at -80°C .

5.2.2 Methods

A bilayer of 1,2-diphytanoylphosphatidylcholine (Avanti Polar Lipids; Alabaster, AL, USA) was formed on an aperture (150 μm) in a Teflon septum (25 μm thick; Goodfellow, Malvern, PA, USA) that divided a planar bilayer chamber into

two compartments, *cis* and *trans*. The formation of the bilayer was achieved by using the Montal-Mueller method,²⁷ and monitored by using a function generator (BK precision 4012A; Yorba Linda, CA, USA). The experiments were performed at 22 ± 1 °C in various electrolyte solutions as described in the “materials” section. The α HL protein (with the final concentration of $0.2\text{--}2.0 \text{ ng}\cdot\text{mL}^{-1}$) was added to the *cis* compartment, which connects to “ground”, while the analyte was added from the *trans* compartment. Once the channel inserts into the bilayer, the mushroom cap of the α HL pore positions towards the *cis* compartment, while the β -barrel of the α HL is located at the *trans* of the chamber device. The applied potential was -40 mV , unless otherwise noted. Currents were recorded with a patch clamp amplifier (Axopatch 200B, Molecular Devices; Sunnyvale, CA, USA). They were low-pass filtered with a built-in four-pole Bessel filter at 5 kHz and sampled at 25 kHz by a computer equipped with a Digidata 1440 A/D converter (Molecular Devices). To shield against ambient electrical noise, a metal box was used to serve as a Faraday cage, inside which the bilayer recording amplifying headstage, stirring system, chamber, and chamber holder were enclosed.

5.2.3 Flow nanopore sensing device

To facilitate adjusting the pH of the solution in the bilayer chamber compartments, a flow set-up was constructed. As shown in Figure 1, four channel peristaltic pump, PP (Dynamax, Rainin, 0.1 in. i.d. pump tubing, 0.8 rotations per minute; rpm), was used to perform buffer exchange, where a polyvinyl chloride (PVC) pump tubing (0.75 mm internal diameter, id) were connected to each channel of the PP. Two tubes, each connected to the *cis* and *trans* inlets of the reaction chamber (RC), supplies the desired electrolyte from the reservoir to the RC, and the other two

tubes connected to the outlet of *cis* and *trans* compartments withdraws the electrolyte to be replaced from the RC to waste (Figure 5.1). The buffer exchange process is carried out in such a way that the liquid level inside the reaction chamber is constant. A low flow rate of 0.2 mL/min was maintained in order to prevent any disruption to the bilayer and the inserted protein channel. Pump tubings were further connected to polytetrafluoroethylene (PTFE) tubes (0.86-mm i.d., 1.68-mm o.d., 20 SW).

pH adjustments and on-line monitoring of pH performed at 22 ± 1 °C by pH microprobe electrode, (P/N MI-414-4 cm pH combination Electrode, Microelectrodes Inc.) connected to a pH meter (Symphony SB70P, VWR) for all the experiments. Pre determined amount of 6M NaOH / 6M HCl was added to both *cis* and *trans* sides, in order to change the pH during on/off-line experiments and confirmed using the pH meter.

The ^1H NMR, and ^{31}P NMR spectra were recorded for 1 M $\text{P}(\text{CH}_2\text{OH})_4\text{-Cl}$ at pH 3.0 then at pH 6.0, which was obtained by the addition of pre-determined amount of 6 M NaOH to the solution, and back at pH 3.0 by adding 6 M HCl to the same solution. The readings were taken after incubation at room temperature for 24 hours and also on-line without any incubation. Further, readings were taken with and without the buffer.

Data analysis was achieved using Clampfit 10.0 software (Molecular Devices) and Origin 6.0 (Microcal, Northampton, MA). Mean residence times (τ values) for the analytes were obtained from dwell time histograms by fitting the distributions to single exponential functions by the Levenberg-Marquardt procedure. All the results were reported as mean values \pm standard deviation.

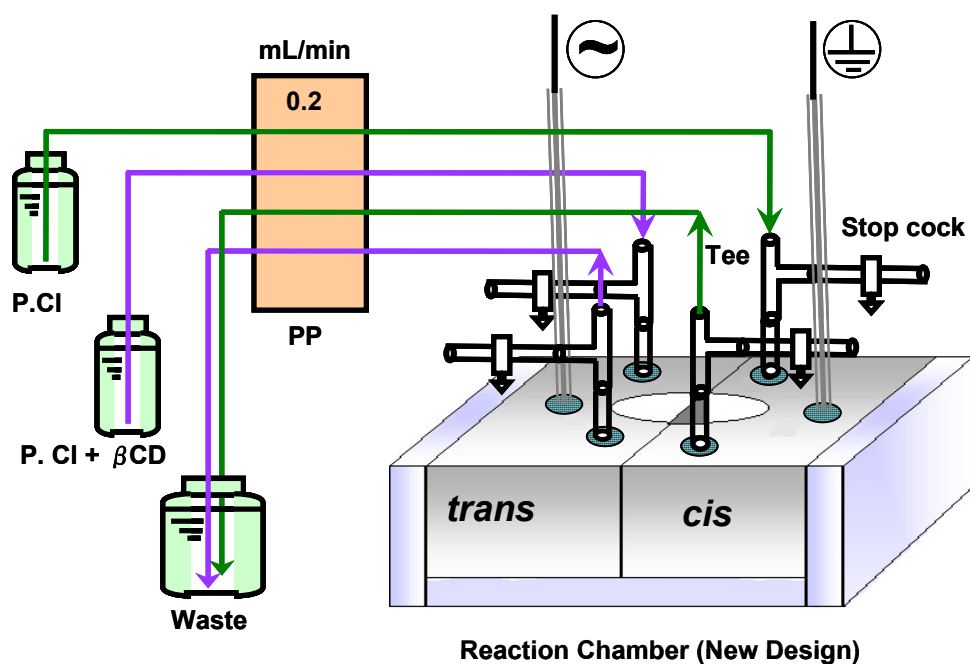


Figure 5.1 Schematic representation of the flow set-up.

5.3 Results and discussion

5.3.1 The effect of pH on the binding of β CD to the α HL pore in the $P(\text{CH}_2\text{OH})_4\text{-Cl}$ solution

The initial experiments were carried out at -40 mV in 1 M $P(\text{CH}_2\text{OH})_4\text{-Cl}$ solutions with various pH, ranging from pH 3.0 to 6.9. The results showed that, with the increase in the pH of the solution, both the channel current and the residence time of β CD decreased (Figures 5.2 and 5.3). When the pH of the solution is larger than ~ 5.6 , β CD events disappeared, and a larger current noise was observed.

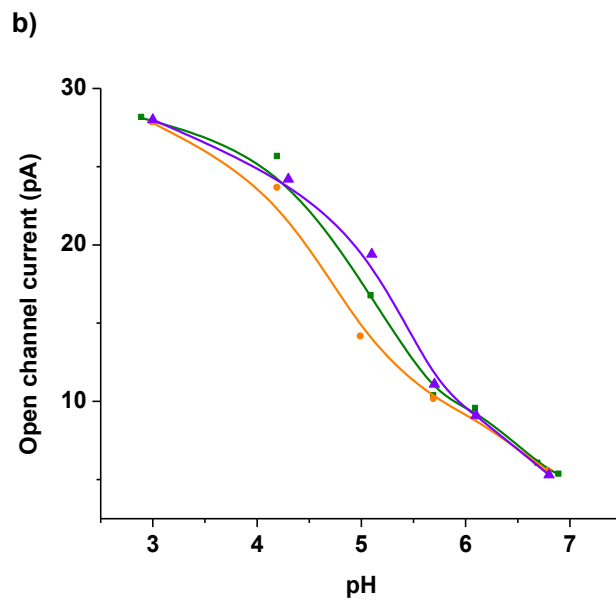
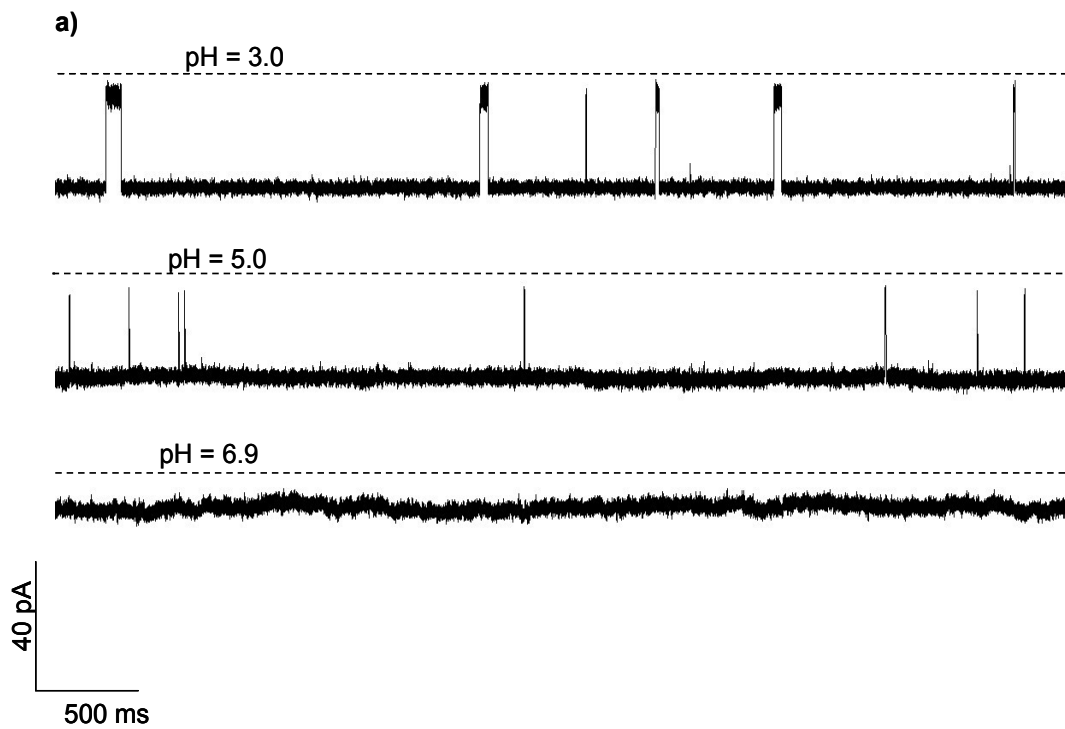


Figure 5.2 The effect of pH on the current of the α -hemolysin channel and the interaction between β CD and the α -hemolysin pore.

a) Single channel current recording traces; and b) the plot of the channel current vs. pH of the solution. The experiments were performed in 1 M phosphonium IL at (-) 40 mV

One likely interpretation is that the gating of the α HL pore might occur, thus preventing β CD's binding to the pore when the pH of the solution is larger than pH 5.6.

5.3.2 The effect of pH on the α HL channel in other electrolytes

To investigate whether the α HL channel gating phenomenon was induced by the $\text{P}(\text{CH}_2\text{OH})_4\text{-Cl}$ solution or was only due to the pH effect, four other solutions were examined including $\text{P}(\text{CH}_2\text{OH})_4\text{-SO}_4$, BMIM-Cl, NaCl and Bis-Tris methane (Zwitter ionic buffer with pKa of 6.46). Our experiments showed that, in the BMIM-Cl, NaCl and Bis-Tris methane solutions, although the channel current and the residence time of β CD decreased with an increase in the pH of the solution, the current noise was not changed significantly; furthermore, the β CD events could still be observed (Figure 5.3). This suggests that the α HL pore does not lose functionality in these electrolytes solutions under various pH values, thus ruling out the possibility that gating was only to the pH effect. When 1M $\text{P}(\text{CH}_2\text{OH})_4\text{-SO}_4$ solution was used, again the gating behavior has been observed (data not shown, $n = 3$). Note that the pH effect on event dwell time was also observed by other researchers, which may be attributed to the charge selectivity of the protein pore.^{59,96}

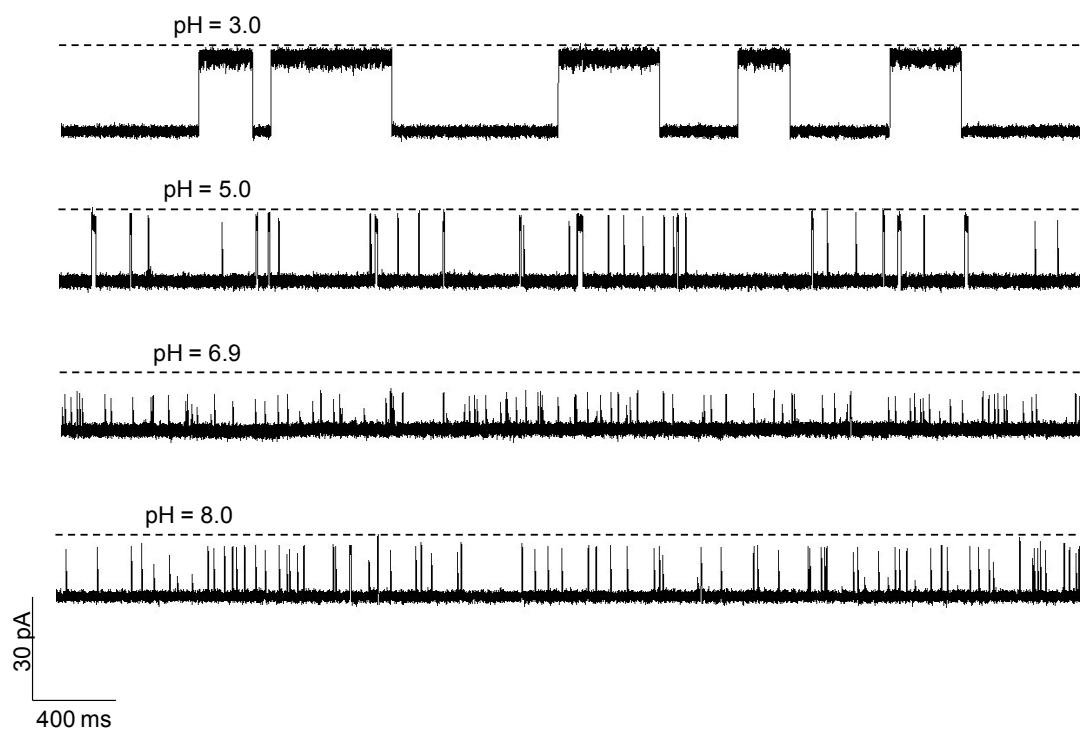


Figure 5.3 pH Dependence of the β -CD's binding to α HL channel.

The experiments were performed in 1 M BMIM-Cl solution at (-) 40 mV. Similar phenomena were observed in 1 M NaCl and 1 M Bis-Tris methane solutions (data not shown) where the channel current and dwell time of the β CD decreased as pH of the solution increased.

5.3.3 Understanding the gating phenomenon

The blockage of the mutant α HL channel by phosphate compounds (ligands) has been reported previously,¹⁵ and shown to be voltage dependent. Moreover, to understand the gating behavior, generating a channel I-V curve and making “noise” measurements are usually employed.^{88,173} Figure 5.4 illustrates the effect of voltage on both gated e.g., at pH 6.0 and open e.g., at pH 3.0 channels in 1 M $P(\text{CH}_2\text{OH})_4\text{-Cl}$ solution. It is clear that at pH 3.0, the channel current varies linearly with the applied

voltage, whereas the applied voltage does not affect the channel current at pH 6.0. Further the α HL channel current showed an increased noise level at pH 6.0 than at pH 3.0 (data not shown).

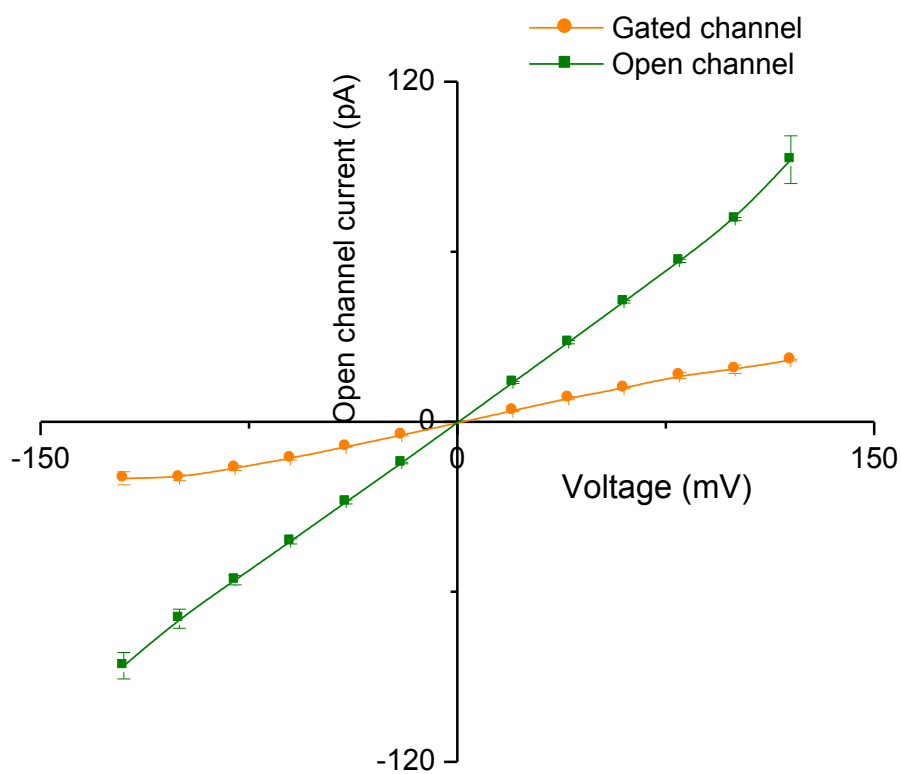
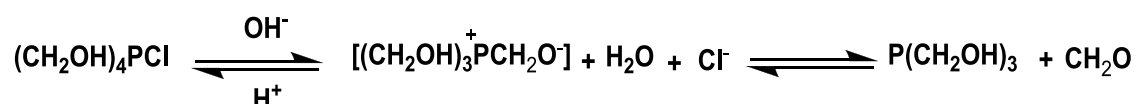


Figure 5.4 Voltage effect on both gated and open channels.

Taken together, the experimental results suggest that $P(\text{CH}_2\text{OH})_4\text{-Cl}$ is responsible for the channel gating, whereas pH acts as the molecular switch. Note

that, P(CH₂OH)₄-Cl is a monoprotic acid, which has an apparent pKa of 5.5.¹⁷⁶ As mentioned previously, we found at pH 5.48, the αHL channel is in open state but at pH 5.6 it is closed.

Further, the extant literature¹⁷⁷ suggests that P(CH₂OH)₄-Cl reacts with NaOH as follows:



To support the proposed mechanism as depicted in the above equation, NMR studies were carried out at different pH values. Data clearly suggests that there is a change in phosphonium moiety at lower and higher pH. At pH 3.0 it behaves as a cationic species which becomes a neutral species above pH 5.6. The results also showed that the reaction is reversible with a high rate constant, even without any incubation. Due to its reversible nature, P(CH₂OH)₄-Cl was subjected for on-line reversibility study.

The preliminary online reversibility was studied with two different directions: one, from lower pH to higher pH, and the other, from higher to lower pH. In the first case, the experiment was carried out at (-) 40 mV in 1M P(CH₂OH)₄-Cl solution at pH 3.0 and in the presence of 80 μM βCD. Then, pre-determined amount of 6M NaOH was added sequentially to both the *cis* and *trans* terminals till the channel gates. For the second case, similar approach was adopted by starting from pH 6.0 with sequential addition of 6 M HCl until the channel opens. Although a desired channel gating was observed while moving from lower pH to higher pH (n=5) (Figure 5.5), but

the reverse direction could not be achieved due to the bilayer instability occurred upon addition of 6M HCl (n=10).

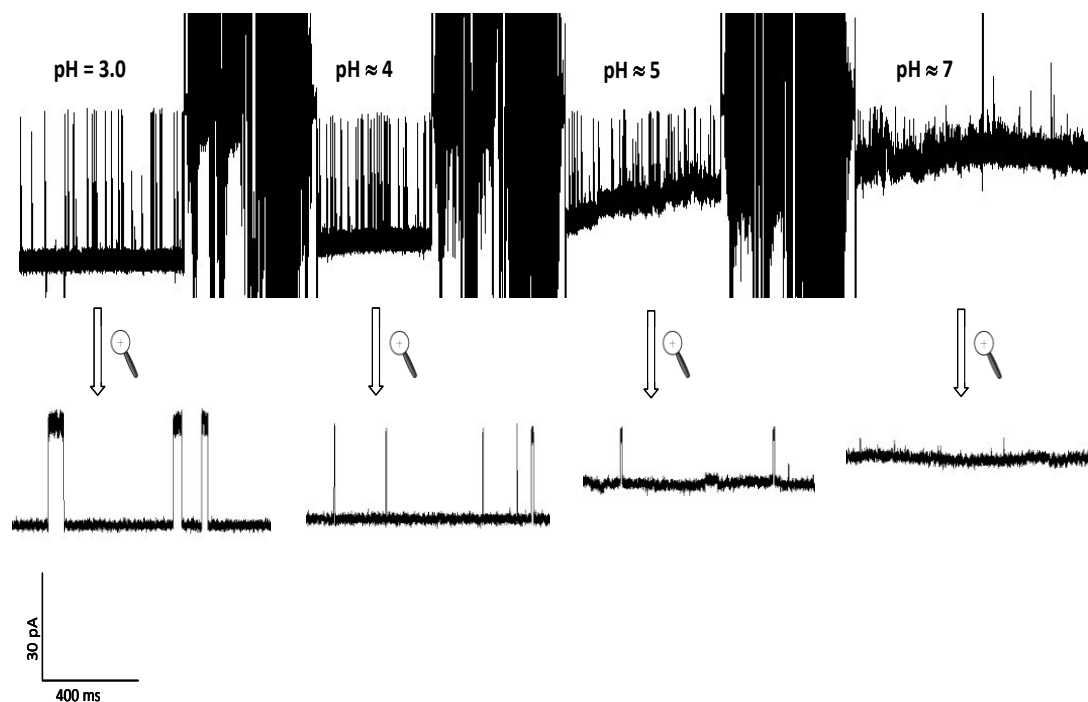


Figure 5.5 Online study of pH dependence while adding NaOH, up to pH 7.0.

To overcome the effect of HCl on the lipid bilayer, a flow set-up was integrated to the nano-pore stochastic sensing device as described in the experimental section, which can efficiently perform buffer exchange without breaking the bilayer and disturbing the channel. In this study, the experiment began with 1M $P(CH_2OH)_4\text{-Cl}$ (pH 6.0), in the presence of βCD . After insertion of the αHL pore into the lipid bilayer and single channel recording for ~2 minutes at (-) 40 mV, the electrolyte solutions in both the *cis* and *trans* compartments were replaced with

1M P(CH₂OH)₄-Cl solution (pH 3.0) via the PP at a flow rate of 0.2 ml/min. To maintain the concentration of the analyte constant throughout the experiment, the solution which would be flowed into the *trans* compartment was pre mixed with 80 μM βCD. Note that the flow rates, as well as the tube length and diameter were prior optimized for maintaining the liquid level, which is critical for the bilayer stability and single channel recording. It takes ~12 minutes to replace the electrolyte solution from the RC using the flow set-up, judged by the open channel current as well as the pH value measured online using a pH microprobe. Once the channel opens, the trace was recorded for another 5 minutes. And then, a pre-determined amount of 6M NaOH was added directly to both the *cis* and *trans* compartments to change the pH of the solution back to pH 6.0. Although the flow setup was capable of refilling the compartment with the pH 6.0 electrolyte solution again, we preferred manual addition of the NaOH solution to raise the pH, as this approach is faster and does not affect the existing bilayer and the protein pore. The online monitoring of pH effect on the αHL channel in 1 M P(CH₂OH)₄-Cl solution was performed with both buffered [(citric acid and sodium citrate) n=3] and unbuffered (n=10) solution. The results are presented in Figure 5.6, which confirms that the gating is indeed reversible.

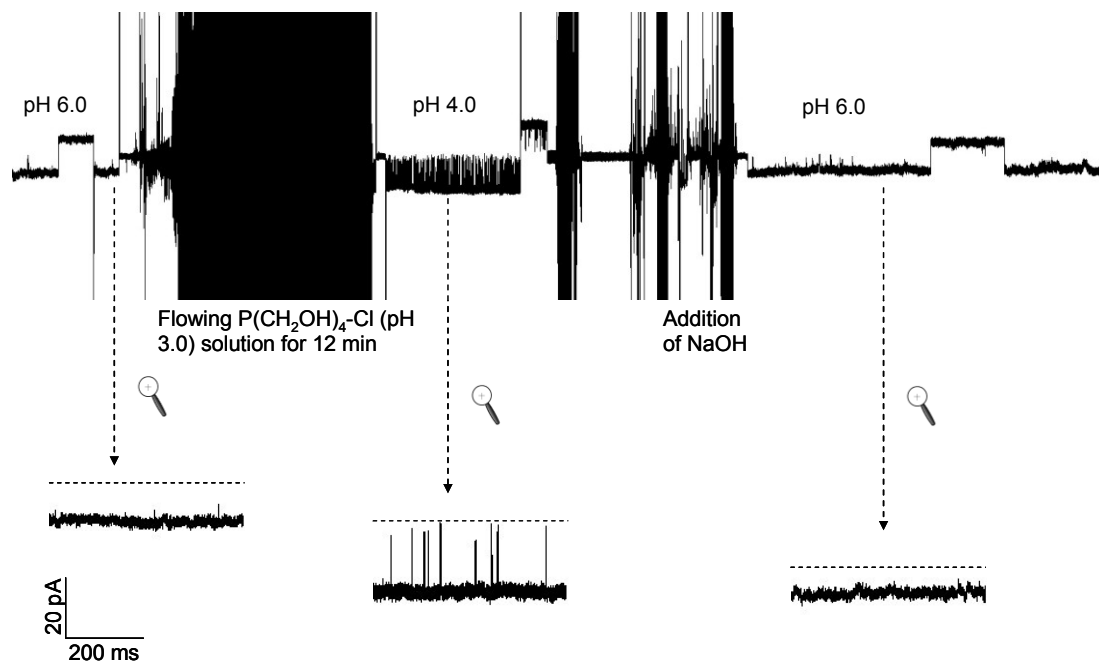


Figure 5.6 On-line monitoring of the pH effect on the α HL channel in the presence of $80 \mu\text{M}$ βCD .

Showing that the gating of the α HL channel by the $\text{P}(\text{CH}_2\text{OH})_4\text{-Cl}$ solution is reversible by adjusting the pH of the solution.

5.3.4 Investigating the gating mechanism in the α HL pore

As described in the previous sections, the gating phenomenon was observed in the $\text{P}(\text{CH}_2\text{OH})_4\text{-Cl}$ solution with pH larger than 5.5. To support our hypothesis that the gating may be attributed to $\text{P}(\text{CH}_2\text{OH})_3$, four sets of experiments were performed in 1M NaCl solution with or without $\text{P}(\text{CH}_2\text{OH})_4\text{-Cl}$ or $\text{P}(\text{CH}_2\text{OH})_3$ in the presence of βCD . Specifically, the first set of experiments involved with 1 M NaCl at pH 3.0 and with the addition of $\text{P}(\text{CH}_2\text{OH})_4\text{-Cl}$ to the *trans* compartment with 10 mM sequential increment (up to 60 mM), and then to the *cis* compartment in the similar fashion. The second set of experiments was the same as the first one with the except that

P(CH₂OH)₄-Cl was added to the *cis* first. The third and fourth sets of experiments were similar to the first and second sets respectively, except that the experiments were carried out at pH 6.0. The results turned out that at pH 3.0, βCD signal (the event mean dwell time and amplitude) didn't change significantly upon addition of P(CH₂OH)₄-Cl even up to 60 mM to both the *cis* and *trans* compartments (n=3). In case the of pH 6.0, the addition of P(CH₂OH)₃ to the *trans* compartment up to 60 mM didn't result the disappearance of the βCD events, but caused a noticeable reduction in both the open channel current and the frequency of the βCD events. In sharp contrast, at pH 6.0, a complete gated channel was observed when 30 mM of P(CH₂OH)₃ was present in the *cis* compartment. Moreover, the voltage effect on these gated channels were also studied, and the experiments showed that the αHL channel could not restore to the open stage at the voltage range (20-300 mV) we tested suggesting a voltage independent gating. Similar experiments were also performed in 1M BMIM-Cl solution instead of the 1 M NaCl solution (n=3), and we observed similar results. This provides further evidence that gating is due to the binding of tris(hydroxymethyl)phosphine to the αHL pore, which occurs in solutions with relatively large pH values.

5.4 Conclusion

By adding phosphonium ion in the αHL pore and adjusting the pH of the electrolyte solution, the αHL channel can be controlled close or open. This approach can be employed to develop a novel molecular switch to regulate molecular transport, which may find useful application as a 'smart' drug delivery method.¹⁷⁸

Furthermore, gating mechanism has been also investigated. A variety of other ILs and their solutions are currently being investigated to examine whether the gating phenomena in the α HL pore is limited to the phosphonium IL.

CHAPTER 6

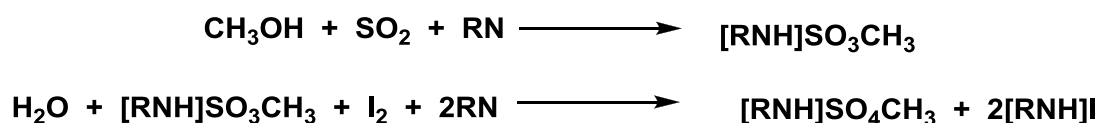
A RAPID GAS CHROMATOGRAPHIC WATER QUANTITATION METHOD, USING IONIC LIQUID STATIONARY PHASES

6.1 Introduction

The determination of water content in consumer products, such as foods, and pharmaceuticals, and to industrial materials/products, like solvents, oil and paint, is of great importance. Indeed analytical testing for the presence and concentration of water is one of the most frequent, important and ubiquitous measurements made in modern industrial society. Thus a versatile and simple analytical technique for the accurate quantification of water is imperative. Due to the essentially universal presence of water, accurate, facile and sensitive techniques are needed. Though various techniques such as gravimetry,³⁷ Karl Fisher titration (KFT),^{38,39} gas chromatography,⁴⁰⁻⁴⁹ near IR spectrophotometry,^{40,50-52} solvatochromic sensing,⁵³ ¹⁹F-NMR spectroscopy,⁵⁴ isotope ratio mass spectrometry (IRMS)⁵⁵ and many more have been reported in the literature, only few are accepted widely and used.

Currently, the most commonly used method for water analysis is KFT, which was first published in 1935 by the chemist, Karl Fischer.³⁸ In this titrametric method, I₂ is reduced to HI in the presence of water.⁴⁵ There are four components in the Karl Fischer reagent consisting of; Iodine, sulfur dioxide, a suitable base [(RN); originally pyridine was used but now imidazole is used] and a suitable solvent (methanol, ethanol, diethylene glycol monomethyl ether..etc).¹⁷⁹

The accepted mechanism of this reaction is composed of two steps;



The end point is determined potentiometrically. There are two types of KFT methods available. They are, coulometric titration and volumetric titration. The former is used to detect trace amounts of water, ranges from 10 µg to 99 µg (1 ppm – 5%), which requires ~ 5 g of sample.¹⁸⁰ On the other hand, volumetric titration is used to detect higher water quantities; > 1 mg (10 ppm – 100%) and the amount of sample required varies from 0.1 mg to 500 mg.¹⁸¹

Despite the fact that this is a well established method, interference of side reactions,⁴⁵ reagent instability, sample insolubility⁵⁶ and pH issues⁴⁰ prevent it from being accepted as a universal method. Some KFT methodologies have been developed in an attempt to overcome these issues^{39,45,56}. However, many issues still remain, not the least of which is that there is residual water in most KFT reagents. Another applied method for water detection is based on gas chromatography. Early attempts using gas chromatography were mainly based on packed (molecular sieves) columns, involving both direct detection by thermal conductivity detector (TCD)^{43-45,47,49} and indirect detection (i.e. reacting water with calcium carbide to convert to acetylene) by flame ionization detection (FID)⁴¹. Peak asymmetry,⁴⁰ poor sensitivity, adsorption of water by the stationary phase,⁴³ overlapping of the water peak by other larger peaks, and the inability to detect higher amounts of water⁴⁰ delayed its practical applications. Attempts to eliminate peak asymmetry,^{40, 57} using wide-diameter open tubular columns⁴² and capillary columns⁴⁶ showed some

success. Also most conventional capillary column GC stationary phases are degraded by water.

In this study, we examine ionic liquid (IL) based capillary gas chromatographic method with TCD for the direct determination of water content in liquid samples. The unique nature of ILs including; high thermal stabilities,⁵⁸ variable polarities^{30, 35} and exceptional stability to water and oxygen make them excellent choices as stationary phases for this methodology. As will be shown, open tubular capillary columns, coated with specific IL stationary phases (developed for water analysis) can tremendously increase the sensitivity and reliability of this technique. Furthermore analysis time can be decreased to 5 min or less in many cases, and samples with virtually any concentration of water can be analyzed. The efficiency of this approach is demonstrated on 50 different solvent samples.

6.2 Experimental

6.2.1 Apparatus

The analysis was performed using an Agilent Technologies 6890N gas chromatograph (Agilent technologies Inc., Wilmington, DE), equipped with a 7683B series autoinjector, TCD and Chemstation plus software (Rev. B.01.03). An agilent technologies 10 µl syringe (5181-1267), has been used with the autosampler, and a Hamilton 10 µl syringe was used for manual injection. The other parameters are shown in Table 6.1.

The fused silica capillary columns were coated with IL stationary phases synthesized as previously reported.^{58, 182} Static coating was done at are from

Supelco (Bellefonte, PA). The columns were 30 m long, 0.25 mm internal diameter (I.D.) and 0.2 μm film thickness.

Table 6.1 GC/TCD parameters for the analysis of water.

Carrier gas	Helium
Carrier gas flow rate (ml/min)	1.0
Inlet temperature ($^{\circ}\text{C}$)	250
Detector temperature ($^{\circ}\text{C}$)	250
Injection volume (μl)	Vary (0.2 – 5)
Oven temperature ($^{\circ}\text{C}$)	Vary (40 – 120)
Analysis mode	Splitless

6.2.2 Materials

The water reference material: 8509, moisture in methanol (MeOH, 93 ± 13 ppm water) was obtained from National Institute of Standards and Technology (NIST, Gaithersburg, MD). The 4 Å molecular sieves, tetrahydrofuran (THF) and both the IS; acetone and acetonitrile were purchased from Sigma-Aldrich (St. Louis, MO). The high purity water was obtained by filtering the deionized water with Millipore, synergy 185. The testing solvents were from, Sigma-Aldrich, Mallinckrodt, EMD, Fisher, Omni solvent, and Acros organics (see Appendix 1 for more information).

6.2.3 Calibration standard and sample preparation

The accurate quantification of water was achieved using two internal standards (ISs); either acetone or acetonitrile to avoid co-elution with the bulk solvent. Hence, two different calibration samples were prepared for the quantification of water per each column. One for the acetone, with MeOH (NIST) matrix and the other for acetonitrile with anhydrous THF matrix. "IS" is used to represent either acetone or acetonitrile and "matrix" represents either THF or MeOH. It should be noted that both ISs and THF were dried beforehand with 4 Å molecular sieves, which were activated by drying overnight at 300 °C, and cooling to ambient temperature. All the samples were prepared in 2 ml, amber autosampler vials sealed with screw caps containing white silicon/red PTFE septums. These vials were dried 100 °C for overnight before use. Also, the sample preparations were done under ultra high purity argon, at room temperature 22±1 °C. All the volumes were measured with Eppendorf adjustable pipettes (0.1 – 2.5 µl, 2 – 20 µl and 100 – 1000 µl).

6.2.4 Methods

For initial screening, the columns were conditioned at 120 °C for 2 hours and high purity water was injected, 0.1 µl, using 100:1 split ratio at the desired temperature. The sample of interest is injected in the splitless mode (0.2 µl to 5 µl), in order to examine the separation between water and the bulk solvent. This helped in determining which IS would be used.

6.2.5 Preparation of IS calibration plots

First, the dried sample vials were sealed with the screw caps and allowed to cool to ambient temperature. Then, the empty bottles were weighed precisely to ± 0.001 g to obtain the initial weight. Predetermined amounts of high purity water, ranging from 0 to 10 mg were added to the vials using eppendorf adjustable pipettes (by opening the vials under high purity argon), they were sealed and re-weighed to get the final weight. After that, the vials were opened under high purity argon, 5 μ l of IS was added to each bottle and the matrix solvent resulting in a total volume of 1 ml. Once they were prepared, the vials were sealed with screw caps, and parafilm and stored in the desiccator, when ever not in use. Then, 0.2 μ l from each vial was injected to GC column at 70 $^{\circ}$ C in the splitless mode, at least three times to obtain successive chromatograms.

The peak area ratio of water and I.S. was calculated in such a way that, dividing the peak area of water by the peak area of IS. Then, the amount of water actually injected was calculated and the calibration curve of ; peak area ratio of water and I.S. vs amount of water injected (ng) was constructed. By obtaining the x-intercept of the plot, the actual amount of water in the 1st point (0 amount of water added) was obtained. With this value, a correction was made only for that point and the graph was re drawn. This graph was used to calculate the amount of water in the sample of interest. It should be noted that all these steps were carried out within one day. Once the calibration plot was constructed for a particular IS, and column, it was used for the entire study. In addition to these IS calibration plots, another calibration plot was constructed using only the water standard (in MeOH, NIST) and injecting different volume to find the linearity of the method. All the calculations and

regression analysis (for 95% confidence limit) of the plots were performed using Microsoft office excel 2003.

6.2.6 Sample preparation and analysis

Samples were prepared in dried, sealed and cooled sample vials. First 5 μl of the IS of choice was added to the sample vial and then the solvent of interest was added to bring the total volume to 1 ml, by opening them under ultra high purity argon. After that, the sealed vials were further secured with parafilm and stored in the desiccator. Every day, a fresh sample of IS was tested, using NIST water standard (8509) as the bulk solvent to determine the amount of water in the IS. Then, the predetermined amount of volume (0.2 μl - 5 μl) was injected in to the GC under splitless mode, at the temperature of desired. The testing was carried out at least three times per sample. After obtaining the chromatograms, the peak area ratio of water and I.S. was calculated for all the samples. Then, using the calibration plot, the actual amount of water in the samples, as well as, in the IS was calculated. After subtracting the amount of water in the IS, the actual amount of water in the sample was obtained. Then using the density of the solvent, the actual amount of water in "ppm" (mg/kg) was obtained. All the data was reported in ppm with the percent relative standard deviation (RSD%).

6.2.7 Detection limit and quantitation limit

The detection limit (DL) and the quantitation limit (QL) were calculated according to the guidelines of the US Food and Drug Administration (FDA),^{183, 184} using the following equations:

$$DL = \frac{3.3 \sigma}{S}$$

$$QL = \frac{10 \sigma}{S}$$

Where,

σ = the standard deviation of the response

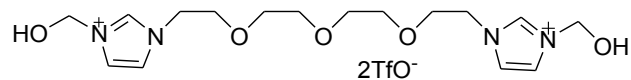
S = the slope of the calibration plot

The σ is normally obtained from the standard deviation of the blank sample.¹⁸⁴ Since it is impossible to obtain a sample without water, the 1st point of the calibration plot, where there is no added water is used as the blank sample and its standard deviation was used as σ . The slope was obtained from the regression analysis of the plot; peak area ratio of water and I.S. vs amount of water.

6.3 Results and discussion

Figure 6.1 shows the structures of the two ILs that were used as stationary phases for this analysis (the structures of all the other ILs tested are available in Appendix 2). Generally, IL stationary phases containing trifluoromethylsulfonate (TfO⁻) anions resulted in more symmetric peak shapes compared to those of that contained bis[(trifluoromethyl)sulfonyl]imide (NTf₂⁻), with the same cation (data not shown). In addition to the IL-based GC columns, a commercially available polyethylene glycol column was also studied for comparison purposes.

1) HMIM-PEG TfO₂⁻



2) TPT TfO₂⁻

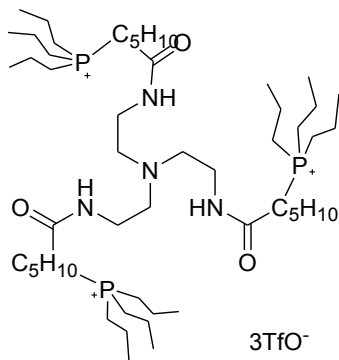


Figure 6.1 The structures of ILs that gave the best separation of water, when coated on fused silica capillary columns.

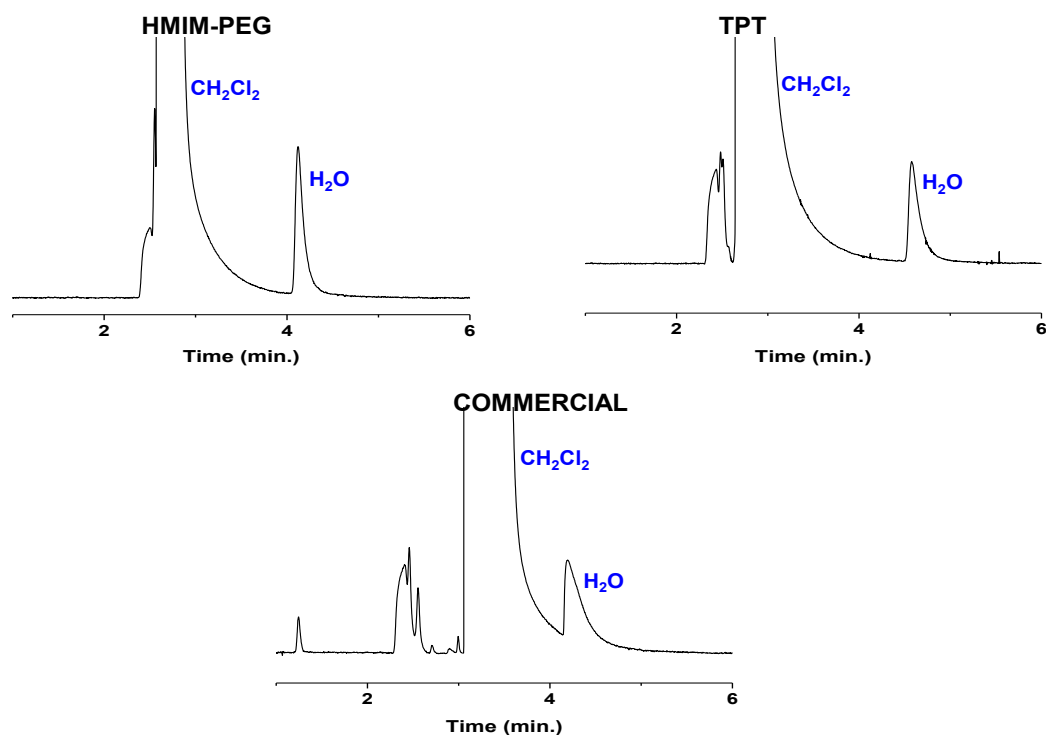


Figure 6.2 Separation of water from CH₂Cl₂ in examined columns at 80 °C.

As shown in Figure 6.2, all the IL columns gave a better separation of water and methylene chloride (CH₂Cl₂) and better peak shapes compared to the commercial column. It should be noted that the Figure 6.2 shows only the separation of water from the solvent CH₂Cl₂ which elutes before the water peak. However, there are solvents, such as dimethylformamide (DMF), dimethyl sulfoxide (DMSO)...etc which elute after the water peak. In all cases (for all solvent samples) the IL separations were substantially better. In addition the IL stationary phases are not adversely affected by water even after 1000 injections (not shown). Virtually all commercial columns (based on polyethylene glycol or polysiloxanes) show appreciable degradation from water coupled with changing/degrading chromatograms.

Table 6.2 Limits of detection and limits of quantitation of water in evaluated columns.

Type of plot	HMIM-PEG		TPT		Commercial	
	DL/ng	QL/ng	DL/ng	QL/ng	DL/ng	QL/ng
MeOH	7.0	21.1	6.7	20.3	23.3	70.5
MeOH/A	3.6	10.9	4.0	12.0	11.8	35.7
THF/C	2.1	6.3	5.6	16.9	12.9	39.1

Table 6.3 Detection of water in 50 solvents. X- couldn't separate the water peak from the solvent peak.

Sample	Reported water content (ppm)	HMIM-PEG			TPT		
		Water (ppm)	Std. dev. (±)	RSD%	Water (ppm)	Std. dev. (±)	RSD%
Acetic acid		105	0.8	0.8	76	7.4	9.6
Acetone	1000	1088	100.6	9.2	954	10.4	1.1
Acetonitrile	10	45	2.9	6.5	38	2.2	5.8
Anisole		x	X	X	232	20.6	8.9
Benzene	200	34	0.8	2.4	38	3.1	8.3
1-Butanol	1000	893	5.7	0.6	554	46.6	8.4
2-Butanol		1145	31.1	2.7	x	x	X
2-Butanone	400	431	16.7	3.9	569	6.9	1.2
<i>t</i> -Butyl alcohol	1000	4846	230.7	4.8	4607	71.0	1.5
Carbon tetrachloride		4	0.1	3.7	6	0.1	1.4
Chlorobenzene		3	0.3	9.2	5	0.4	8.0
1-Chlorobutane		20	0.8	4.0	12	1.0	8.2
Chloroform	200	56	1.5	2.7	42	5.6	8.0
2-Chloropropane		44	2.4	5.6	38	2.1	5.6
Cyclohexane		7	0.1	1.8	21	0.6	3.0
Cyclohexanone		168	3.3	2.0	149	14.7	9.9

Table 6.3 continued

1,2-Dichlorobenzene		x	X	X	3	0.2	6.0
1,2-Dichloroethane	60	91	1.9	2.1	81	6.8	8.4
1,3-Dichloropropane		458	19.3	4.2	X	x	X
Diethyl ether	300	264	4.9	1.8	266	4.6	1.7
Di(ethyleneglycol) ethyl ether		405	1.2	0.3	372	36.9	9.9
1,2-Dimethoxy-ethane (glyme, DME)	30	261	4.2	1.6	176	8.0	4.6
Dimethyl-formamide (DMF)	50	159	3.3	2.1	158	6.5	4.1
Dimethylsulfoxide (DMSO)	50	1347	2.4	0.2	931	24.2	2.6
Dioxane	30	2961	150.6	5.1	1428	7.5	0.5
Ethanol	30	1426	14.5	1.0	899	7.4	0.8
Ethyl acetate	2000	2302	42.9	1.9	2538	172.6	6.8
Ethylene glycol		85215	551.7	0.6	89873	8807.6	9.8
Heptane	71	12	0.6	5.2	11	0.2	1.7
Hexane	1	8	0.2	2.1	6	0.5	8.2
Methanol	500	3218	280.0	8.7	3361	200.0	6.0
Methyl <i>t</i> -butyl ether (MTBE)	200	262	3.1	1.2	232	2.8	1.2
Methylene chloride	147 ppt	5	0.3	5.6	21	1.5	6.8

Table 6.3 continued

<i>N</i> -methyl-2-pyrrolidinone (NMP)		2306	216.3	9.4	2830	25.7	0.9
Nitrobenzene		2	0.1	5.7	13	1.0	8.0
Nitromethane	500	564	29.6	5.2	x	x	X
Nitroethane		676	22.3	3.3	X	x	X
Octane		20	0.2	1.0	22	1.1	5.2
1-Octanol		302	1.9	0.6	72	6.6	9.1
Pentane	10	9	0.1	0.9	12	0.1	0.6
Petroleumether (ligroine)		19	0.1	0.4	28	1.2	4.1
1-Propanol	2000	5935	82.3	1.4	X	x	X
2-Propanol	1000	1609	25.0	1.6	465	35.5	7.6
Pyridine	30	X	X	X	312	15.1	4.8
Tetrahydrofuran (THF)	20	348	9.8	2.8	223	14.2	6.4
Toluene	10	32	0.1	0.3	15	0.3	1.8
Triethyl amine		56	0.2	0.3	57	0.1	0.2
<i>o</i> -Xylene		91	4.9	5.4	X	x	x
<i>m</i> -Xylene		3	0.3	8.2	X	x	x
<i>p</i> -Xylene		4	0.4	9.3	x	x	x

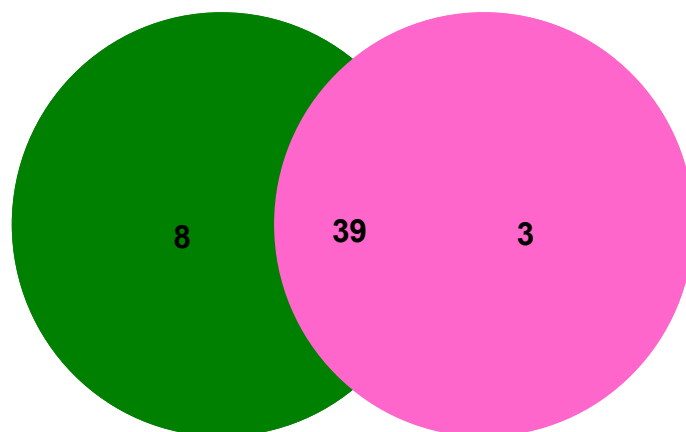


Figure 6.3 Summary of the detection of water by two IL columns; green is HMHM-PEG and pink is TPT.

The limits of detection and the limits of quantitation of IL columns (Table 6.2) are superior to those of the best commercial column (calibration plots are available in the Appendix 3). The detection limit of coulometric KFT is 10 μg , which requires 5 g of the sample. The IL based GC method required only 0.2 μl of sample to obtain a more lower detection limit (~ 2.0 ng or $\sim 5,000$ x greater sensitivity).

Table 6.3 consists of the final data for the water quantification in 50 different solvent samples using the two IL columns. Only 25 samples were investigated using the commercial column, for comparison. As illustrated in figure 6.3, the water peak of 39 samples out of 50, was separated from the solvent peak and quantified by both the columns. IL HMIM-PEG TfO⁻ showed the best results, as it was useful in the quantification of water in 47 samples, including 8 samples that were not amenable to separation on the other tested column. IL TPT TfO⁻ was used to quantify water in 42 solvents, including three samples which was not possible using the other column that

was investigated.

The commercial column was only able to quantify water in 18 solvents (out of 25 that were investigated). Additionally, the commercial PEG column cannot withstand as high operating temperature or water concentrations as the IL based columns can.

A study was carried out to check the absorption of atmospheric water during 24 hour period, in to the tested solvents, using IL HMIM-PEG TfO⁻ column under 40% - 60% relative humidity. It was done in two different sets. First set included low boiling point solvents; MeOH, Heptane and THF, which are representatives of water miscible, immiscible and moderately miscible respectively. Two identical sample vials were prepared for each solvent, keeping one vial well sealed, inside the desiccator, and the other outside, with the screw cap on, but without sealing the punched hole by the injector. According to the results, when desiccated and undesiccated samples are compared, the significant change in absorption of atmospheric water has been occurred after 1 hr, for MeOH and THF; and for Heptane (Appendix 4), it is after 2 hr. This is due to the low miscibility of water in Heptane.

The second set of samples included high boiling point solvents; DMF and DMSO, water miscible and moderately miscible, respectively. Here, three identical sample vials were prepared for each solvent, one kept inside the desiccator, completely sealed, the other outside with the screw cap on, and the third one, outside, without the screw cap i. e. open. The same trend as above has been observed for the desiccated and undesiccated, closed samples. In contrast to that,

the open solvent samples kept on absorbing water throughout the study (Appendix 5).

According to this study, the absorption of atmospheric water is minimal up to 1 hr when the samples are stored in sample vials sealed with screw caps containing white silicon/red PTFE septums.

6.4 Conclusions

In conclusion, an IL GC method has been successfully validated for the quantification of water in extremely diverse solvent samples. Limits of detection using this technique are far superior when compared to KFT. Furthermore, IL-CG methodology requires less sample and is free from other complications associated with KFT. Also, the IL GC method is independent of the chemical nature of the substance and is a solvent free method. When compared to other GC methods using a commercially available PEG columns, the IL based columns possessed superior selectivity for water in a plethora of materials. This approach has a potential to be developed as a rapid and ultra sensitive method to detect water, not only in liquids, but also in air and solid samples.

CHAPTER 7

SUMMARY

Ionic liquids (ILs), the salts which melt at or below 100 °C is an important class of compounds. The main focus of this dissertation is on their application on stochastic sensing technique and gas chromatography (GC).

The chapter 2 presented the systematic investigation of the translocation of aromatic peptides through the α -hemolysin pores in traditional NaCl background electrolyte. With a properly engineered protein pore, a series of short peptides, including those differing by only an amino acid were successfully differentiated. Further, the feasibility of utilizing the engineered protein pore for simultaneous detection of a mixture of peptides and even differentiation of peptide sequences were demonstrated.

After that, the implementation of ILs has been discussed. In chapter 3, the successful introduction of IL as the supporting electrolyte solution in nanopore technology for the first time was demonstrated. They permit the analysis of compounds that are difficult or even impossible to achieve in NaCl or KCl solution, e.g., liquid explosives and their sensitizers. Furthermore, the nanopore sensor sensitivity was enhanced in BMIM-Cl, IL solution as compared to NaCl solutions of the same concentrations.

Chapter 4 represented how IL salt solution slowed the DNA translocation velocities through the nanopore, which has been one of the key challenges to

nanopore DNA sequencing. The enhanced resolution achieved by this, permitted the convenient differentiation between various DNA molecules.

A new concept; pH triggered reversible ligand gating of α -hemolysin was demonstrated in the phosphonium IL salt solution, in chapter 5. The observations from chapter 3 through 5, showed the importance of IL supporting electrolyte in stochastic sensing technique. Further studies on the effect of other multifunctional ionic liquid solutions (see Appendix 6) and even with pure ionic liquids are currently in progress.

The last portion of this dissertation, the chapter 6 presented development of IL based capillary CG method for the determination of water content in 50 liquid samples. The increased sensitivity, speed, solvent free analysis, absence of interference and side reactions made this method superior to the existing methods.

APPENDIX A

DESCRIPTION OF SOLVENTS THAT ARE USED TO DETECT THE WATER CONTENT

Table A.1 Properties of the solvents

Sample Name	B.P. (°C)	Reported water content (ppm)	Vendor	Density (g/ml)
Acetic acid	118		Sigma	1.049
Acetone	56.2	1000	Fisher	0.786
Acetonitrile	81.6	10	Sigma	0.786
Anisole	154		Aldrich	0.995
Benzene	80.1	200	EMD	0.879
1-Butanol	117.6	1000	Sigma	0.81
2-Butanol	98		Fluka	0.808
2-Butanone	79.6	400	Fisher	0.805
<i>t</i> -Butyl alcohol	82.2	1000	Sigma	0.786
Carbon tetrachloride	76.7		Aldrich	1.594
Chlorobenzene	131.7		Aldrich	1.106
1-Chlorobutane	79		Aldrich	0.886
Chloroform	61.7	200	Sigma	1.498
2-Chloropropane	36		Aldrich	0.859
Cyclohexane	80.7		Fluka	0.779
Cyclohexanone	156		Sigma	0.947
1,2-Dichlorobenzene	179		Sigma	1.306
1,2-Dichloroethane	83.5	60	Acros org	1.245

Table A.1 continued

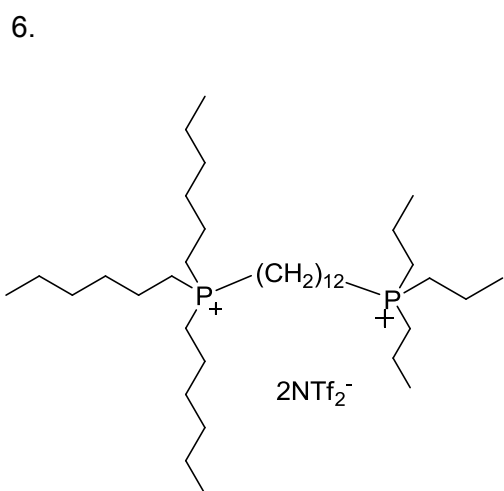
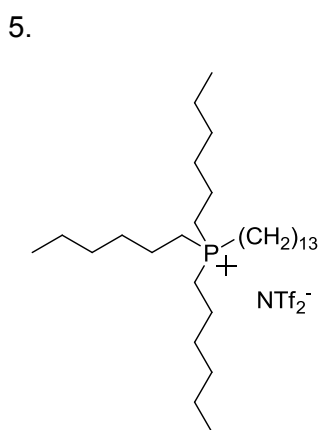
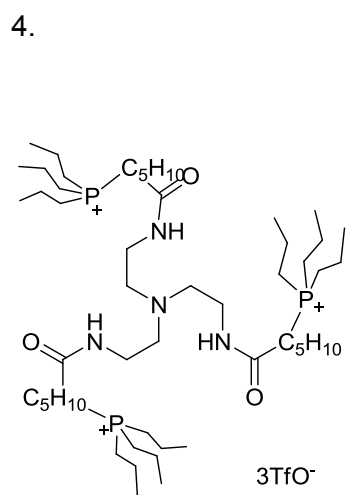
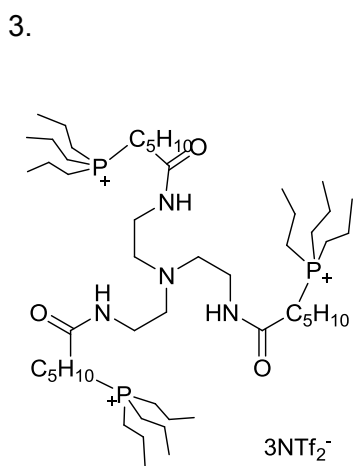
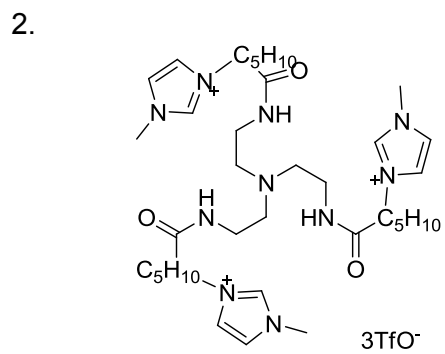
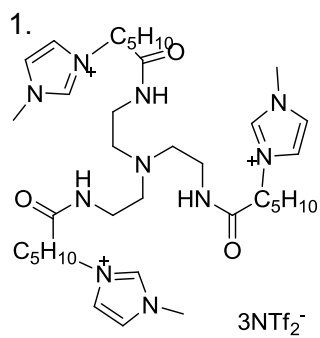
1,3-Dichloropropane	104		TCI	1.19
Diethyl ether	34.6	300	Sigma	0.713
Di (ethylene glycol) ethyl ether	196-202		Sigma	0.999
1,2-Dimethoxy-ethane (glyme, DME)	85	30	Sigma	0.868
Dimethyl- formamide (DMF)	153	50	Sigma	0.944
Dimethyl sulfoxide (DMSO)	189	50	Sigma	1.092
Dioxane	101.1	30	Sigma	1.033
Ethanol	78.5	30	Sigma	0.789
Ethyl acetate	77	2000	Mallinckrodt	0.895
Ethylene glycol	195		Sigma	1.115
Heptane	98	71	EMD	0.684
Hexane	69	1	Fisher	0.659
Methanol	64.6	500	EMD	0.791
Methyl <i>t</i> -butyl ether (MTBE)	55.2	200	Omni solv.	0.741
Methylene chloride	39.8	147 ppt	Omni solv.	1.326
<i>N</i> -methyl-2-pyrrolidinone (NMP)	202		Sigma	1.033
Nitrobenzene	210		Sigma	1.196
Nitromethane	101.2	500	Sigma	1.382
Nitroethane	112-116		Sigma	1.045
Octane	125		Sigma	0.703
1-Octanol	195		Sigma	0.827
Pentane	36.1	10	EMD	0.626
Petroleum ether (ligroine)	30-60		Mallinckrodt	0.656
1-Propanol	97	2000	Sigma	0.803

Table A.1 continued

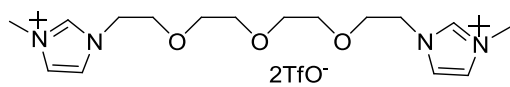
2-Propanol	82.4	1000	EMD	0.785
Pyridine	115.2	30	Sigma	0.982
Tetrahydrofuran (THF)	66	20	Sigma	0.886
Toluene	110.6	10	Sigma	0.867
Triethyl amine	88.9		Fluka	0.728
<i>o</i> -Xylene	144		Aldrich	0.897
<i>m</i> -Xylene	139.1		Acros Org.	0.868
<i>p</i> -Xylene	138.4		Fisher	0.861

APPENDIX B

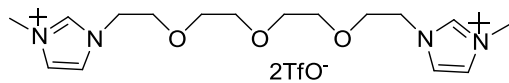
STRUCTURES OF ILS THAT ARE TESTED AS GC STATIONARY PHASES FOR
THE DETECTION OF WATER



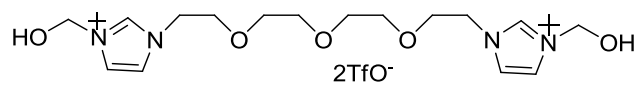
7.



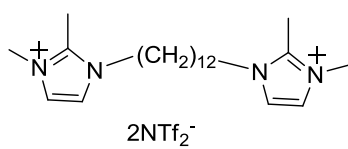
8.



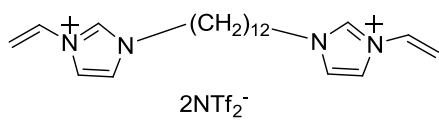
9.



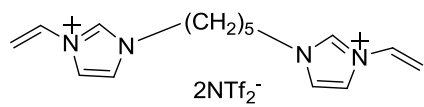
10.



11.

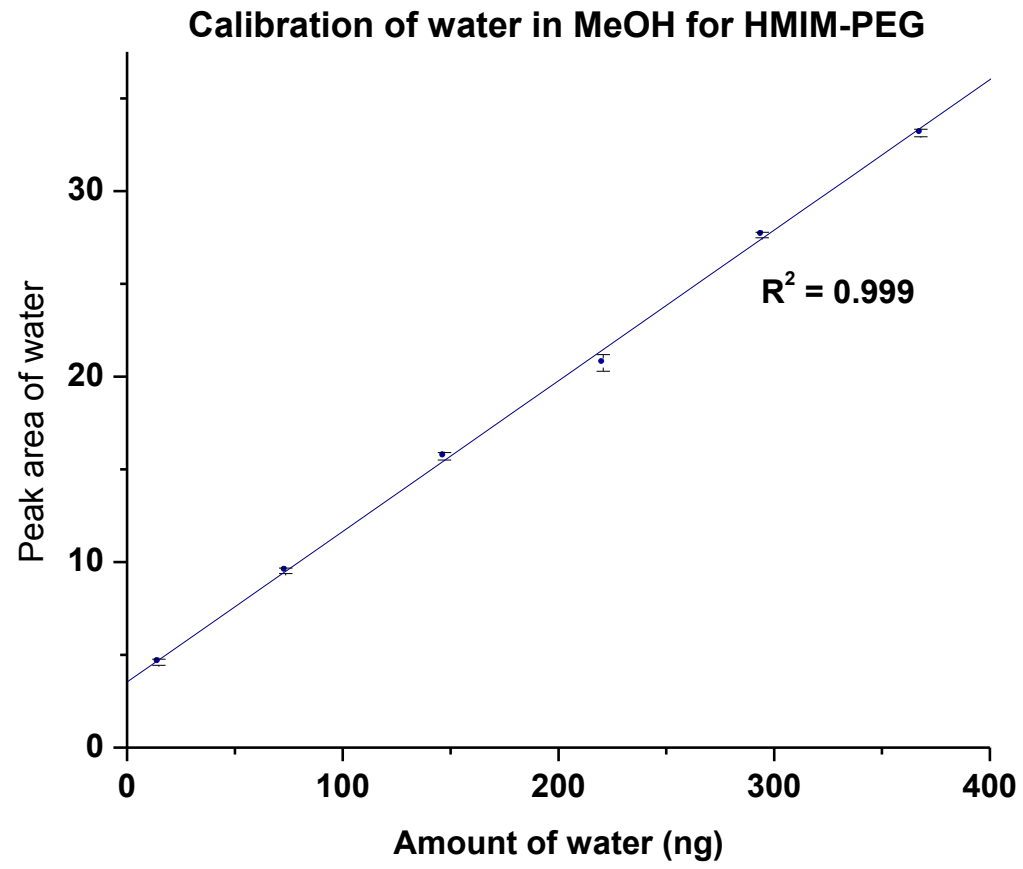


12.

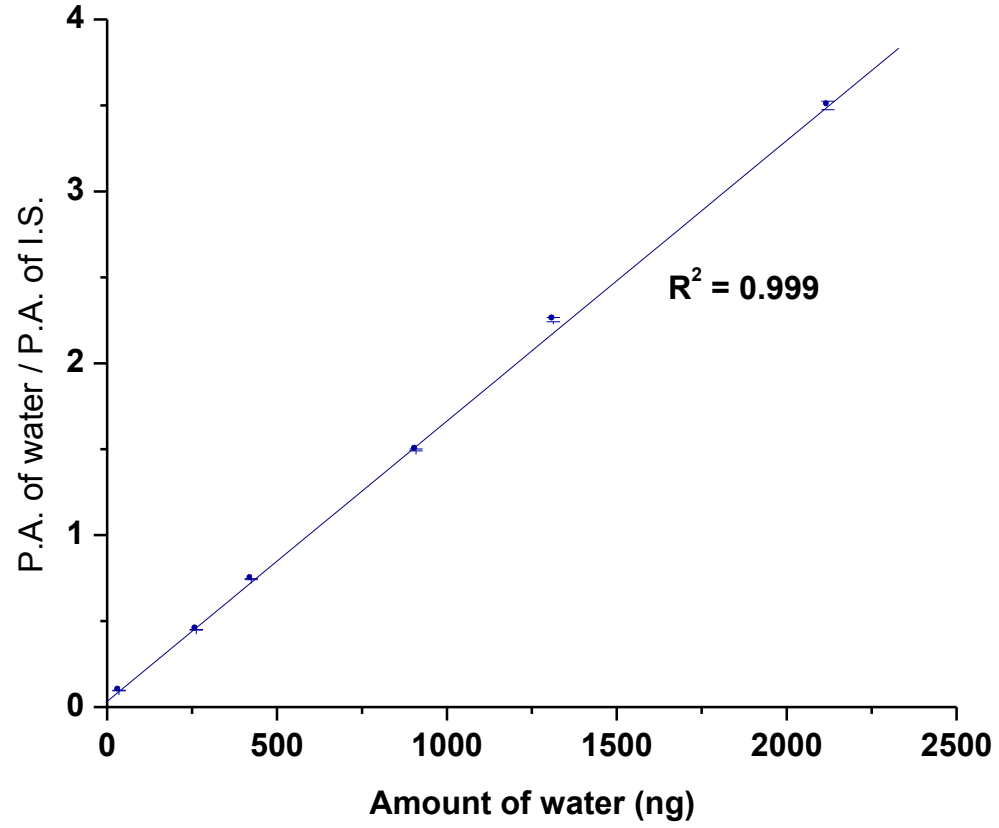


APPENDIX C

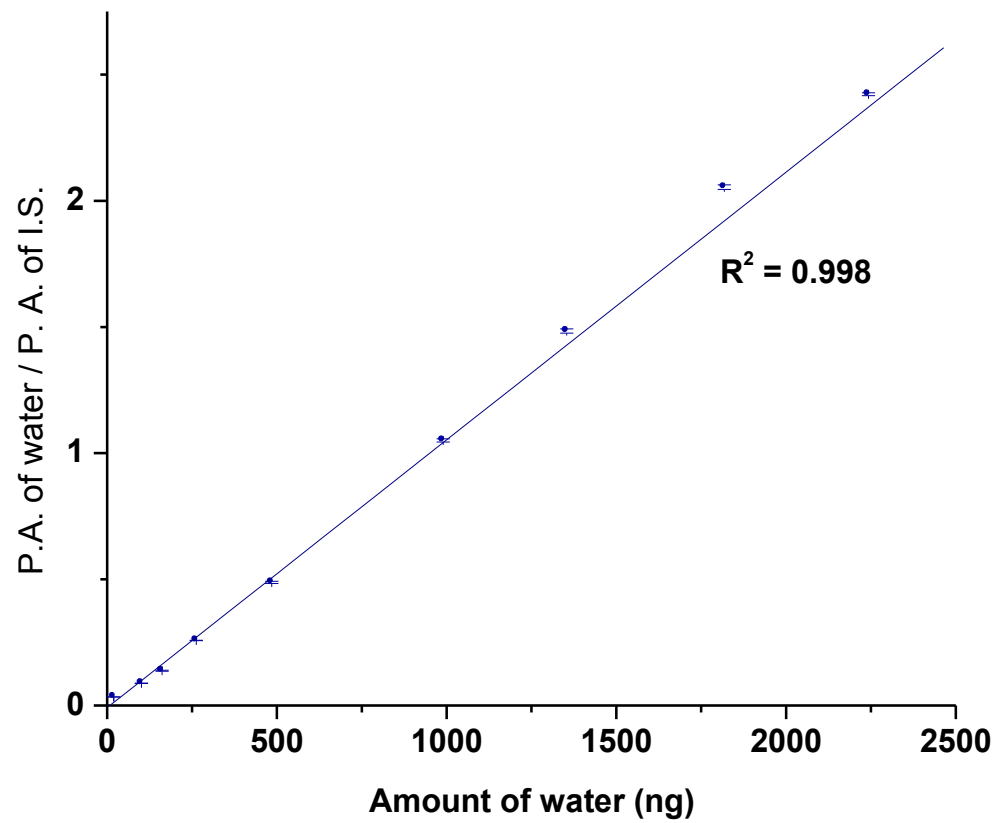
CALIBRATION PLOTS FOR WATER DETECTION STUDY

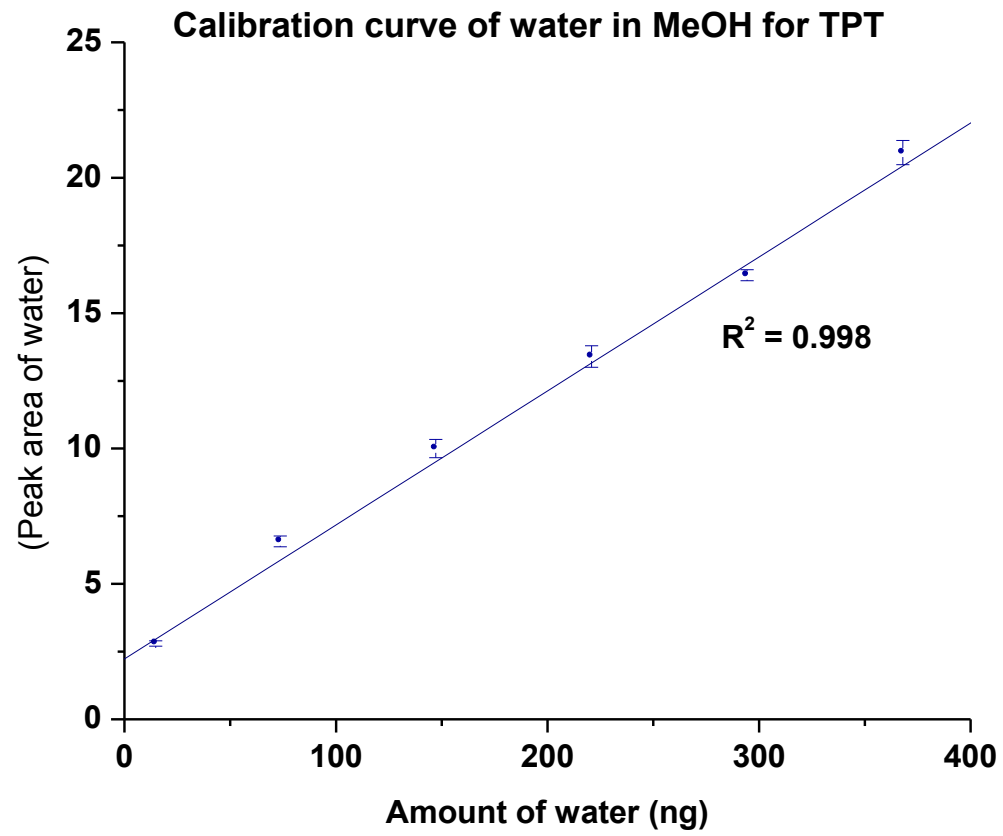


Calibration curve of water with acetone I.S. in MeOH for HMIM-PEG

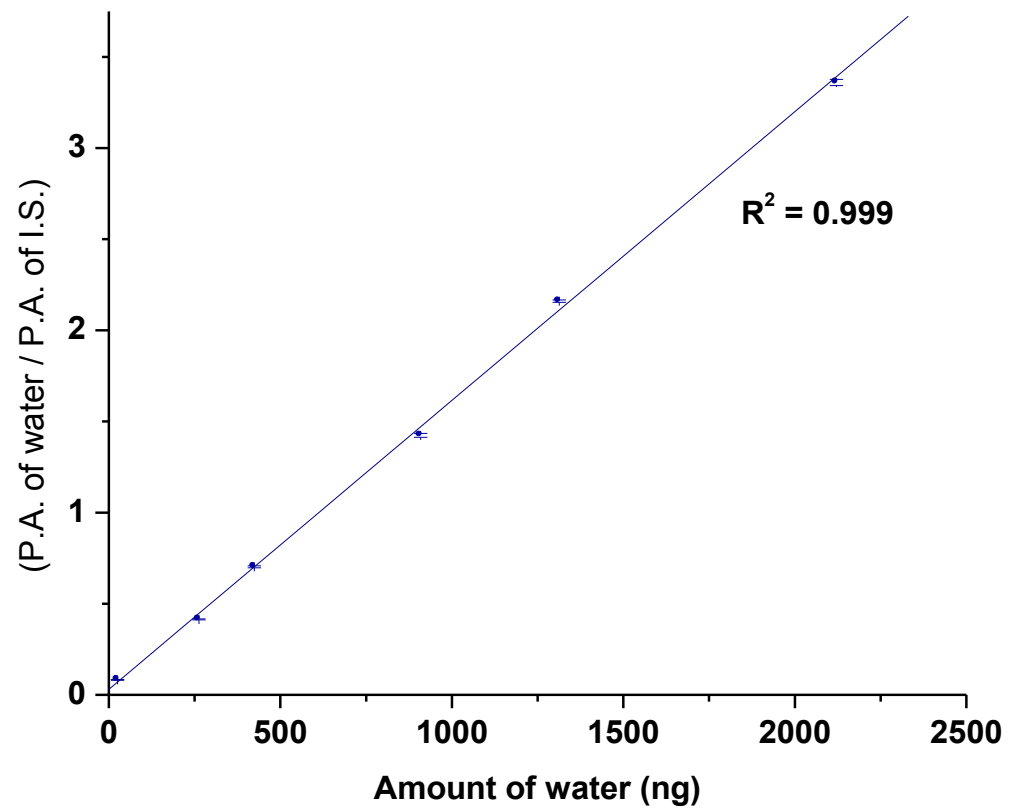


Calibration curve of water with acetonitrile I.S. in THF for HMHM-PEG

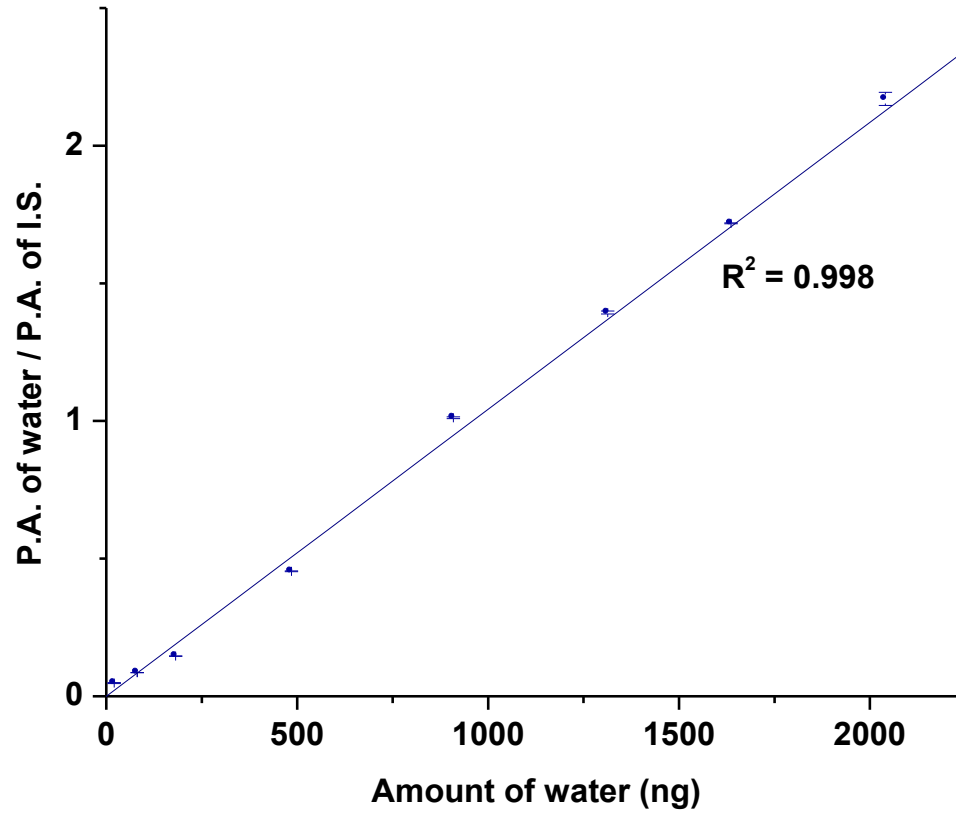




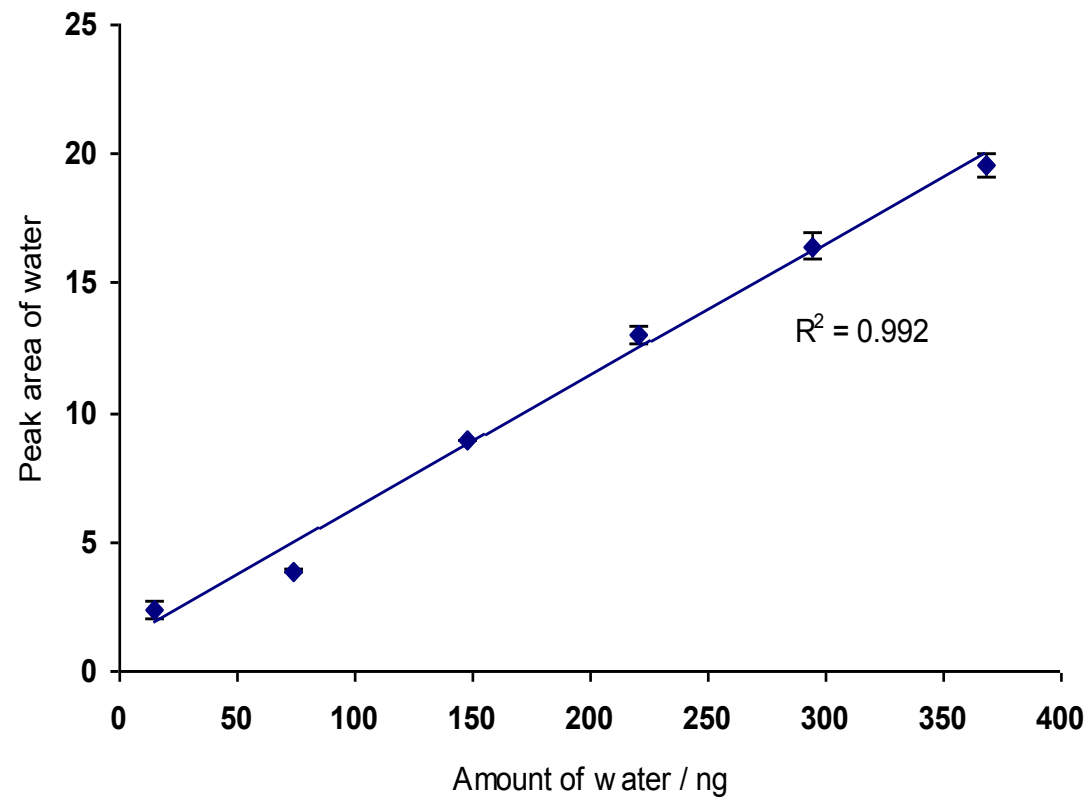
Calibration curve of water with acetone I.S. in MeOH for TPT



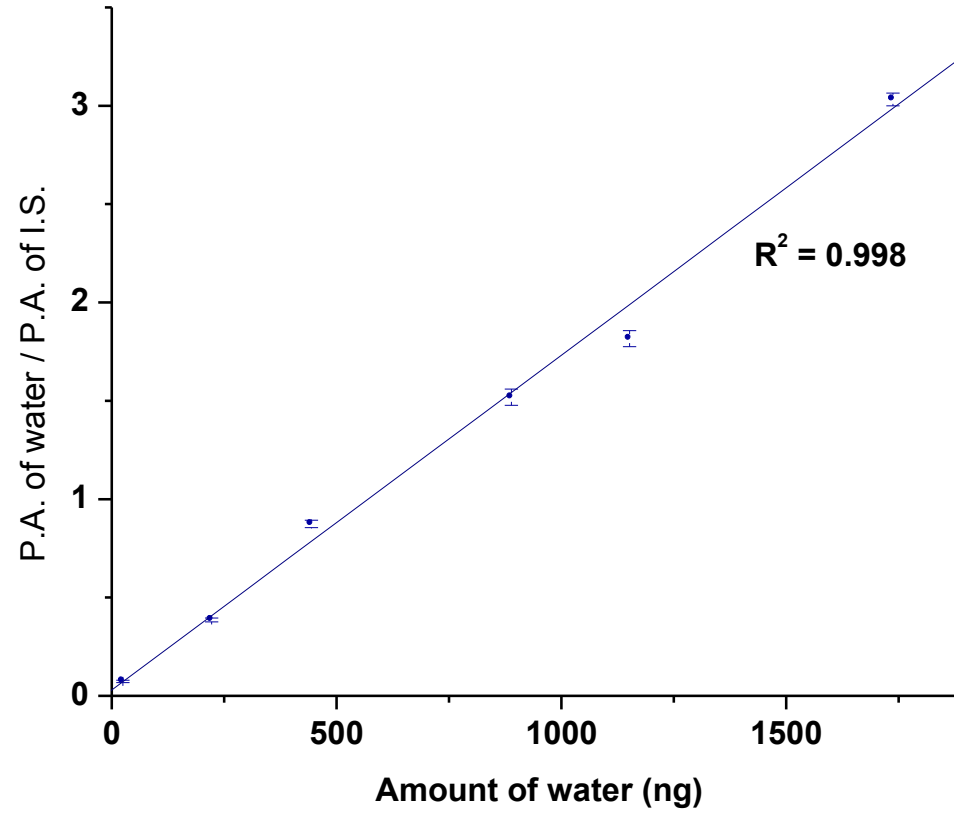
Calibration curve of water with acetonitrile I.S. in THF for TPT



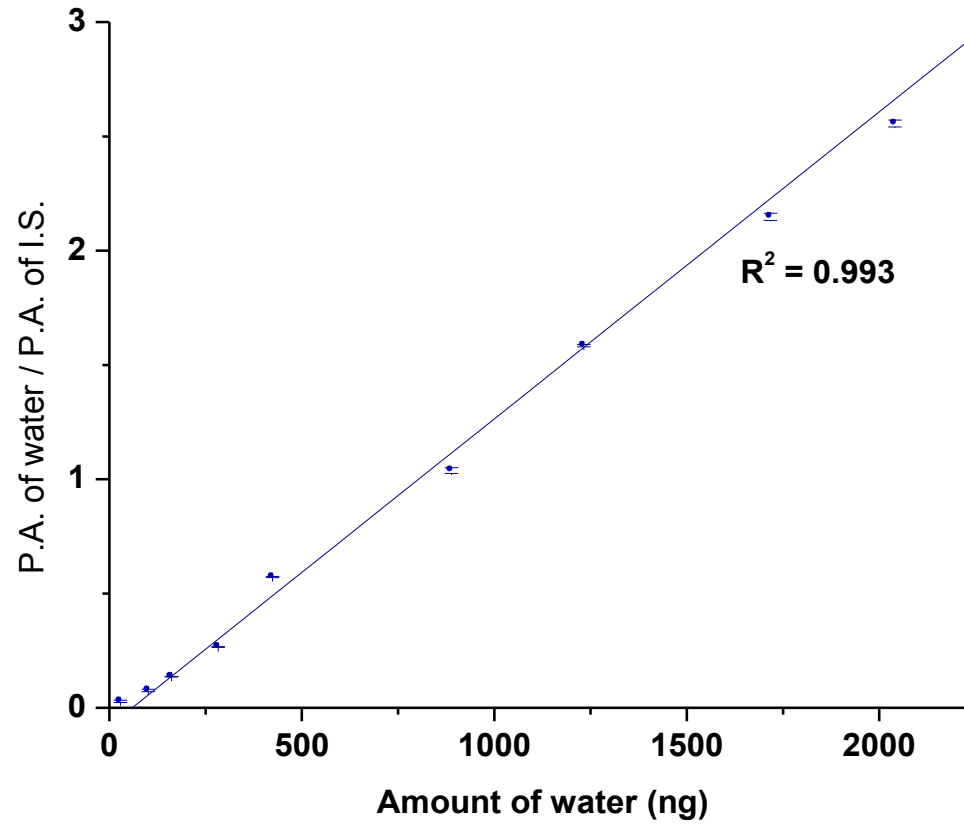
Calibration curve of water in MeOH for commercial column



Calibration curve of water with acetone I.S. in MeOH for Commercial C.



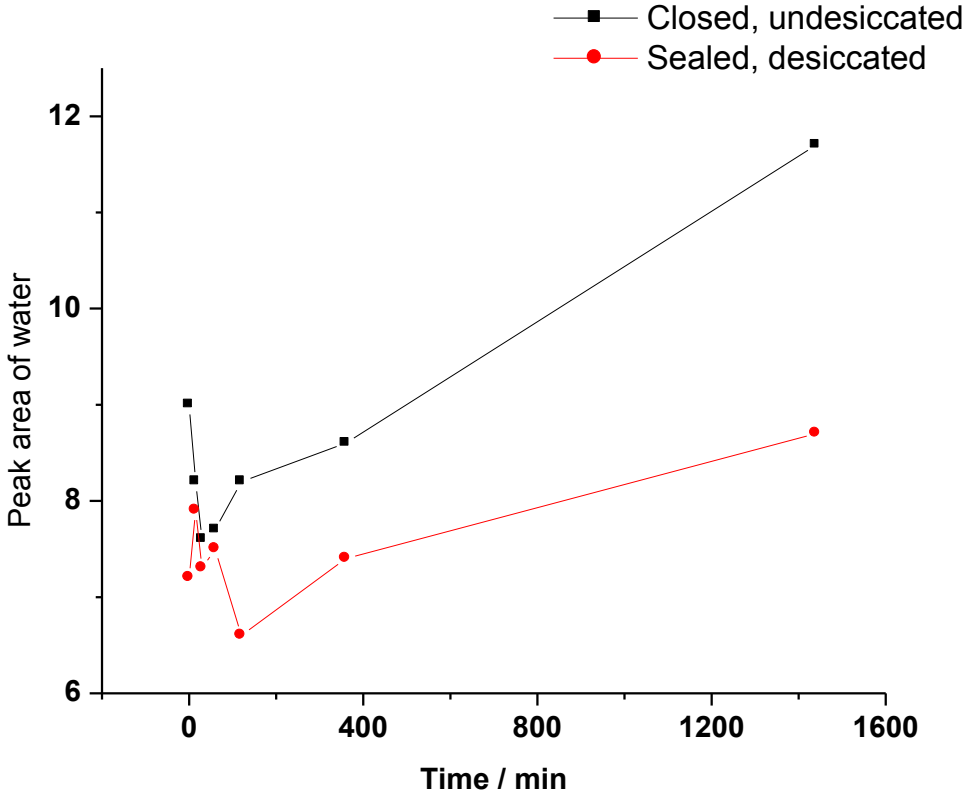
Calibration curve of water with acetonitrile in THF with Commercial C.



APPENDIX D

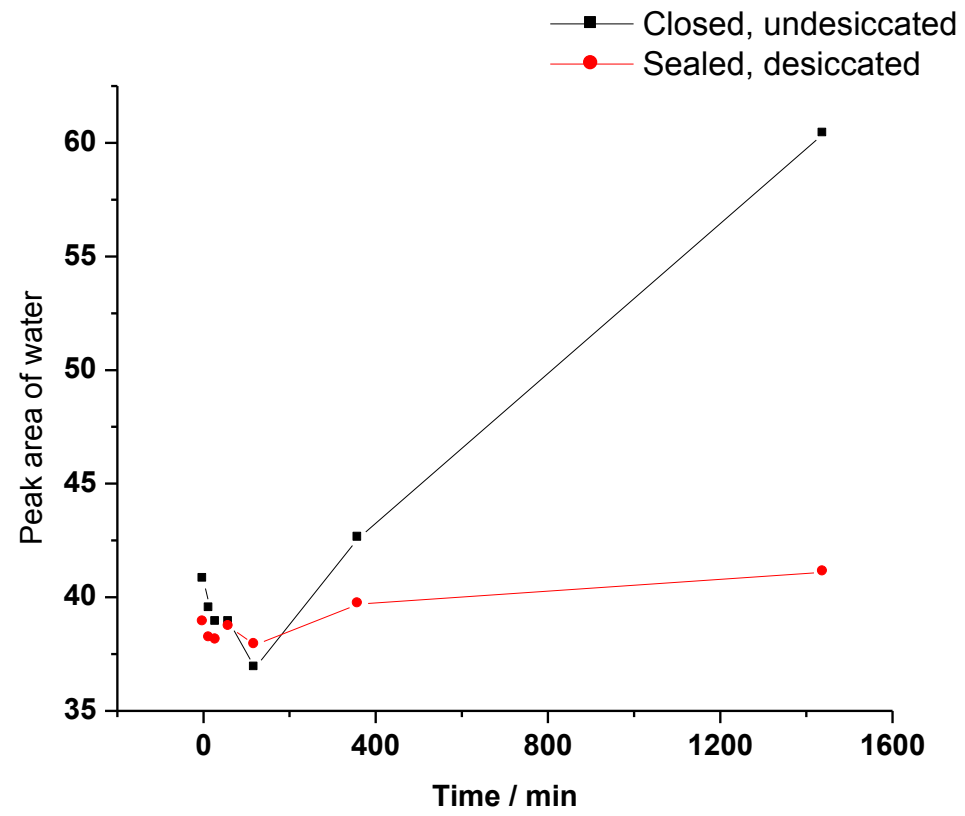
THE STUDY OF ATMOSPHERIC WATER ABSORPTION ON DIFFERENT
SOLVENTS: THE INCREMENT OF WATER PEAK AREA AS A FUNCTION OF
TIME

The study of atmospheric water absorption on MeOH.

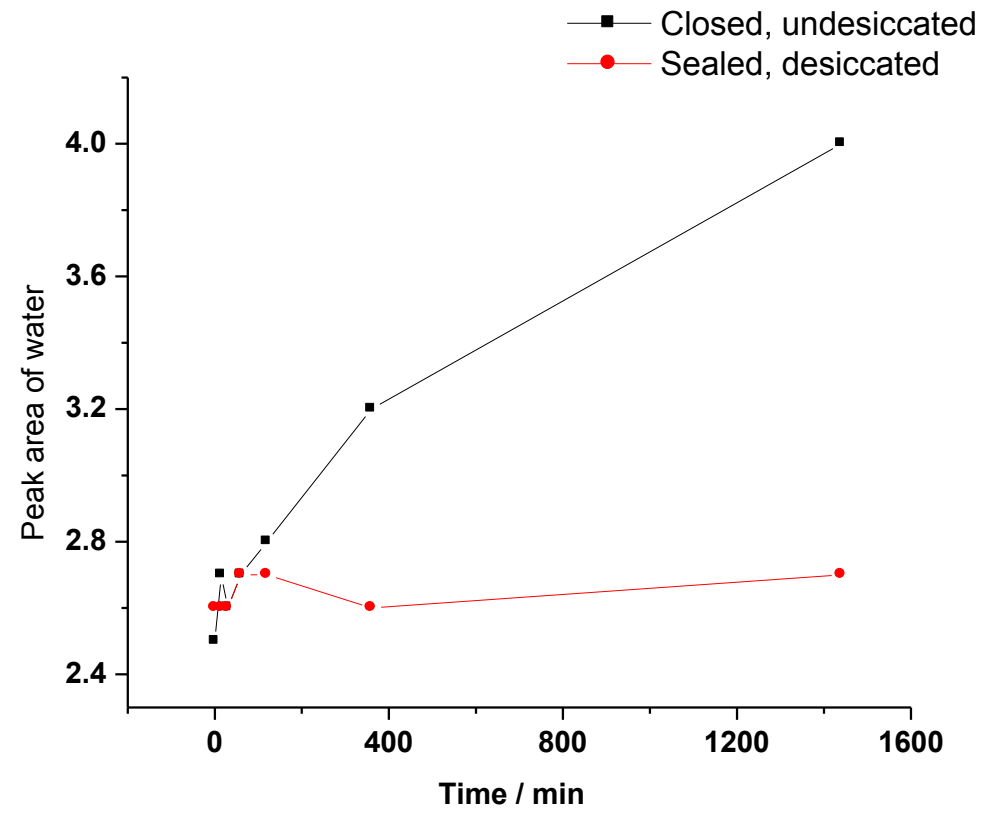


140

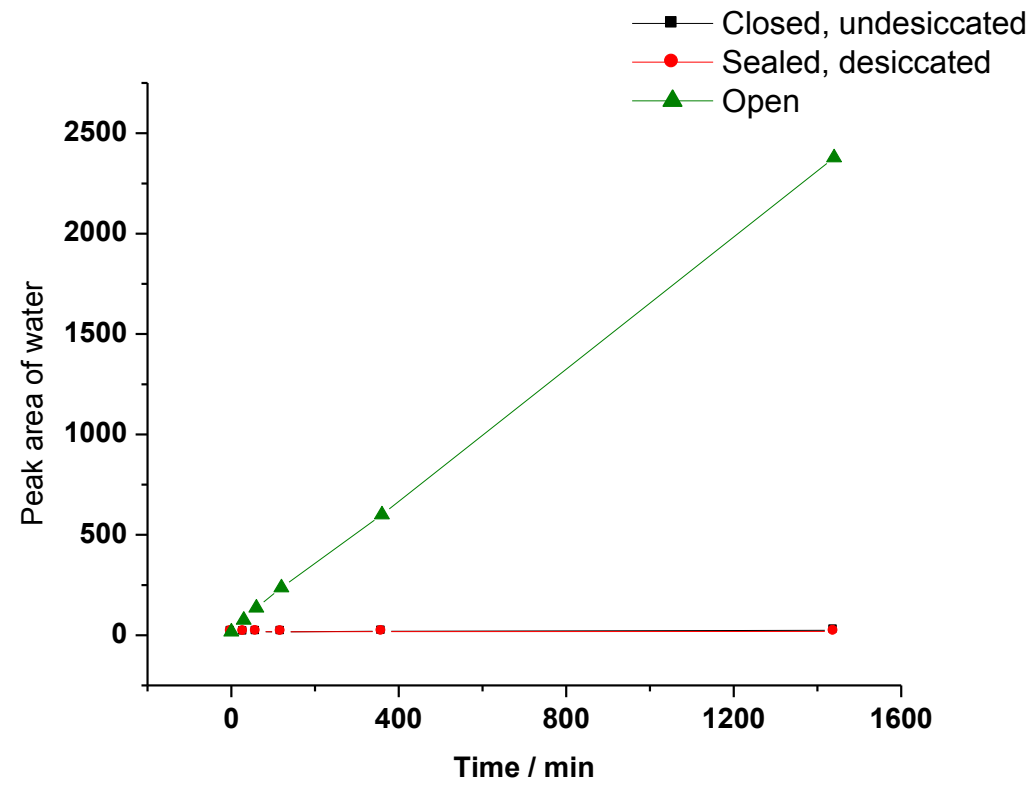
The study of atmospheric water absorption on THF.



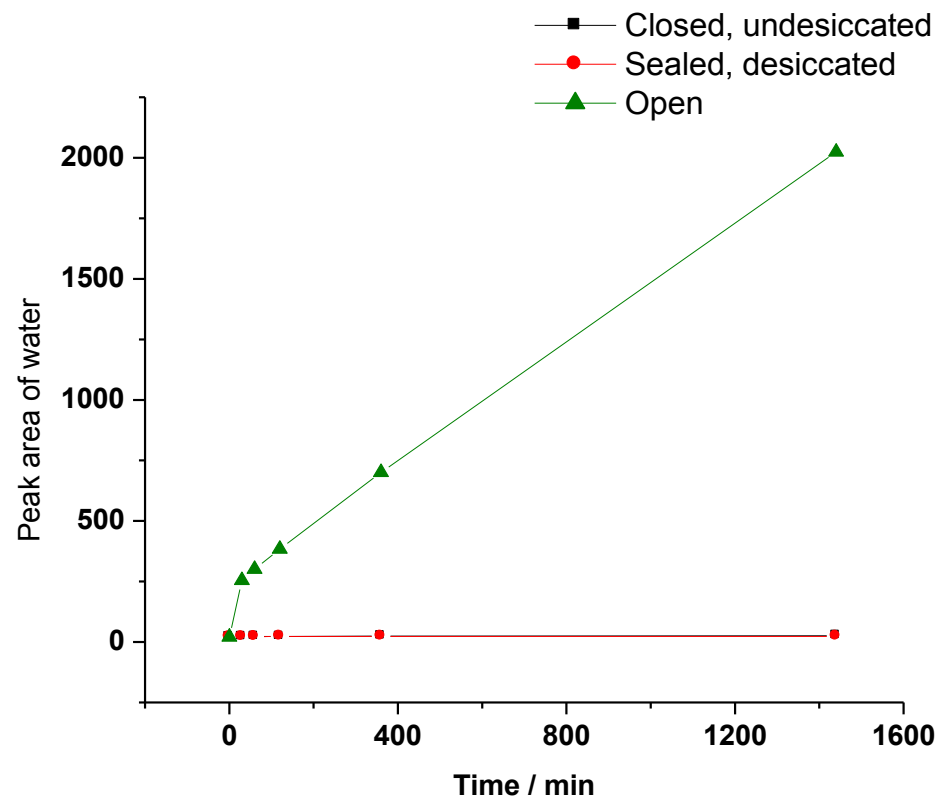
The study of atmospheric water absorption on heptane.



The study of atmospheric water absorption on DMSO.



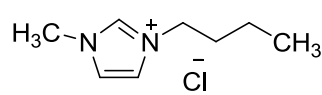
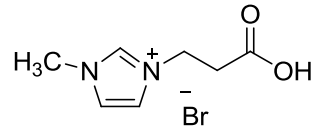
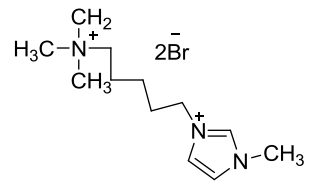
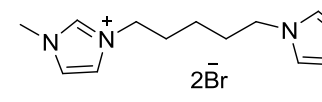
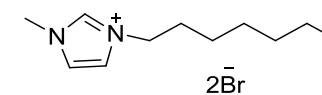
The study of atmospheric water absorption on DMF.

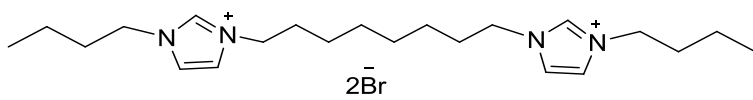


APPENDIX E

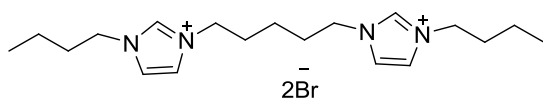
STUDY OF THE EFFECT OF DIFFERENT ILS ON STOCHASTIC SENSING

The detection of β CD at (-)100 mV and pH 6.0

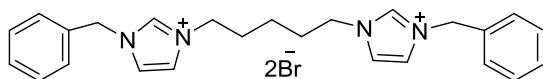
IL	Dwell time
	1.89 ± 0.02
	1.55 ± 0.04
	2.07 ± 0.03
	13.25 ± 0.06
	0.845 ± 0.005



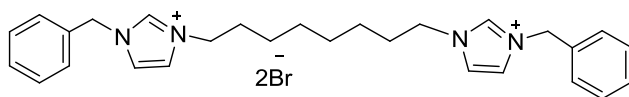
0.49 ± 0.003



17.26 ± 0.08



Did not work



Did not work

APPENDIX F

RIGHTS AND PERMISSIONS

**AMERICAN CHEMICAL SOCIETY LICENSE
TERMS AND CONDITIONS**

This is a License Agreement between Dilani A Jayawardhana ("You") and American Chemical Society ("American Chemical Society") provided by Copyright Clearance Center ("CCC"). The license consists of your order details, the terms and conditions provided by American Chemical Society, and the payment terms and conditions.

All payments must be made in full to CCC. For payment instructions, please see information listed at the bottom of this form.

License Number 2554280959164

License Date Nov 22, 2010

Licensed content publisher American Chemical Society

Licensed content The Journal of Physical Chemistry B
publication

Licensed content title Study of Peptide Transport through Engineered Protein
Channels

Licensed content author Qitao Zhao et al.

Licensed content date Mar 1, 2009

Volume number 113

Issue number	11
Type of Use	Thesis/Dissertation
Requestor type11	Not specified
Format	Print
Portion	50% or more of original article
Author of this ACS article	Yes
Order reference number	
Title of the thesis / dissertation	Nanopore stochastic sensing with ionic liquid supporting electrolyte and ionic liquid based water quantitation using gas chromatography
Expected completion date	Dec 2010
Estimated size(pages)	175
Billing Type	Invoice
Billing Address	700 Planetarium place RM 130 Arlington, TX 76019 United States

AMERICAN CHEMICAL SOCIETY LICENSE

TERMS AND CONDITIONS

This is a License Agreement between Dilani A Jayawardhana ("You") and American Chemical Society ("American Chemical Society") provided by Copyright Clearance Center ("CCC"). The license consists of your order details, the terms and conditions provided by American Chemical Society, and the payment terms and conditions.

All payments must be made in full to CCC. For payment instructions, please see information listed at the bottom of this form.

License Number 2554280436311

License Date Nov 22, 2010

Licensed content publisher American Chemical Society

Licensed content Analytical Chemistry
publication

Licensed content title Nanopore Stochastic Detection of a Liquid Explosive
Component and Sensitizers Using Boromycin and an
Ionic Liquid Supporting Electrolyte

Licensed content author Dilani A. Jayawardhana et al.

Licensed content date Jan 1, 2009

Volume number 81

Issue number	1
Type of Use	Thesis/Dissertation
Requestor type11	Not specified
Format	Print
Portion	Full article
Author of this ACS article	Yes
Order reference number	
Title of the thesis / dissertation	Nanopore stochastic sensing with ionic liquid supporting electrolyte and ionic liquid based water quantitation using gas chromatography
Expected completion date	Dec 2010
Estimated size(pages)	175
Billing Type	Invoice
Billing Address	700 Planetarium place RM 130 Arlington, TX 76019 United States

AMERICAN CHEMICAL SOCIETY LICENSE

TERMS AND CONDITIONS

This is a License Agreement between Dilani A Jayawardhana ("You") and American Chemical Society ("American Chemical Society") provided by Copyright Clearance Center ("CCC"). The license consists of your order details, the terms and conditions provided by American Chemical Society, and the payment terms and conditions.

All payments must be made in full to CCC. For payment instructions, please see information listed at the bottom of this form.

License Number	2554280665918
License Date	Nov 22, 2010
Licensed content publisher	American Chemical Society
Licensed content publication	The Journal of Physical Chemistry B
Licensed content title	Slowing DNA Translocation through Nanopores Using a Solution Containing Organic Salts
Licensed content author	Ranulu Samanthi S. de Zoysa et al.
Licensed content date	Oct 1, 2009
Volume number	113

Issue number	40
Type of Use	Thesis/Dissertation
Requestor type ¹¹	Not specified
Format	Print
Portion	50% or more of original article
Author of this ACS article	Yes
Order reference number	
Title of the thesis / dissertation	Nanopore stochastic sensing with ionic liquid supporting electrolyte and ionic liquid based water quantitation using gas chromatography
Expected completion date	Dec 2010
Estimated size(pages)	175
Billing Type	Invoice
Billing Address	700 Planetarium place RM 130 Arlington, TX 76019 United States
Customer reference info	
Total	0.00 USD

REFERENCES

- (1) Bayley, H.; Cremer, P. S. *Nature (London, U. K.)* **2001**, *413*, 226-230.
- (2) Schmidt, J. J. *Mater. Chem.* **2005**, *15*, 831-840.
- (3) Hladky, S. B.; Haydon, D. A. *Nature (London)* **1970**, *225*, 451-453.
- (4) Bayley, H.; Martin, C. R. *Chem. Rev. (Washington, D. C.)* **2000**, *100*, 2575-2594.
- (5) Miyazawa, A.; Fujiyoshi, Y.; Unwin, N. *Nature (London, U. K.)* **2003**, *423*, 949-955.
- (6) Burkhart, B. M.; Li, N.; Langs, D. A.; Pangborn, W. A.; Duax, W. L. *Proc. Natl. Acad. Sci. U. S. A.* **1998**, *95*, 12950-12955.
- (7) Doyle, D. A.; Cabral, J. M.; Pfuetzner, R. A.; Kuo, A.; Gulbis, J. M.; Cohen, S. L.; Chait, B. T.; MacKinnon, R. *Science (Washington, D. C.)* **1998**, *280*, 69-77.
- (8) MacKinnon, R. *FEBS Lett.* **2003**, *555*, 62-65.
- (9) Bezrukov, S. M.; Kullman, L.; Winterhalter, M. *FEBS Lett.* **2000**, *476*, 224-228.
- (10) Kullman, L.; Winterhalter, M.; Bezrukov, S. M. *Biophys. J.* **2002**, *82*, 803-812.
- (11) Song, L.; Hobaugh, M. R.; Shustak, C.; Cheley, S.; Bayley, H.; Gouaux, J. E. *Science (Washington, D. C.)* **1996**, *274*, 1859-1866.
- (12) Bayley, H.; Braha, O.; Gu, L. *Adv. Mater. (Weinheim, Ger.)* **2000**, *12*, 139-142.
- (13) Braha, O.; Gu, L.; Zhou, L.; Lu, X.; Cheley, S.; Bayley, H. *Nat. Biotechnol.* **2000**, *18*, 1005-1007.
- (14) Braha, O.; Walker, B.; Cheley, S.; Kasianowicz, J. J.; Song, L.; Gouaux, J. E.; Bayley, H. *Chem. Biol.* **1997**, *4*, 497-505.
- (15) Cheley, S.; Gu, L.; Bayley, H. *Chem. Biol.* **2002**, *9*, 829-838.
- (16) Movileanu, L.; Howorka, S.; Braha, O.; Bayley, H. *Nat. Biotechnol.* **2000**, *18*, 1091-1095.

- (17) Howorka, S.; Nam, J.; Bayley, H.; Kahne, D. *Angew. Chem. , Int. Ed.* **2004**, *43*, 842-846.
- (18) Meller, A.; Nivon, L.; Brandin, E.; Golovchenko, J.; Branton, D. *Proc. Natl. Acad. Sci. U. S. A.* **2000**, *97*, 1079-1084.
- (19) Li, J.; Stein, D.; McMullan, C.; Branton, D.; Aziz, M. J.; Golovchenko, J. A. *Nature* **2001**, *412*, 166-169.
- (20) Howorka, S.; Cheley, S.; Bayley, H. *Nat. Biotechnol.* **2001**, *19*, 636-639.
- (21) de Zoysa, R. S. S.; Jayawardhana, D. A.; Zhao, Q.; Wang, D.; Armstrong, D. W.; Guan, X. *J. Phys. Chem. B* **2009**, *113*, 13332-13336.
- (22) Kang, X.; Cheley, S.; Guan, X.; Bayley, H. *J. Am. Chem. Soc.* **2006**, *128*, 10684-10685.
- (23) Guan, X.; Gu, L.; Cheley, S.; Braha, O.; Bayley, H. *ChemBioChem* **2005**, *6*, 1875-1881.
- (24) Jayawardhana, D. A.; Crank, J. A.; Zhao, Q.; Armstrong, D. W.; Guan, X. *Anal. Chem. (Washington, DC, U. S.)* **2009**, *81*, 460-464.
- (25) Gu, L.; Braha, O.; Conlan, S.; Cheley, S.; Bayley, H. *Nature (London)* **1999**, *398*, 686-690.
- (26) Shin, S.; Luchian, T.; Cheley, S.; Braha, O.; Bayley, H. *Angew. Chem. , Int. Ed.* **2002**, *41*, 3707-3709.
- (27) Montal, M.; Mueller, P. *Proc. Nat. Acad. Sci. U. S. A.* **1972**, *69*, 3561-3566.
- (28) Kang, X.; Cheley, S.; Rice-Ficht, A. C.; Bayley, H. *J. Am. Chem. Soc.* **2007**, *129*, 4701-4705.
- (29) Sexton, L. T.; Horne, L. P.; Martin, C. R. *Mol. BioSyst.* **2007**, *3*, 667-685.
- (30) Sun, P.; Armstrong, D. W. *Anal. Chim. Acta* **2010**, *661*, 1-16.
- (31) Soukup-Hein, R. J.; Warnke, M. M.; Armstrong, D. W. *Annu. Rev. Anal. Chem.* **2009**, *2*, 145-168.
- (32) Welton, T. *Chem. Rev. (Washington, D. C.)* **1999**, *99*, 2071-2083.
- (33) Welton, T. *Coord. Chem. Rev.* **2004**, *248*, 2459-2477.
- (34) Anderson, J. L.; Armstrong, D. W.; Wei, G. *Anal. Chem.* **2006**, *78*, 2893-2902.
- (35) Han, X.; Armstrong, D. W. *Acc. Chem. Res.* **2007**, *40*, 1079-1086.

- (36) Galinski, M.; Lewandowski, A.; Stepniak, I. *Electrochim. Acta* **2006**, *51*, 5567-5580.
- (37) de Jong, G. M.; Huizenga, J. R.; Wolthers, B. G.; Jansen, H. G.; Uges, D. R.; Hindriks, F. R.; Gips, C. H. *Clin Chim Acta* **1987**, *166*, 187-194.
- (38) Fischer, K. *Angew. Chem.* **1935**, *48*, 394-396.
- (39) Scholz, E. *Anal. Chem.* **1985**, *57*, 2965-2971.
- (40) Streim, H. G.; Boyce, E. A.; Smith, J. R. *Anal. Chem.* **1961**, *33*, 85-89.
- (41) Knight, H. S.; Weiss, F. T. *Anal. Chem.* **1962**, *34*, 749-751.
- (42) Quiram, E. R. *Anal. Chem.* **1963**, *35*, 593-595.
- (43) Hogan, J. M.; Engel, R. A.; Stevenson, H. F. *Anal. Chem.* **1970**, *42*, 249-252.
- (44) MacDonald, J. C.; Brady, C. A. *Anal. Chem.* **1975**, *47*, 947-948.
- (45) Houston, T. E. *Met. Finish.* **1997**, *95*, 36-38.
- (46) Jalbert, J.; Gilbert, R.; Tetreault, P. *Anal. Chem.* **1999**, *71*, 3283-3291.
- (47) Nussbaum, R.; Lischke, D.; Paxmann, H.; Wolf, B. *Chromatographia* **2000**, *51*, 119-121.
- (48) Lee, C.; Chang, S. *Atmos. Environ.* **2002**, *36*, 1883-1894.
- (49) O'Keefe, W. K.; Ng, F. T. T.; Rempel, G. L. *J. Chromatogr. , A* **2008**, *1182*, 113-118.
- (50) Vornheder, P. F.; Brabbs, W. J. *Anal. Chem.* **1970**, *42*, 1454-1456.
- (51) Li, M.; Pacey, G. E. *Talanta* **1997**, *44*, 1949-1958.
- (52) Zhou, X.; Hines, P. A.; White, K. C.; Borer, M. W. *Anal. Chem.* **1998**, *70*, 390-394.
- (53) Pinheiro, C.; Lima, J. C.; Parola, A. J. *Sens. Actuators, B* **2006**, *B114*, 978-983.
- (54) Sun, H.; Wang, B.; DiMagno, S. G. *Org. Lett.* **2008**, *10*, 4413-4416.
- (55) Jamin, E.; Guerin, R.; Retif, M.; Lees, M.; Martin, G. J. *J. Agric. Food Chem.* **2003**, *51*, 5202-5206.
- (56) Isengard, H. D.; Striffler, U. *Fresenius. J. Anal. Chem.* **1992**, *342*, 287-291.

- (57) Knight, H. S. *Anal. Chem.* **1958**, *30*, 2030-2032.
- (58) Huang, K.; Han, X.; Zhang, X.; Armstrong, D. W. *Anal. Bioanal. Chem.* **2007**, *389*, 2265-2275.
- (59) Gu, L.; Cheley, S.; Bayley, H. *J. Gen. Physiol.* **2001**, *118*, 481-493.
- (60) Kang, X.; Gu, L.; Cheley, S.; Bayley, H. *Angew. Chem., Int. Ed.* **2005**, *44*, 1495-1499, S1495/1-S1495/21.
- (61) Jung, Y.; Bayley, H.; Movileanu, L. *J. Am. Chem. Soc.* **2006**, *128*, 15332-15340.
- (62) Kuyucak, S.; Bastug, T. *J. Biol. Phys.* **2003**, *29*, 429-446.
- (63) Zhao, Q.; Jayawardhana, D. A.; Guan, X. *Biophys. J.* **2008**, *94*, 1267-1275.
- (64) Wu, H.; Bayley, H. *J. Am. Chem. Soc.* **2008**, *130*, 6813-6819.
- (65) Kasianowicz, J. J.; Brandin, E.; Branton, D.; Deamer, D. *Proc. Natl. Acad. Sci. U. S. A.* **1996**, *93*, 13770-13773.
- (66) Benner, S.; Chen, R. J. A.; Wilson, N. A.; Abu-Shumays, R.; Hurt, N.; Lieberman, K. R.; Deamer, D. W.; Dunbar, W. B.; Akeson, M. *Nat. Nanotechnol.* **2007**, *2*, 718-724.
- (67) Sutherland, T. C.; Long, Y.; Stefureac, R.; Bediako-Amoa, I.; Kraatz, H.; Lee, J. S. *Nano Lett.* **2004**, *4*, 1273-1277.
- (68) Stefureac, R.; Long, Y.; Kraatz, H.; Howard, P.; Lee, J. S. *Biochemistry* **2006**, *45*, 9172-9179.
- (69) Movileanu, L.; Schmittschmitt, J. P.; Scholtz, J. M.; Bayley, H. *Biophys. J.* **2005**, *89*, 1030-1045.
- (70) Wolfe, A. J.; Mohammad, M. M.; Cheley, S.; Bayley, H.; Movileanu, L. *J. Am. Chem. Soc.* **2007**, *129*, 14034-14041.
- (71) Mohammad, M. M.; Movileanu, L. *Eur. Biophys. J.* **2008**, *37*, 913-925.
- (72) Rathert, P.; Dhayalan, A.; Murakami, M.; Zhang, X.; Tamas, R.; Jurkowska, R.; Komatsu, Y.; Shinkai, Y.; Cheng, X.; Jeltsch, A. *Nat. Chem. Biol.* **2008**, *4*, 344-346.
- (73) Asara, J. M.; Schweitzer, M. H.; Freemark, L. M.; Phillips, M.; Cantley, L. C. *Science (Washington, DC, U. S.)* **2007**, *316*, 280-285.
- (74) Baker, D.; Sali, A. *Science (Washington, DC, U. S.)* **2001**, *294*, 93-96.

- (75) Rajendran, L.; Schneider, A.; Schlechtingen, G.; Weidlich, S.; Ries, J.; Braxmeier, T.; Schwille, P.; Schulz, J. B.; Schroeder, C.; Simons, M.; Jennings, G.; Knoelker, H.; Simons, K. *Science (Washington, DC, U. S.)* **2008**, *320*, 520-523.
- (76) Barnham, K. J.; Kenche, V. B.; Ciccotosto, G. D.; Smith, D. P.; Tew, D. J.; Liu, X.; Perez, K.; Cranston, G. A.; Johanssen, T. J.; Volitakis, I.; Bush, A. I.; Masters, C. L.; White, A. R.; Smith, J. P.; Cherny, R. A.; Cappai, R. *Proc. Natl. Acad. Sci. U. S. A.* **2008**, *105*, 6813-6818.
- (77) Hintersteiner, M.; Enz, A.; Frey, P.; Jatou, A.; Kinzy, W.; Kneuer, R.; Neumann, U.; Rudin, M.; Staufienbiel, M.; Stoeckli, M.; Wiederhold, K.; Gremlich, H. *Nat. Biotechnol.* **2005**, *23*, 577-583.
- (78) Szegedi, V.; Juhasz, G.; Rozsa, E.; Juhasz-Vedres, G.; Datki, Z.; Fulop, L.; Bozso, Z.; Lakatos, A.; Laczko, I.; Farkas, T.; Kis, Z.; Toth, G.; Soos, K.; Zarandi, M.; Budai, D.; Toldi, J.; Penke, B. *Faseb J.* **2006**, *20*, 1191-1193, 10.1096/fj.05-4891fje.
- (79) Chen, C.; Wagner, H.; Still, W. C. *Science (Washington, D. C.)* **1998**, *279*, 851-853.
- (80) Koo, T.; Chan, S.; Berlin, A. A. *Opt. Lett.* **2005**, *30*, 1024-1026.
- (81) Kalkum, M.; Lyon, G. J.; Chait, B. T. *Proc. Natl. Acad. Sci. U. S. A.* **2003**, *100*, 2795-2800.
- (82) Villafranca, J. J.; Editor **1991**, 579.
- (83) Molle, D.; Morgan, F.; Bouhallab, S.; Leonil, J. *Anal. Biochem.* **1998**, *259*, 152-161.
- (84) Lee, B.; Krisnanchettiar, S.; Lateef, S. S.; Gupta, S. *Rapid Commun. Mass Spectrom.* **2005**, *19*, 886-892.
- (85) Barrera, N. P.; Di Bartolo, N.; Booth, P. J.; Robinson, C. V. *Science (Washington, DC, U. S.)* **2008**, *321*, 243-246.
- (86) Cheley, S.; Braha, O.; Lu, X.; Conlan, S.; Bayley, H. *Protein Sci* **1999**, *8*, 1257-1267.
- (87) Andrews, P. *Methods Biochem. Anal.* **1970**, *18*, 1-53.
- (88) Hille, B., Ed.; In *Ion channels of excitable membranes*; Sinauer associates, Inc.: Sunderland, Massachusetts U.S.A., 2001; , pp 722.
- (89) Ananthaswamy, J.; Atkinson, G. *J. Solution Chem.* **1982**, *11*, 509-527.
- (90) Pitzer, K. S.; Mayorga, G. *J. Phys. Chem.* **1973**, *77*, 2300-2308.

- (91) Trias, J.; Benz, R. *J. Biol. Chem.* **1993**, *268*, 6234-6240.
- (92) Bauer, W. R.; Nadler, W. *Proc. Natl. Acad. Sci. U. S. A.* **2006**, *103*, 11446-11451.
- (93) Movileanu, L.; Cheley, S.; Bayley, H. *Biophys. J.* **2003**, *85*, 897-910.
- (94) Kasianowicz, J. J.; Nguyen, T. L.; Stanford, V. M. *Proc. Natl. Acad. Sci. U. S. A.* **2006**, *103*, 11431-11432.
- (95) Zamyatnin, A. A. *Prog Biophys Mol Biol* **1972**, *24*, 107-123.
- (96) Gu, L.; Bayley, H. *Biophys. J.* **2000**, *79*, 1967-1975.
- (97) Vlassioux, I.; Smirnov, S.; Siwy, Z. *Nano Lett.* **2008**, *8*, 1978-1985.
- (98) Gu, L.; Dalla Serra, M.; Vincent, J. B.; Vigh, G.; Cheley, S.; Braha, O.; Bayley, H. *Proc. Natl. Acad. Sci. U. S. A.* **2000**, *97*, 3959-3964.
- (99) Gu, L.; Cheley, S.; Bayley, H. *Proc. Natl. Acad. Sci. U. S. A.* **2003**, *100*, 15498-15503.
- (100) White, R. J.; Ervin, E. N.; Yang, T.; Chen, X.; Daniel, S.; Cremer, P. S.; White, H. S. *J. Am. Chem. Soc.* **2007**, *129*, 11766-11775.
- (101) <http://www.globalsecurity.org/military/systems/munitions/explosives-liquid.htm>.
- (102) Senesac, L.; Thundat, T. G. *Mater. Today (Oxford, U. K.)* **2008**, *11*, 28-36.
- (103) Kanda, J. *Water Res.* **1995**, *29*, 2746-2750.
- (104) Frenzel, W.; Liu, C. Y. *Fresenius. J. Anal. Chem.* **1992**, *342*, 276-280.
- (105) Slanina, J.; ten Brink, H. M.; Otjes, R. P.; Even, A.; Jongejan, P.; Khlystov, A.; Waijers-Ijpelaar, A.; Hu, M.; Lu, Y. *Atmos. Environ.* **2001**, *35*, 2319-2330.
- (106) Holmes, R. M.; Aminot, A.; Kerouel, R.; Hooker, B. A.; Peterson, B. J. *Can. J. Fish. Aquat. Sci.* **1999**, *56*, 1801-1808.
- (107) Bertocchi, P.; Compagnone, D.; Palleschi, G. *Biosens. Bioelectron.* **1996**, *11*, 1-10.
- (108) Reichert, J.; Sellien, W.; Ache, H. J. *Sens. Actuators, A* **1991**, *A26*, 481-482.
- (109) Hu, X.; Takenaka, N.; Takasuna, S.; Kitano, M.; Bandow, H.; Maeda, Y.; Hattori, M. *Anal. Chem.* **1993**, *65*, 3489-3492.
- (110) Lee, Y. I.; Sneddon, J. *Analyst (Cambridge, U. K.)* **1994**, *119*, 1441-1443.

- (111) Destandau, E.; Lefevre, J.; Chouai Fakhr Eddine, A.; Desportes, S.; Jullien, M. C.; Hierle, R.; Leray, I.; Valeur, B.; Delaire, J. A. *Anal. Bioanal. Chem.* **2007**, *387*, 2627-2632.
- (112) Lopez, J. A.; Manriquez, J.; Mendoza, S.; Godinez, L. A. *Electrochem. Commun.* **2007**, *9*, 2133-2139.
- (113) Yam, V. W.; Li, C.; Chan, C. *Angew. Chem., Int. Ed.* **1998**, *37*, 2857-2859.
- (114) Wu, G.; Wong, A.; Gan, Z.; Davis, J. T. *J. Am. Chem. Soc.* **2003**, *125*, 7182-7183.
- (115) Bente, M.; Adam, T.; Ferge, T.; Gallavardin, S.; Sklorz, M.; Streibel, T.; Zimmermann, R. *Int. J. Mass Spectrom.* **2006**, *258*, 86-94.
- (116) Grate, J. W.; Rose-Pehrsson, S.; Barger, W. R. *Langmuir* **1988**, *4*, 1293-1301.
- (117) Wang, J.; Chen, L. *Anal. Chem.* **1995**, *67*, 3824-3827.
- (118) Guerra, S. V.; Kubota, L. T.; Xavier, C. R.; Nakagaki, S. *Anal. Sci.* **1999**, *15*, 1231-1234.
- (119) Raoof, J. B.; Ojani, R.; Kiani, A.; Khosravi, M.; Adnani, A. *Bull. Chem. Soc. Jpn.* **2005**, *78*, 258-261.
- (120) Virji, S.; Kaner, R. B.; Weiller, B. H. *Chem. Mater.* **2005**, *17*, 1256-1260.
- (121) Ozoemena, K. I.; Nyokong, T. *Talanta* **2005**, *67*, 162-168.
- (122) Thomas, S. W., III; Swager, T. M. *Adv. Mater. (Weinheim, Ger.)* **2006**, *18*, 1047-1050.
- (123) Baron, R.; Sljukic, B.; Salter, C.; Crossley, A.; Compton, R. G. *Electroanalysis* **2007**, *19*, 1062-1068.
- (124) Umar, A.; Rahman, M. M.; Kim, S. H.; Hahn, Y. *Chem. Commun. (Cambridge, U. K.)* **2008**, 166-168.
- (125) Neiderhiser, D. H.; Fuller, R. K. *J. Chromatogr., Biomed. Appl.* **1982**, *229*, 470-474.
- (126) Chen, Y.; Lin, Z.; Sun, J.; Chen, G. *Electrophoresis* **2007**, *28*, 3250-3259.
- (127) Gilbert, R.; Rioux, R.; Saheb, S. E. *Anal. Chem.* **1984**, *56*, 106-109.
- (128) Lindahl, R.; Wasterby, A.; Levin, J. *Analyst (Cambridge, U. K.)* **2001**, *126*, 152-154.

- (129) White, J. D.; Avery, M. A.; Choudhry, S. C.; Dhingra, O. P.; Gray, B. D.; Kang, M. C.; Kuo, S. C.; Whittle, A. J. *J. Am. Chem. Soc.* **1989**, *111*, 790-792.
- (130) Wang, C.; Armstrong, D. W.; Risley, D. S. *Anal. Chem. (Washington, DC, U. S.)* **2007**, *79*, 8125-8135.
- (131) Tinker, A.; Lindsay, A. R. G.; Williams, A. J. *J. Membr. Biol.* **1992**, *127*, 149-159.
- (132) Tinker, A.; Lindsay, A. R. G.; Williams, A. J. *Biophys. J.* **1992**, *61*, 1122-1132.
- (133) Anderson, J. L.; Ding, J.; Welton, T.; Armstrong, D. W. *J. Am. Chem. Soc.* **2002**, *124*, 14247-14254.
- (134) Ohno, H. In *Electrochemical aspects of ionic liquids*; John Wiley & Sons: New Jersey, 2005; .
- (135) Atkins, P.; de Paula, J. **2002**, 1149.
- (136) Robertson, J. W. F.; Rodrigues, C. G.; Stanford, V. M.; Rubinson, K. A.; Krasilnikov, O. V.; Kasianowicz, J. J. *Proc. Natl. Acad. Sci. U. S. A.* **2007**, *104*, 8207-8211.
- (137) Anderson, J. L.; Ding, R.; Ellern, A.; Armstrong, D. W. *J. Am. Chem. Soc.* **2005**, *127*, 593-604.
- (138) Payagala, T.; Huang, J.; Breitbach, Z. S.; Sharma, P. S.; Armstrong, D. W. *Chem. Mater.* **2007**, *19*, 5848-5850.
- (139) Breitbach, Z. S.; Armstrong, D. W. *Anal. Bioanal. Chem.* **2008**, *390*, 1605-1617.
- (140) Franca, L. T. C.; Carrilho, E.; Kist, T. B. L. *Q. Rev. Biophys.* **2002**, *35*, 169-200.
- (141) <http://grants1.nih.gov/grants/guide/rfa-files/RFA-HG-04-003.html>.
- (142) Bayley, H. *Curr. Opin. Chem. Biol.* **2006**, *10*, 628-637.
- (143) Branton, D.; Deamer, D. W.; Marziali, A.; Bayley, H.; Benner, S. A.; Butler, T.; Di Ventra, M.; Garaj, S.; Hibbs, A.; Huang, X.; Jovanovich, S. B.; Krstic, P. S.; Lindsay, S.; Ling, X. S.; Mastrangelo, C. H.; Meller, A.; Oliver, J. S.; Pershin, Y. V.; Ramsey, J. M.; Riehn, R.; Soni, G. V.; Tabard-Cossa, V.; Wanunu, M.; Wiggins, M.; Schloss, J. A. *Nat. Biotechnol.* **2008**, *26*, 1146-1153.
- (144) Meller, A.; Branton, D. *Electrophoresis* **2002**, *23*, 2583-2591.
- (145) Meller, A.; Nivon, L.; Branton, D. *Phys Rev Lett* **2001**, *86*, 3435-3438.

- (146) Sanchez-Quesada, J.; Saghatelian, A.; Cheley, S.; Bayley, H.; Ghadiri, M. R. *Angew. Chem., Int. Ed.* **2004**, *43*, 3063-3067.
- (147) Astier, Y.; Braha, O.; Bayley, H. *J. Am. Chem. Soc.* **2006**, *128*, 1705-1710.
- (148) Purnell, R. F.; Mehta, K. K.; Schmidt, J. J. *Nano Lett.* **2008**, *8*, 3029-3034.
- (149) Sigalov, G.; Comer, J.; Timp, G.; Aksimentiev, A. *Nano Lett.* **2008**, *8*, 56-63.
- (150) Nakashima, K.; Kubota, F.; Maruyama, T.; Goto, M. *Ind. Eng. Chem. Res.* **2005**, *44*, 4368-4372.
- (151) Zhao, Q.; Jayawardhana, D. A.; Wang, D.; Guan, X. *J. Phys. Chem. B* **2009**, *113*, 3572-3578.
- (152) Zhao, Q.; Wang, D.; Jayawardhana, D. A.; Guan, X. *Nanotechnology* **2008**, *19*, 505504/1-505504/8.
- (153) Butler, T. Z.; Gundlach, J. H.; Troll, M. *Biophys. J.* **2007**, *93*, 3229-3240.
- (154) Miller, C. *Biophys J* **1982**, *38*, 227-230.
- (155) Colquhoun, D.; Hawkes, A. G., Eds.; In *The principles of stochastic interpretation of ion-channel mechanisms. In Single-Channel Recording.* Sakmann, B., Neher, E., Ed.; Plenum Press: New York, NY, **1983**
- (156) Kawano, R.; Schibel, A. E. P.; Cauley, C.; White, H. S. *Langmuir* **2009**, *25*, 1233-1237.
- (157) Marziali, A.; Akeson, M. *Annu. Rev. Biomed. Eng.* **2001**, *3*, 195-223.
- (158) Zhang, Y.; Gao, F.; Popov, V. L.; Wen, J. W.; Hamill, O. P. *J. Physiol.* **2000**, *523 Pt 1*, 117-130.
- (159) Shen, X.; Xu, G.; Shao, C. *Solid State Commun.* **2009**, *149*, 852-854.
- (160) Berthod, A.; Kozak, J. J.; Anderson, J. L.; Ding, J.; Armstrong, D. W. *Theor. Chem. Acc.* **2007**, *117*, 127-135.
- (161) Wang, J.; Cheng, D.; Chen, X.; Du, Z.; Fang, Z. *Anal. Chem.* **2007**, *79*, 620-625.
- (162) Xie, Y.; Wang, S.; Zhang, Z.; Pang, D. *J. Phys. Chem. B* **2008**, *112*, 9864-9868.
- (163) Fologea, D.; Gershow, M.; Ledden, B.; McNabb, D. S.; Golovchenko, J. A.; Li, J. *Nano Lett.* **2005**, *5*, 1905-1909.

- (164) Keyser, U. F.; Koeleman, B. N.; Van Dorp, S.; Krapf, D.; Smeets, R. M. M.; Lemay, S. G.; Dekker, N. H.; Dekker, C. *Nat. Phys.* **2006**, *2*, 473-477.
- (165) Gershow, M.; Golovchenko, J. A. *Nat. Nanotechnol.* **2007**, *2*, 775-779.
- (166) Takeuchi, K.; Takahashi, H.; Kawano, S.; Shimada, I. *J. Biol. Chem.* **2007**, *282*, 15179-15186.
- (167) Kocer, A.; Walko, M.; Meijberg, W.; Feringa, B. L. *Science (Washington, DC, U. S.)* **2005**, *309*, 755-758.
- (168) Cuello, L. G.; Romero, J. G.; Cortes, D. M.; Perozo, E. *Biochemistry* **1998**, *37*, 3229-3236.
- (169) Collarini, M.; Amblard, G.; Lazdunski, C.; Pattus, F. *Eur. Biophys. J.* **1987**, *14*, 147-153.
- (170) Tavernarakis, N.; Shreffler, W.; Wang, S.; Driscoll, M. *Neuron* **1997**, *18*, 107-119.
- (171) Mounsey, K. E.; Dent, J. A.; Holt, D. C.; McCarthy, J.; Currie, B. J.; Walton, S. F. *Invertebr. Neurosci.* **2007**, *7*, 149-156.
- (172) Jiang, Y.; MacKinnon, R. *J. Gen. Physiol.* **2000**, *115*, 269-272.
- (173) Nowak, L.; Bregestovski, P.; Ascher, P.; Herbet, A.; Prochiantz, A. *Nature (London)* **1984**, *307*, 462-465.
- (174) Wirtz, M.; Martin, C. R. *Sens. Update* **2003**, *11*, 35-64.
- (175) Zhao, Q.; de Zoysa, R. S. S.; Wang, D.; Jayawardhana, D. A.; Guan, X. *J. Am. Chem. Soc.* **2009**, *131*, 6324-6325.
- (176) Vullo, W. J. *J. Org. Chem.* **1968**, *33*, 3665-3667.
- (177) Ellzey, S. E., Jr.; Connick, W. J., Jr.; Boudreaux, G. J.; Klapper, H. *J. Org. Chem.* **1972**, *37*, 3453-3457.
- (178) Cao, Y. C. *Nanomedicine (Lond)* **2008**, *3*, 467-469.
- (179) EMD Chemicals AQUASTAR Tech Notes *Fischer Titration Basics*.
- (180) <http://www.jmscience.com/AQ-300-Karl-Fischer-Coulometric-Titrator.htm>.
- (181) http://www.jmscience.com/AQ_2200/AQ-2200.htm.
- (182) Sharma, P. S.; Payagala, T.; Wanigasekara, E.; Wijeratne, A. B.; Huang, J.; Armstrong, D. W. *Chem. Mater.* **2008**, *20*, 4182-4184.

- (183) Center for Drug Evaluation and Research (CDER), US Food and Drug Administration (FDA) **1994**, 1-30.
- (184) Center for Drug Evaluation and Research (CDER), US Food and Drug Administration (FDA) **1996**, 1-10.

BIOGRAPHICAL INFORMATION

Dilani A. Jayawardhana, born in Kegalle, Sri Lanka, obtained her B.S in special degree in chemistry with a second class honors in 2004, from The University of Peradeniya, Peradeniya, Sri Lanka. After working as an assistant lecturer and then as a research assistant at The University of Peradeniya, she moved to The United States in 2005 and began her doctoral study at the University of Texas at Arlington, with Professors Daniel W. Armstrong and Richard X. Guan. Her research interests include stochastic nanopore sensing and introduction of novel background electrolytes to that technique. She is also interested in developing an ionic liquid based water quantitation method using gas chromatography. She obtained her Doctor of Philosophy degree in 2010.